GUANIDINATES: A NEW CLASS OF LIGANDS FOR DIMETAL UNITS WITH MULTIPLE METAL-METAL BONDS

A Dissertation

by

CHAD C. WILKINSON

Submitted to the Office of Graduate Studies of
Texas A&M University
in partial fulfillment of the requirements for the degree of

DOCTOR OF PHILOSOPHY

May 2005

Major Subject: Chemistry

GUANIDINATES: A NEW CLASS OF LIGANDS FOR DIMETAL UNITS WITH MULTIPLE METAL-METAL BONDS

A Dissertation

by

CHAD C. WILKINSON

Submitted to the Office of Graduate Studies of
Texas A&M University
in partial fulfillment of the requirements for the degree of

DOCTOR OF PHILOSOPHY

Approved as to style and content by:

F. A. Cotton (Co-Chair of Committee)	J. P. Fackler, Jr. (Co-Chair of Committee)
C. A. Murillo (Member)	G. W. Kattawar (Member)
E. A. Schweikert (Head of Department)	

May 2005

Major Subject: Chemistry

ABSTRACT

Guanidinates: A New Class of Ligands for Dimetal Units with Multiple Metal-Metal Bonds. (May 2005)

Chad C. Wilkinson, B.S., Baylor University

Co-Chairs of Advisory Committee: Dr. F. A. Cotton
Dr. J. P. Fackler, Jr.

This dissertation concerns the discovery of the ability of the guanidinate ligand hpp (hpp = anion of 1,3,4,6,7,8-hexahydropyrimido[1,2-a]pyrimidine) to stabilize high oxidation states of dimetal units (particularly dimolybdenum species) and attempts to control solubility and redox potential through modification of the ligand. Two general strategies were used for the ligand modifications: alteration of the ring size, and addition of alkyl substituents.

All of the dimetal complexes using these ligands show a significant shift in redox potential compared to other commonly used classes of ligands (i.e. carboxylates and formamidinates) allowing access to the Mo_2^{4+}, Mo_2^{5+} and Mo_2^{6+} oxidation states. The solubility of the complexes increases with increasing ring size, or with increasing length of the alkyl substituent. The physical and chemical properties of the ligands and their dimolybdenum complexes are described in detail.

DEDICATION

I dedicate this work to my good friend Mervin J. Bazile, Jr.

Your light faded from this world far too soon.

"Always remember, a crystal shines in every heart."
— *Final Fantasy* (video game)

ACKNOWLEDGEMENTS

I sincerely thank Prof. F. A. Cotton for giving me the opportunity to work on a highly challenging and rewarding project. I could not have asked for a greater adventure.

I thank Dr. Carlos A. Murillo for his guidance and helpful discussions as I worked on this project. His wealth of synthetic knowledge has made this road less difficult to travel. If not for his suggestion to turn to the patent literature, this work would not exist.

I truly appreciate the help of Dr. Lee M. Daniels and Dr. Xiaoping Wang concerning X-ray crystallography. The training and advice they have provided as well as their assistance with particularly difficult structures has been a great boon to this project.

I thank Dr. Shane Tichey and Vanessa Santiago for their help with obtaining the mass spectra of many air-sensitive compounds.

I thank Dr. Brant Boren and Joseph Grill for helpful discussion regarding organic synthesis.

I greatly appreciate Dino Villagrán's assistance with theoretical calculations and measurements of magnetic susceptibility.

Finally, I would like to thank all the members of the LMSB, past and present, my friends and my family for their support and encouragement through the years.

TABLE OF CONTENTS

LIST OF TABLES

TABLE Page

LIST OF FIGURES

FIGURE Page

FIGURE Page

FIGURE Page

CHAPTER I

INTRODUCTION*

A wealth of knowledge[1] on multiple metal-metal bonded complexes has accumulated since the correct formulation of the first quadruply bonded species, $Re_2Cl_8^{2-}$, was published almost four decades ago.[2] Since then, other halide species $M_2X_8^{n-}$, **I**, having direct and unsupported metal-metal bonds have been made for four other metals, M = Mo, W, Tc and Os, as shown in Figure 1.

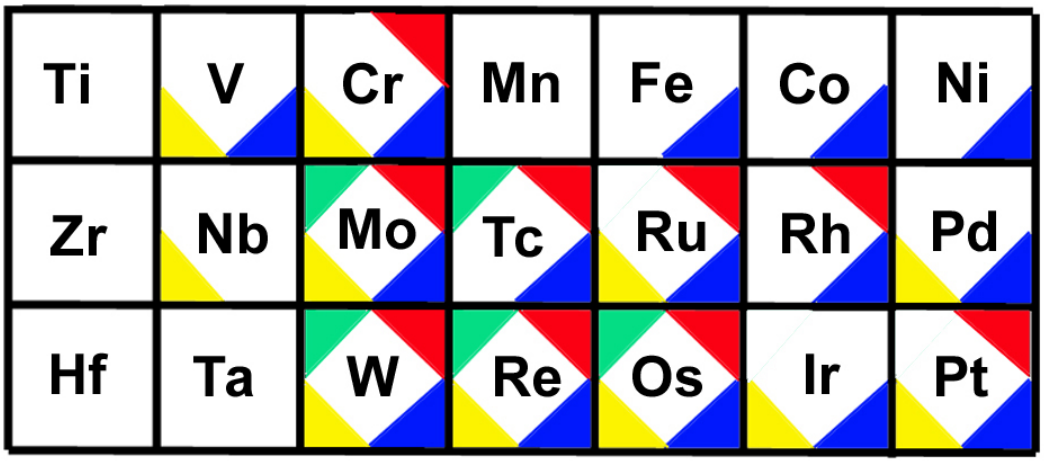

Figure 1. Portion of the periodic table depicting the groups 4 through 10 transition metals that form paddlewheel structures. Green represents halides, red represents carboxylates, blue represents formamidinates, and yellow represents hpp compounds.

This dissertation follows the format and style of *Inorganic Chemistry*.

*Portions of this chapter are reprinted in part from *J. Am. Chem. Soc.*, *124*, Cotton, F. A.; Daniels, L. M.; Murillo, C. A.; Timmons, D. J.; Wilkinson, C. C., "The Extraordinary Ability of Guanidinate Derivatives to Stabilize Higher Oxidation Numbers in Dimetal Units by Modification of Redox Potentials: Structures of Mo_2^{5+} and Mo_2^{6+} Compounds", 9249, Copyright 2002, with permission from the American Chemical Society.

Much of the progress in this field has come in quantum jumps closely associated with the development of new types of ligands. For example, substitution of the halide ions by carboxylate anions brought about an almost explosive growth. This allowed the preparation of hundreds of compounds having two metal atoms bridged by four monoanions, providing structures of type **II**, commonly known as paddlewheel or tetragonal lantern structures. As shown in Figure 1, metal atoms capable of forming such structural types include Cr, Ru and Rh as well as those known to form $M_2X_8^{n-}$ species.

Further expansion of the number of elements capable of forming paddlewheel compounds had to wait until amidinate-type ligands, such as the formamidinates, **III**, were used.[1] These ushered in yet another stage of development, allowing isolation of the first Ni_2^{5+} complex having a bond order of 1/2,[3] as well as the first V_2^{4+},[4] $Fe_2^{3+,4+}$,[5] $Co_2^{3+,4+,5+}$,[6] and Ir_2^{4+},[7] and $Pt_2^{4+,5+,6+}$ compounds[8] (see Figure 1), although for the latter, other types of Pt–Pt bonded species were already known.[1]

Optimism about filling still more holes in the periodic table was tempered by the discovery that formamidinates are cleaved rather easily in the presence of certain low-valent metal species, for example those of Nb and Ta.[9] It was then necessary to find a more sturdy ligand that would not be cleaved as easily. One that seemed to have those desirable characteristics was the anion of 1,3,4,6,7,8-hexahydro-2*H*-pyrimido[1,2-*a*]pyrimidine, hpp (**IV**). The parent guanidinate-type compound had the advantage of being commercially available and the anion had been shown to stabilize Ru_2^{6+} units.[10] Using this ligand, it was possible to synthesize the first triply-bonded Nb_2^{4+} complex.[11]

As indicated in Figure 1, this anion can also form paddlewheel complexes with many other transition metal atoms.[12]

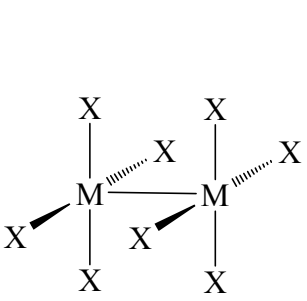

I

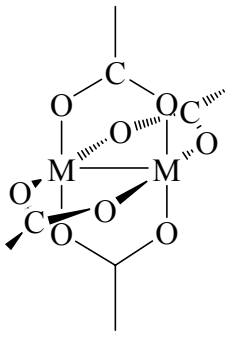

II

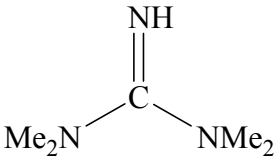

V

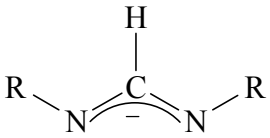

III

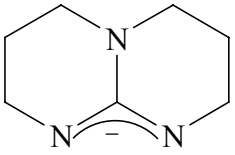

IV

More importantly, it is now clear that not only is the hpp ligand more robust than the formamidinates but also that there are significant electronic differences. The Hhpp compound has been considered a weak nucleophile for organic synthesis but studies of the electronic structure[13] have shown it is a very strong Brønsted base. It has been estimated that Hhpp is nearly 100 times more basic than tetramethylguanidine,[14] **V**. From UV photoelectron spectroscopy, it has been established that the HOMO ionization of Hhpp corresponds to a nitrogen lone pair at the N(1) position (the N at the top in **IV**).[13] It has been argued that there are possible intramolecular interactions between orbitals localized on imine (n_{CN}, π_{CN}) and amine (n_N) moieties with the lone pairs from

N(1) interacting more strongly with the π_{CN} orbital than with the lone pair orbital at the non-protonated nitrogen atom. Thus, it is likely that such large electronic differences between hpp and formamidinate ligands are responsible for the stabilization of a series of highly oxidized M_2 species by hpp ligands. Because of the high basicity of bicyclic amines such as Hhpp, they have been used extensively as catalysts in many organic reactions such as nitroaldol (Henry) reactions,[15] addition of dialkyl phosphates to a variety of carbonyl compounds and imines,[15] and transesterification reactions.[16] More recently, there has been great interest in the study of proton affinities of polyguanidines.[17] For those, their very large intrinsic basicity has been traced to a dramatic increase in the resonance stabilization of the conjugate bases. Also, an extensive review on the coordination chemistry of the simpler guanidines and guanidinates has appeared.[18]

The aim of this dissertation is to advance the utility of guanidinates as a new class of ligand for dimetal units, separate and distinct from halides, carboxylates and formamidinates. The distinction is made in Chapter II by examining the effect of hpp on the dimolybdenum unit. This chapter not only establishes guanidinates as a separate ligand class, but also serves as a point of reference for the work achieved in subsequent chapters.

Chapters III, IV and V describe the development of ligands that expand the guanidinate class and their dimolybdenum complexes. Chapter III discusses the preparation of ligands which incorporate 5-membered rings, the anion of 1,3,6-triazabicyclo[3.3.0]oct-4-ene, tbo (**VI**), and the anion of 1,3,6-triazabicyclo[3.4.0]non-4-ene, tbn (**VII**). The geometry of the 5-membered ring results in nitrogen orbitals that

have a divergent bite angle. The effect this divergence has on the physical and chemical properties of the dimolybdenum complexes (particularly the Mo–Mo distances) is examined.

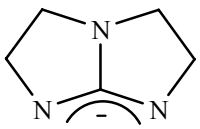

VI

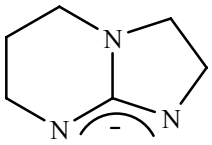

VII

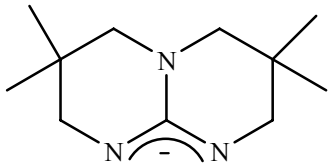

VIII

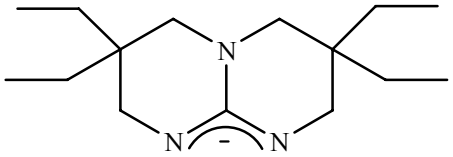

IX

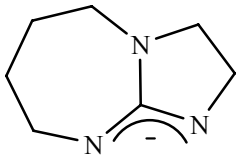

X

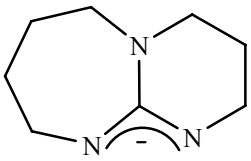

XI

Derivatives of hpp which incorporate alkyl substituents are the topic of Chapter IV. Two ligands incorporating methyl groups, TMhpp (**VIII**), and ethyl groups, TEhpp (**IX**) are developed. These derivatives show a substantial increase in solubility compared to hpp as well as other important changes in physical and chemical properties.

The use of 7-membered rings is discussed in Chapter V. The anion of 1,4,6-triazabicyclo[3.5.0]dec-4-ene, tbd (**X**), results in nitrogen orbitals which are essentially parallel as in hpp. In the case of the anion of 1,5,7-triazabicyclo[4.5.0]undec-5-ene, tbu (**XI**), the nitrogen orbitals are convergent. The effects produced by the inclusion of 7-

membered rings on the physical and chemical properties of the dimolybdenum complexes are explored.

The results from each chapter that encompass the overarching theme in this dissertation are brought together in Chapter VI. Some concluding thoughts are provided as well as suggestions for further work in the area to more fully develop guanidinates as a unique class of ligands.

CHAPTER II

THE EXTRAORDINARY ABILITY OF GUANIDINATE DERIVATIVES TO STABILIZE HIGHER OXIDATION NUMBERS IN DIMETAL UNITS BY MODIFICATION OF REDOX POTENTIALS: STRUCTURES OF Mo_2^{5+} AND Mo_2^{6+} COMPOUNDS*

Introduction

In a preliminary communication, the first triply-bonded tetragonal lantern compounds having the Mo_2^{6+} units surrounded by nitrogen donor ligands were reported.[19] Likewise, the first and only known singly-bonded Pd_2^{6+} and doubly-bonded Ir_2^{6+} tetragonal lantern compounds were prepared recently with the aid of the hpp ligand, **IV**.[20,21] Unfortunately, $M_2(hpp)_4^{n+}$ species tend to have low solubility. Thus reactions have been difficult to accomplish in a fully controlled manner. For example, when the oxidation of $Mo_2(hpp)_4$ with $AgBF_4$ was attempted for the first time, the doubly oxidized $[Mo_2(hpp)_4](BF_4)_2$ compound was the only product isolated and the intermediate

---

*Portions of this chapter are reprinted from parts of *J. Am. Chem. Soc*., *124*, Cotton, F. A.; Daniels, L. M.; Murillo, C. A.; Timmons, D. J.; Wilkinson, C. C., "The Extraordinary Ability of Guanidinate Derivatives to Stabilize Higher Oxidation Numbers in Dimetal Units by Modification of Redox Potentials: Structures of Mo_2^{5+} and Mo_2^{6+} Compounds", 9249, Copyright 2002, with permission from the American Chemical Society.

*Portions of this chapter are reprinted from parts of *Inor. Chim. Acta*, *351*, Cotton, F. A.; Murillo, C. A.; Wang, X.; Wilkinson C. C., "Resolving Conformational Ambiguities in $M_2(hpp)_4Cl_2$ Paddlewheel Compounds: M = Mo, W, Re, Ru, Os, Ir, Pd, Pt", 191, Copyright 2003, with permission from Elsevier Science. DOI: 10.1016/S0020-1693(03)00113-0.

$[Mo_2(hpp)_4]^+$ species was not observed.[19] However, a few crystals of $Mo_2(hpp)_4Cl$ were isolated at a later stage.[22]

We have now overcome the synthetic problems encountered earlier after realizing that, contrary to what was known for other quadruply bonded Mo_2^{4+} species, the Mo_2^{4+} unit is very easy to oxidize when it is embraced by hpp ligands. In fact, mere dissolution of $Mo_2(hpp)_4$ in CH_2Cl_2 causes formation of Mo_2^{5+} in essentially quantitative yield. In this solvent, addition of stronger oxidation agents such as $AgBF_4$ will proceed with further oxidation to Mo_2^{6+} and beyond. Based on recognition of these facts, the series of $Mo_2(hpp)_4^{n+}$ species, for n = 0, 1 and 2 has been completed. This is the first truly homologous series having Mo_2^{n+} units with bond orders of 4, 3.5 and 3 with an electronic configuration of the type $\sigma^2\pi^4\delta^x$, x = 2, 1, 0. Here we also report voltammetric studies on these molybdenum complexes and show the existence of an enormous difference in the oxidation potential of the Mo_2^{4+} unit of *ca* 1.5 V for compounds with N-donor ligands of the formamidinate type and those with hpp. There exists a tremendous capability for tuning the oxidation potential of the Mo_2^{4+} unit by modifying the ligands, a situation that could be relevant in the creation of electrochemical sensors, an area of much current interest,[23] and other applications. Furthermore, it is important to recognize that the backbone of the hpp ligand is the guanidinate group, N_3C, derived from guanidine, **XII**. Guanidine has been recognized as an important biological molecule with many of its derivatives having important biological functions.[24]

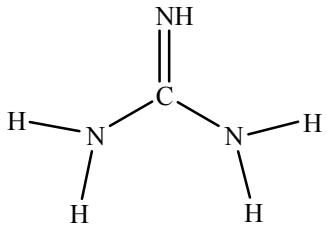

XII

Experimental Section

General Procedures. All synthetic techniques were performed under a nitrogen atmosphere, and all glassware was oven-dried prior to use. Hexanes, toluene, THF, CH_2Cl_2, Bu_4NBF_4 and Hhpp were purchased from Aldrich. Butyllithium (1.6 M) in hexanes was purchased from Acros and used as received. The solvents THF, toluene, ether, and hexanes were dried over Na/K alloy and CH_2Cl_2 over P_2O_5. All solvents were freshly distilled under nitrogen prior to use. Hhpp was sublimed and Bu_4NBF_4 was oven-dried prior to use. $TlBF_4$ was prepared by titrating Tl_2CO_3 with $HBF_4{\cdot}2Et_2O$, both purchased from Strem and used as received. $Mo_2(hpp)_4$, **1**, was made using a modification of a previous synthesis where the solvent of reaction/crystallization was switched to THF.[12a]

Physical Measurements. Elemental analyses were performed by Canadian Microanalytical Service, Ltd., Delta, British Columbia, Canada. UV-Vis spectra were recorded on a Cary 17D spectrophotometer for **4** and a Shimadzu UV-1601 PC spectrophotometer for **2** and **3**. ^{1}H NMR spectra were recorded on a Unity Plus 300 NMR spectrometer, using CH_2Cl_2 and pyridine to reference chemical shifts (δ). Cyclic

voltammetry was recorded using a BAS 100 electrochemical analyzer with a 2 mm diameter Pt disk working electrode, Ag/AgCl reference electrode, and Pt wire auxillary electrode with Bu_4NBF_4·3toluene as solvent.[25,26] The scan rate for the voltammograms was 200 mV/s. Potentials are reported *vs* Ag/AgCl.

Preparation of $Mo_2(hpp)_4Cl$, 2. $Mo_2(hpp)_4$ (0.20 g, 0.27 mmol) was dissolved in 20 mL of CH_2Cl_2. The deep red solution turned brown within 5 min, and was stirred for 1 h. The brown solution was transferred to a 50 mL Schlenk tube via cannula and layered with hexanes. Brown crystals (0.18 g) were collected after two weeks giving a yield of 71%. X-ray studies confirmed the product as **2**·$2CH_2Cl_2$. Anal. Calcd for $C_{30}H_{52}Cl_5Mo_2N_{12}$: C, 37.93; H, 5.52; N, 17.69%. Found: C, 38.31; H, 5.77; N, 18.07%. Magnetism: 1.64 BM. EPR (CH_2Cl_2, 13 K) singlet, g = 1.94. Visible absorption spectrum (CH_2Cl_2): λ_{MAX}, nm; (ε_M, L/mol·cm) 770 (200), 500 (shoulder). IR (KBr, cm^{-1}): 2929(m), 2841(m), 2820(m), 1636(w), 1522(s), 1492(s), 1473(m), 1442(s), 1380(m), 1308(s), 1280(s), 1205(s), 1137(m), 1068(w), 1028(w), 739(m), 720(m), 414(w).

$Mo_2(hpp)_4(BF_4)$, 3. $Mo_2(hpp)_4$ (0.20 g, 0.27 mmol) was dissolved in 20 mL of CH_2Cl_2. Once the red solution had turned brown, it was transferred via cannula to a flask with $TlBF_4$ (0.10 mg, 0.34 mmol) and stirred for 2 h. The brown solution was filtered into a 50 mL Schlenk tube and layered with hexanes. Brown crystals of **3**·$2CH_2Cl_2$ (0.15 g) were collected after 3 weeks giving a 61% yield. Anal. Calcd for $C_{28}H_{48}BF_4Mo_2N_{12}$: C, 40.45; H, 5.82; N, 20.22. Found: C, 40.26; H, 6.12; N, 19.94. Visible absorption spectrum (CH_2Cl_2): λ_{MAX}, nm; (ε_M, L/mol·cm) 760 (200), 520

(shoulder). IR (KBr, cm^{-1}): 2934(m), 2847(m), 2821(m), 1629(w), 1522(s), 1490(s), 1467(s), 1445(s), 1382(s), 1308(s), 1281(m), 1207(s), 1139(m), 1054(s), 1026(s), 743(m), 720(w), 417(w).

$Mo_2(hpp)_4Cl_2$, 4. In a Schlenk flask charged with $Mo_2(hpp)_4$ (0.300 g, 0.403 mmol) CH_2Cl_2 (20 ml) was added. After stirring for 10 min under nitrogen, the contents of the flask were exposed to air for 1.5 min. Then the flask was purged of air and filled with nitrogen. The brown solution was transferred to a Schlenk tube and layered with ether. After 1 week brown block crystals of **4** were collected. Yield: 0.202 g (61%). By layering the CH_2Cl_2 solution obtained from a similar preparation with hexanes, brown block crystals of **4**·$4CH_2Cl_2$ were obtained. Yield: 0.257 g (55%). ^{1}H NMR (C_6D_5N, ppm): 3.08 (t, $(CH_2)_2$), 2.82 (t, $(CH_2)_2$), 1.50 (quin, $(CH_2)_2$). UV/Vis (CH_2Cl_2): λ_{max}, nm; (ε_M, L mol^{-1} cm^{-1}) 763 (360), 651 (270), 513 (shoulder). IR (KBr, cm^{-1}): 2932 (m), 2840 (m), 2815 (m), 1637 (w), 1522 (s), 1492 (s), 1474 (m), 1443 (s), 1388 (m), 1367 (w), 1323 (m), 1308 (s), 1280 (s), 1192 (m), 1137 (m), 1112 (w), 1066 (w), 1025 (w), 738 (w), 718 (w), 415 (w).

$Mo_2(hpp)_4Cl(BF_4)$, 5. $Mo_2(hpp)_4$ (0.20 g, 0.27 mmol) was dissolved in 20 mL of CH_2Cl_2. Once the red solution had turned brown it was transferred via cannula to a flask containing $AgBF_4$ (0.60 g, 0.31 mmol). The mixture was stirred for 2 h, then filtered into a 50 mL Schlenk tube and the solution layered with hexanes. Brown crystals (0.13 g) were obtained after two weeks giving a 56% yield. Anal. Calcd for $C_{28}H_{48}BClF_4Mo_2N_{12}$: C, 38.79; H, 5.58; N, 19.39 . Found: C, 38.98; H, 5.42; N, 19.61. ^{1}H NMR (CD_2Cl_2, ppm): 3.30 (t, $(CH_2)_2$), 2.01 (quin, CH_2). Visible absorption spectrum

(CH_2Cl_2): λ_{MAX}, nm; (ε_M, L/mol·cm) 610 (270), 427 (15,000). IR (KBr, cm^{-1}): 2934(m), 2860(m), 1636(m), 1538(s), 1492(s), 1448(s), 1383(s), 1311(s), 1217(s), 1137(s), 1067(s), 1029(s), 880(w), 802(w), 751(s), 728(m), 518(w), 413(w).

X-ray Crystallography. Single crystals of **2**·$2CH_2Cl_2$,**4**, **4**·$4CH_2Cl_2$ and **5** were attached to quartz fibers with a minimum of silicone grease. Data were collected at 213 K on a Bruker SMART area detector using the SMART and SAINT programs[27,28] for **2**·$2CH_2Cl_2$, **4**, **4**·$4CH_2Cl_2$ and **5**. The crystal structures were solved via direct methods and refined using SHELXL-97.[29] Hydrogen atoms were placed at calculated positions. Non-hydrogen atoms were refined with anisotropic displacement parameters. Cell parameters and refinement results for compounds **2**·$2CH_2Cl_2$, **4**, **4**·$4CH_2Cl_2$ and **5** are summarized in Table 1. The Laue symmetry was determined to be *4/m* for **4** based on the combined figure-of-merit (CFOM) obtained from reflection intensity statistics. Each of the possible space groups, *I4*, *I4* and *I4/m* was tested for initial structure solution and refinement. The best results were obtained when the structures were refined in the centrosymmetric space group *I4/m*. Refinement in space group *I4/m* gave better agreement between chemically equivalent bonds and clarified the nature of the disordered hpp ligands.

Table 1. Crystallographic Parameters for Compounds **2**·CH_2Cl_2,**4**, **4**·4CH_2Cl_2, and **5**.				
Compound	**2**·2CH_2Cl_2	**4**	**4**·4CH_2Cl_2	**5**
Formula	$C_{30}H_{52}Cl_5Mo_2N_{12}$	$C_{28}H_{48}Cl_2Mo_2N_{12}$	$C_{32}H_{56}Cl_{10}Mo_2N_{12}$	$C_{28}H_{48}BClF_4Mo_2N_{12}$
Fw	949.97	815.56	1155.27	866.92
Space Group	*P4/nnc*	*I4/m*	$P2_1/c$	*P4/ncc*
a (Å)	13.6912(8)	10.0244(4)	11.423(8)	14.4878(8)
b (Å)	13.6912(8)	10.0244(4)	19.262(1)	14.4878(8)
c (Å)	20.475(1)	15.925(1)	11.3100(8)	16.3787(9)
β	90	90	104.426(1)	90
V (Å^3)	3838.1(4)	1600.3(2)	2350.9(3)	3437.8(5)
Z	4	2	2	4
d_{calc} (g/cm^{-3})	1.644	1.693	1.632	1.675
μ (mm^{-1})	1.042	0.993	1.142	0.870
radiation	Mo-K_α (λ_α = 0.71073 Å)			
T (K)	213(2) K			
R1,[a] wR2[b]	0.027, 0.062	0.027, 0.077	0.033, 0.081	0.070, 0.135

[a] $R1 = \Sigma \| F_o | - | F_c \| / \Sigma | F_o |$

[b] $wR2 = [\Sigma[w(F_o^2 - F_c^2)^2]/\Sigma w(F_o^2)^2]^{1/2}$, $w = 1/[\sigma^2(F_o^2) + (aP)^2 + bP]$, where $P = [\max(0 \text{ or } F_o^2) + 2(F_c^2)]/3$

Results and Discussion

Syntheses. The quadruply-bonded starting material, $Mo_2(hpp)_4$, was prepared as before by reaction of $Mo_2(O_2CCF_3)_4$ and Lihpp.[12a] However, we made a simple but important modification by replacing toluene with THF as the solvent for the reaction. This switch from toluene to THF increased the yield of red crystalline material from 22% to 73%.

We had found earlier that this quadruply-bonded compound could be oxidized, in low yield, to the triply-bonded $Mo_2(hpp)_4(BF_4)_2$ species by reaction with $AgBF_4$ in CH_2Cl_2. Interestingly, the oxidation always resulted in the isolation of the Mo_2^{6+} species, even when the ratio of Mo_2^{4+} to Ag^+ was 1:1. An attempt to oxidize a solution of **1** with $C_6H_5I{\cdot}Cl_2$ in CH_3CN finally provided the first few crystals of $Mo_2(hpp)_4Cl$, **2**, which allowed us to determine its structure.[22] While working to improve the yield, the reaction conditions were monitored in various ways. Whenever the ^1H NMR spectrum of $Mo_2(hpp)_4$ was checked, we noticed a change occurring as a function of time when the solvent was CD_2Cl_2 but not in other solvents such as CD_3CN. The longer the time after preparation of the samples, the broader the weak NMR signals became. There was also a noticeable darkening of the dilute solution. It soon became apparent that the broadening of the signals was due to the presence of the paramagnetic Mo_2^{5+} species, with CD_2Cl_2 unexpectedly acting as an oxidizing agent. Thus, bulk samples of the brown crystalline and paramagnetic material $Mo_2(hpp)_4Cl$ were prepared simply by dissolving $Mo_2(hpp)_4$ in CH_2Cl_2 and then stirring the solution at room temperature for an hour. After layering the solution with hexanes, crystals of **2**$\cdot 2CH_2Cl_2$ were isolated in

about 71% yield. It is worth mentioning that although dichloromethane is seldom thought of as an oxidizing agent, it has been used in our laboratory for the oxidation of W_2^{4+} quadruple bonds[30] and the reduction of alkyl halides has been a topic of much interest,[31] and has been studied extensively (*vide infra*).

The chloride ion in **2** can be substituted by reaction with $TlBF_4$ whereby brown, paramagnetic $Mo_2(hpp)_4(BF_4)$, **3**, can be isolated.[32,33] Compounds **2** and **3** are slightly air-sensitive; crystals will decompose within one hour when exposed to air. Like the parent $Mo_2(hpp)_4$ complex, **2** and **3** exhibit very limited solubility in most common laboratory solvents. They are however slightly more soluble in CH_2Cl_2 giving brown solutions.

Further oxidation to the corresponding Mo_2^{6+} species was accomplished quite easily by allowing $Mo_2(hpp)_4$ to react with CH_2Cl_2 to give the corresponding Mo_2^{5+} complex and then adding one equivalent of $AgBF_4$. After work-up of the reaction, the very dark brown and diamagnetic compound **5** was isolated in reasonably good yield (56%). Compound **5** also shows relatively low solubility in most common organic solvents. Further oxidation of $Mo_2(hpp)_4Cl$ to **4** can be performed also by introduction of oxygen into the reaction mixture. $Mo_2(hpp)_4Cl_2$, **4** is prepared by exposing a dichloromethane solution of $Mo_2(hpp)_4$ to air for about 1.5 min. The reaction is very facile, but care must be taken not to expose solutions to air for an extended time. The oxidation product is hygroscopic and tends to decompose upon lengthy exposure to air. Despite this difficulty, reasonable yields of the product are obtained if the reaction conditions are carefully controlled. Crystals of the product are obtained by slow diffusion of a layering

solvent into a CH_2Cl_2 solution. It is interesting to note that the crystallization process is solvent-dependent. When diethyl ether is used, **4** crystallizes without interstitial solvent molecules. If the layering solvent is changed to hexanes, crystals with solvent molecules, **4**·4CH_2Cl_2, are formed. Thus the sequence of events leading from Mo_2^{4+} to Mo_2^{6+} via Mo_2^{5+} can be summarized as:

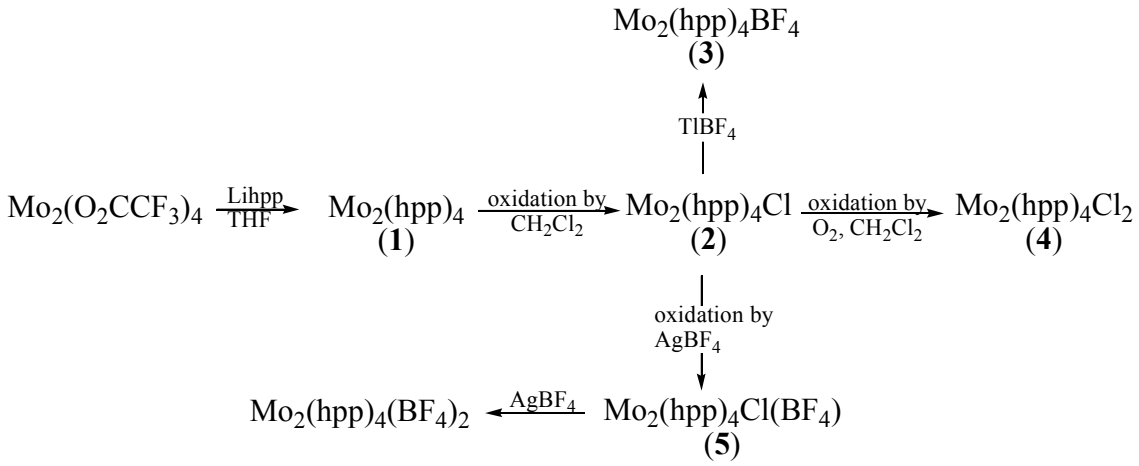

Structural Studies. All three complexes **2**·2CH_2Cl_2, **4**, **4**·4CH_2Cl_2 and **5** crystallized in a tetragonal space group and their structures are shown in Figures 2, 3, 4 and 5 respectively. For each of them, selected interatomic distances are given in the corresponding figure caption. There is a common structural motif whereby four guanidinate groups wrap the dimetal unit giving a paddlewheel or tetragonal lantern structure with the Mo_2^{n+} unit located along the 4-fold axes, where the axial chloride ions

are also found. These are at distances that are too long to be considered as making significant bonding contributions. The molecules of **2**·2CH_2Cl_2 and **5** are well ordered with the hpp ligands being such that in one ring the central CH_2 group deviates in one direction and in the other ring the corresponding CH_2 group deviates in the opposite direction (i.e. a chair conformation).

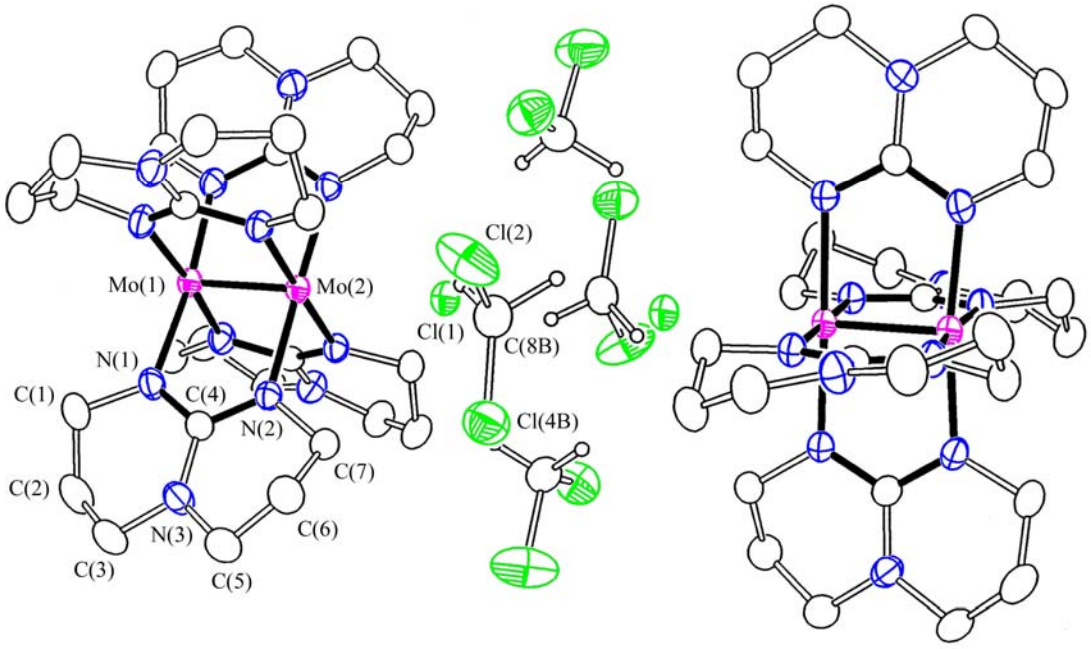

Figure 2. The crystal environment in **2**·2CH_2Cl_2. Labels are on the crystallographically independent hpp ligand, and the probability ellipsoids are shown at the 50% level. Each CH_2Cl_2 has a 50% occupancy. Selected interatomic distances (Å) are: Mo(1)–Mo(2) = 2.1281(4), Mo(1)–N(1) = 2.102(2), Mo(2)–N(2) = 2.160(1), Mo(2)–Cl(1) = 2.838(1).

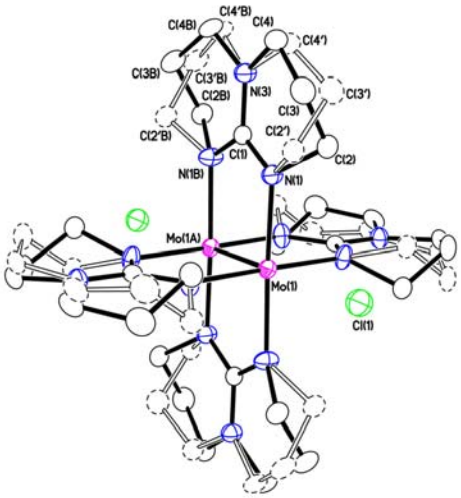

Figure 3. Perspective view of the molecule of **4** showing the disorder of the CH_2 groups on the hpp ligands, with ellipsoids at the 30% probability level. Atoms C(2), C(3), and C(4) are disordered over two positions. Selected interatomic distances (Å) are Mo(1)–Mo(1A) = 2.1727(7), Mo(1)–N(1) = 2.104(2), Mo(1)–Cl(1) = 3.115(2).

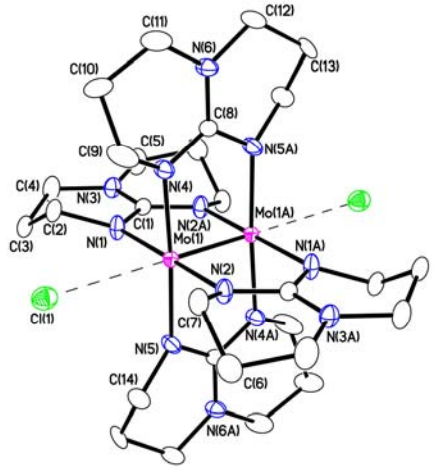

Figure 4. Perspective view of the disordered molecules of **4**•4CH_2Cl_2, with ellipsoids at the 30% probability level. Atoms except C(1) and N(3) in the hpp ligand are disordered over two positions. Selected interatomic distances (Å) are Mo(1)–Mo(1A) = 2.1735(5), Mo(1)–N(1) = 2.094(3), Mo(1)–N(2) = 2.099(3), Mo(1)–N(4) = 2.102(3), Mo(1)–N(5) = 2.099(3), Mo(1)–Cl(1) = 3.175(1).

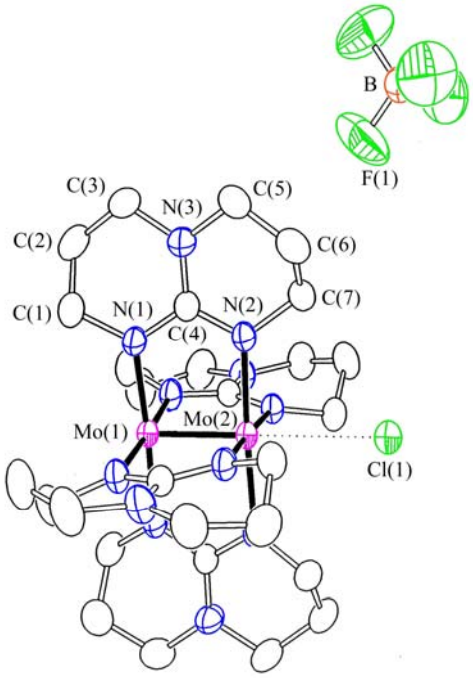

Figure 5. Thermal ellipsoid plot of the triply-bonded $Mo_2(hpp)_4Cl(BF_4)$ compound, **5**, showing displacement ellipsoids at the 50% probability level. Selected interatomic distances (Å) are: Mo(1)–Mo(2) = 2.1722(9), Mo(1)–N(1) = 2.092(4), Mo(2)–N(2) = 2.108(4), Mo(2)–Cl(1) = 2.983(2), Mo(1)–Cl(1) = 3.034(2).

Compound **4** crystallized in tetragonal space group *I4/m* with $Z = 2$. This requires that the molecules have *4/m* symmetry – unless there is crystallographic disorder. In this case disorder exists, but is minor. The disorder arises because the six-membered rings are puckered and each one puckers half the time one way and half the time the other. The central core of the molecule, the Mo_2 unit and the planar guanidinate part (NC(N)N) of each ligand conform to the *4/m* site symmetry. The rotational conformation is eclipsed.

The $P2_1/c$ space group is unambiguously assigned to **4**·4CH_2Cl_2 based on the observed systematic absence conditions of $l = 2n$ for *h0l* reflections. A drawing of the molecule of **4** in **4**·4CH_2Cl_2 is shown in Figure 5 and selected interatomic distances are included in the caption. The Mo–Mo distance of 2.1735(5) Å and Mo to Cl separation of 3.175(1) Å are essentially the same as those observed in **4**. The molecule sits on an inversion center with two independent hpp ligands in the asymmetric unit. Although the CH_2 groups on each hpp are disordered, the coordinating nitrogen atoms are not. This is consistent with very small (but not precisely zero) torsion angles (1.0(1)° and 2.5(1)°) for the Mo_2N_8 core in **4**·4CH_2Cl_2.

For all four complexes the distances within the hpp ligands are very similar. Outside the guanidine core, CN_3, the C–N and C–C distances are *ca* 1.45 Å and *ca* 1.50 Å, respectively. For the core, the two chemically equivalent C–N distances in each of the hpp ligands are significantly shorter and fall in the range 1.33 - 1.35 Å while those C–N distances between the atoms shared by the two rings of the hpp ligands are just slightly longer and in the range between 1.35 - 1.39 Å. This is consistent with the four atoms of the guanidinate core being regarded as sp^2 hybridized with some of their electrons occupying $p\pi$ molecular orbitals leading to near planarity of the CN_3 unit.

Structural Trends among the Dimetal Cores. With this report concerning the first two $Mo_2(hpp)_4^+$ species, we can now for the first time track accurately how the Mo–Mo distances vary as the charge of the Mo_2^{n+} unit changes from 4 to 5 and 6 on a series of homologous compounds. The data are presented in Table 2 which also includes the results of a parallel study on $W_2(hpp)_4^{n+}$ analogs.[34] When the average Mo–N

distances are compared, the general trend is for a small but significant decrease as the oxidation state increases. This is consistent with the generally observed shrinking of the atomic radii as the charge increases. The overall change in going from Mo_2^{4+} to Mo_2^{6+} is 0.08-0.10 Å with the difference roughly split for the Mo_2^{5+} species. Slightly smaller differences have been observed for the only other Mo_2^{4+}/Mo_2^{5+} couples surrounded by nitrogen ligands, also shown in Table 2.

What is more remarkable is the magnitude of the difference for comparable oxidation numbers in changing the ligand from the formamidinate DTolF[35] to the guanidinate-type μ_2-η^2-$(NPh)_2CNHPh$[36] and hpp. It appears that the shorter Mo–N distances for the latter are a reflection of stronger binding that is likely to be due to the higher basicity of the hpp ligand, a derivative of the extremely basic prototype guanidine, $(H_2N)_2C{=}NH$.

The Mo–Mo distances in Table 2 also show a marked variation as the oxidation state increases. However, the variation is the opposite of that for the Mo–N distances. Clearly, there is an even, stepwise increase of the metal–metal distance in going from Mo_2^{4+} to Mo_2^{5+} and Mo_2^{6+}. This is consistent with the decrease in bond order combined with the increase in charge. In the parent compound **1** the electronic configuration of the Mo_2^{4+} is that of a typical quadruply-bonded unit where the eight bonding electrons give a $\sigma^2\pi^4\delta^2$ configuration. The removal of an electron reduces the bond order to 3.5 and the Mo–Mo separation increases by 0.06 Å. Further removal of another electron from the δ orbital brings the bond order to 3 and the Mo–Mo distance increases by 0.01-0.04 Å compared to $Mo_2(hpp)_4(BF_4)_2$, **4**, **4**·$4CH_2Cl_2$ and **5**.

Table 2. Variations of the M–M and M–N and Selected M···Cl Distances (Å) for Paddlewheel Families (M = Mo, W) and Differences in the Metal–Metal Distance Between the Corresponding Cationic and Neutral Species.

Compound	M–M	Δ(M–M) species		M–N (av)	M···Cl	Charge of M_2^{n+} unit	Ref
		M_2^{5+}–M_2^{4+}	M_2^{6+}–M_2^{5+}				
$Mo_2(DTolF)_4$[a]	2.085(4)			2.17		4	36, 46
$[Mo_2(DTolF)_4]PF_6$[a]	2.122(3)	0.037		2.15		5	36
$Mo_2\{\mu\text{-}\eta^2\text{-}(NPh)_2CNHPh\}_4$	2.0839(9)			2.17		4	37
$[Mo_2\{\mu\text{-}\eta^2\text{-}(NPh)_2CNHPh\}_4]BF_4$	2.119(1)	0.035		2.14		5	37
$Mo_2(hpp)_4$	2.067(1)			2.16		4	12a
$Mo_2(hpp)_4Cl$	2.128(2)	0.061		2.13	3.091(6)	5	this work
$Mo_2(hpp)_4Cl\cdot 2CH_2Cl_2$	2.1280(4)	0.061		2.13	2.838(1)	5	this work
$Mo_2(hpp)_4Cl_2$	2.1773(7)		0.049	2.10	3.115(2)	6	this work
$Mo_2(hpp)_4Cl_2\cdot 4CH_2Cl_2$	2.1735(5)		0.046	2.09	3.175(1)	6	this work
$Mo_2(hpp)_4Cl(BF_4)$	2.1722(9)		0.044	2.10	2.983(2)	6	this work
$Mo_2(hpp)_4(BF_4)_2$	2.142(2)		0.014	2.08		6	19
$W_2(hpp)_4\cdot 2NaHBEt_3$	2.1607(4)			2.15		4	35
$W_2(hpp)_4Cl_{0.5}Cl_{0.5}$[b]	2.209(1)	0.048		2.12	2.8425(9)	5	35
$W_2(hpp)_4Cl$	2.2131(8)	0.052		2.12	2.938(4)	5	35
$W_2(hpp)_4Cl_2$	2.250(2)		0.041 (0.037)[c]	2.08	3.064(9)	6	12b

[a]DTolF = *N*,*N*′-di-*p*-tolyformamidinate anion
[b]The net stoichiometry is $W_2(hpp)_4Cl$. Each axial position is half occupied by a chlorine atom.
[c]The number outside the parentheses is relative to $W_2(hpp)_4Cl$; that within the parentheses is relative to $W_2(hpp)_4Cl_{0.5}Cl_{0.5}$.

The relatively small magnitudes of the changes are likely due to the fact that the electrons are being removed from δ orbitals which do not make a major contribution to the total Mo–Mo bond strength. Nevertheless, the trend clearly supports the change in electronic configuration from $\sigma^2\pi^4\delta^2$ to $\sigma^2\pi^4\delta$ and $\sigma^2\pi^4$ as the value of *n* in the Mo_2^{n+} species changes from 4 to 5 and 6, respectively.

Variations in the same direction are also observed for the other two Mo_2^{4+}/Mo_2^{5+} couples shown in Table 2. For another pair, namely that of $Mo_2(SO_4)_4^{4-}$ [37] $Mo_2(SO_4)_4^{3-}$, [38] the metal–metal distances show a similar increase as they vary from 2.110(3) to 2.164(3) Å. It is important to note that entirely analogous trends are to be found[34] for the $W_2(hpp)_4$, $W_2(hpp)_4^+$ and $W_2(hpp)_4^{2+}$ series with the metal–metal distances increasing by *ca* 0.04 Å and the average W–N distances decreasing by a similar amount. Again, this is consistent with the corresponding configurations of $\sigma^2\pi^4\delta^2$, $\sigma^2\pi^4\delta$ and $\sigma^2\pi^4$.

Although there are a large number of structures of quadruply-bonded $Mo_2(carboxylate)_4$ compounds known having Mo–Mo distances of *ca* 2.07-2.10 Å,[1] the actual isolation of oxidized Mo_2^{5+} species has been challenging and it was not until very recently that structures of the first three compounds having $Mo_2(carboxylate)_4^+$ monocations were reported.[39] Once again a small lengthening of metal to metal distances of *ca* 0.06 Å with respect to that of the corresponding parent compound was observed. As expected, the increase in the charge on the Mo_2 core from the loss of one electron caused the Mo–O bonds in the cations to shrink by *ca* 0.025 Å. Unfortunately, the only previously reported $Mo_2(carboxylate)_4^{2+}$ species cannot be included in the

comparison for the following reasons. This is a tetraacetate derivative having a neopentyl (np) group at each of the axial sites.[40]

Here the Mo–Mo distance is 2.1302(6) Å and the average Mo–O distance is 2.103(1) Å. For comparison, the Mo–Mo bond length in Mo_2(2,4,6,-triisopropylphenyl-carboxylate)$_4PF_6$, Mo_2(2,4,6,-triisopropylphenylcarboxylate)$_4BF_4$ and Mo_2(pivalate)$_4PF_6$ are 2.1364(8), 2.1441(5) and 2.1512(5) Å, respectively, and the corresponding average Mo–O distances are 2.066, 2.067 and 2.077 Å. Thus the Mo–Mo bond distance in the Mo_2^{6+} species is slightly shorter than those in Mo_2^{5+} compounds and the corresponding average Mo–O distances are longer. It is important to note, however, that in the triply bonded Mo_2^{6+} species the axially coordinated neopentyl groups are presumably covalently bonded to the Mo atoms (M–C = 2.103(1) Å) while the anions in the Mo_2^{5+} carboxylates do not interact strongly with axial ligands. It does not seem reasonable to compare a compound of the $Mo_2(O_2CR)_4RN_2$ type with the $Mo_2(O_2CR)_4^+$ or $Mo_2(hpp)_4^{n+}$ (n = 1, 2) types. The bonding in the $Mo_2(O_2CR)_4RN_2$ type molecule, along with several analogous W_2^{6+} complexes was described as $\pi^4\delta^2$. However, this does not appear to be an entirely satisfactory explanation, since it seems very peculiar that removal of a σ bond from the M_2 manifold would strengthen the M_2 bond enough to break the trend of increasing M–M distances as the oxidation of Mo_2^{4+} species takes place. More work will be needed to reconcile this apparent discrepancy.

Magnetic Behavior. ^{1}H NMR data clearly show that **4** and **5**, having the Mo_2^{6+} core, are diamagnetic as is **1**, the parent Mo_2^{4+} complex. For **5** there are a sharp triplet and quintet centered at 3.30 and 2.01 ppm, respectively, that integrate in the expected

ratio of 2:1. In the case of **4**, the NMR signals reveal a strong dependence on solvent; in pyridine the two triplets and quintet appear at 3.08, 2.82, and 1.50 ppm, respectively. For all the Mo_2^{5+} compounds the ^1H NMR gives only very broad signals which are typical of paramagnetic substances. The presence of the expected unpaired electron was confirmed by variable temperature magnetic measurements and the EPR spectrum of **2** in CH_2Cl_2 glass at 13 K which shows a metal-centered free radical signal with values of $g_\perp = g_\parallel = 1.94$ similar to those found in $Mo_2(carboxylate)_4^+$ species.[39] In a tetraguanidinato complex of Cr_2^{5+}, namely $Cr_2[(PhN)_2CN(CH_2)_4]_4PF_6$, the *g* value was 1.973.[41]

Electrochemistry. The recent creation of extended structures with multiple Mo_2^{4+} units, e.g. pairs, loops, triangles, squares, cages, and more complex architectures has allowed further electrochemical study of Mo_2^{4+} units.[42] In these a range of electronic interactions between Mo_2 units occur through the linker ligands as oxidation of the entire supramolecule proceeds.[43] In this class of compounds the maximum extent of electrochemical oxidation so far observed leads to four Mo_2^{5+} units in one molecule and never to an Mo_2^{6+} species.[44] Thus, to gain insight into the apparent ability of hpp to stabilize higher oxidation numbers in dimetal units we decided to study the electrochemistry of the $Mo_2(hpp)_4$ system. Solubility problems precluded the use of the traditional conditions in obtaining a cyclic voltammogram (CV) or a differential pulse voltammogram (DPV). However, a search of less common electrochemical media revealed Bu_4NBF_4·3toluene, first described by Pickett[25] and further characterized by Fry and Touster,[26] to be suitable for this purpose. The CV and DPV of $Mo_2(hpp)_4$ shows

two waves corresponding to reversible one-electron processes at E_1 = –0.444 V and E_2 = –1.271 V vs Ag/AgCl (Figure 6). Under these conditions, the ferrocene/ferrocenium couple is found at +0.524 V and the $Mo_2(DTolF)_4/Mo_2(DTolF)_4^+$ couple is at +0.417 V. For comparison, the latter was reported at 333 mV for a measurement carried out in CH_2Cl_2 with Bu_4NBF_4 as the supporting electrolyte.[45]

For these values to be compatible with the chemistry described above, the dominant species at the resting point must be the doubly oxidized Mo_2^{6+} species. Thus the E_1 must correspond to the reduction to Mo_2^{5+} and the E_2 at –1.271 V must be associated with the second reduction to the neutral $Mo_2(hpp)_4$ complex.

The number of reports on electrochemical behavior of M_2 (Mo and W) formamidinates, carboxylates and related ligands is rather limited. Some have already been mentioned above[39, 40, 42-45] but others are also relevant.[46] Some data are summarized in Figure 7. It is important to note that potentials are relative to Ag/AgCl and that the data have been collected in a variety of conditions that might be expected to change the potentials by a few millivolts. Nevertheless, some of the trends observed are overwhelmingly clear. For example, oxidation of comparable quadruply-bonded W_2^{4+} species is significantly easier (by > 0.5 V) than those having Mo_2^{4+} units. It is also apparent that oxidation of formamidinates is not significantly different than that of carboxylates, although variation of substituents in the aryl groups provides considerable tunability of the potentials. However, the most amazing observation is the very large magnitude of the change of the potential as the ligands are modified to include the

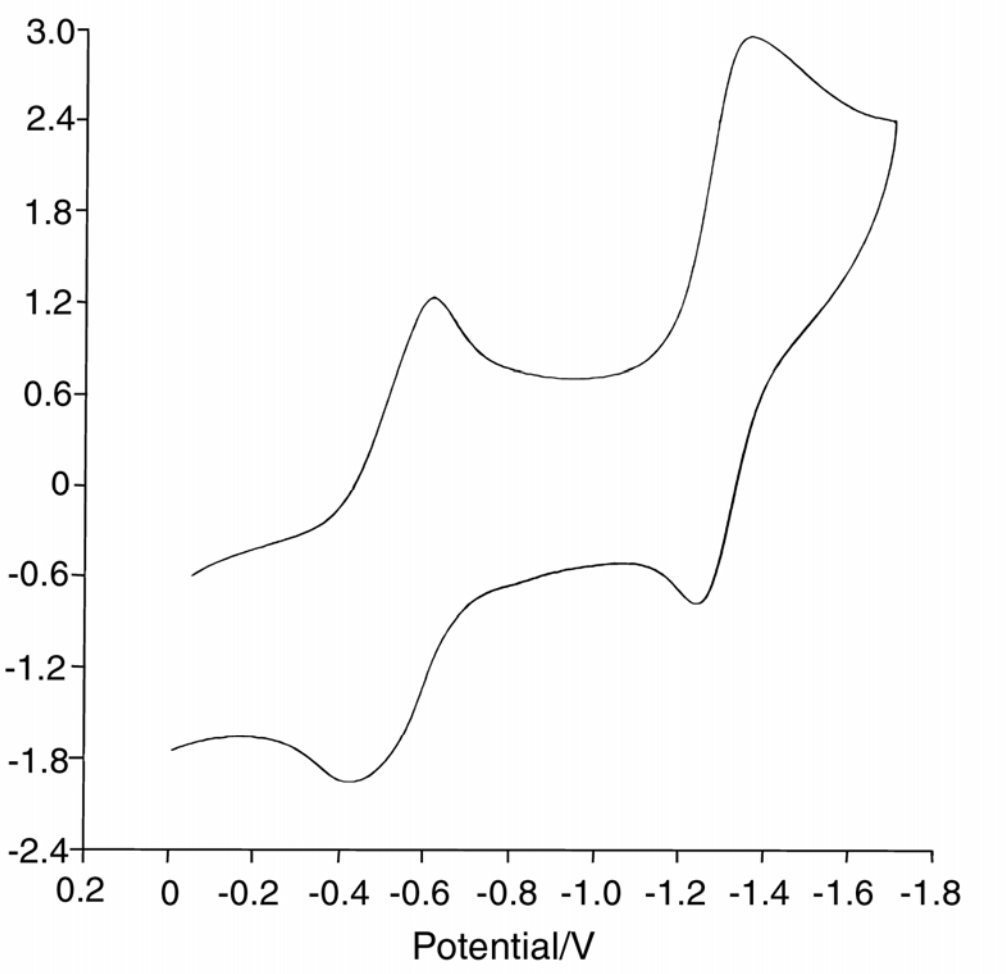

Figure 6. Cyclic voltammogram of $Mo_2(hpp)_4$, **1**, in Bu_4NBF_4·3toluene with potentials referenced vs Ag/AgCl showing two reversible one-electron events at $E^1_{1/2}$ = -0.444 V and $E^2_{1/2}$ = -1.271 V. Under these conditions, the ferrocene/ferrocenium couple appeared at +0.524 V.

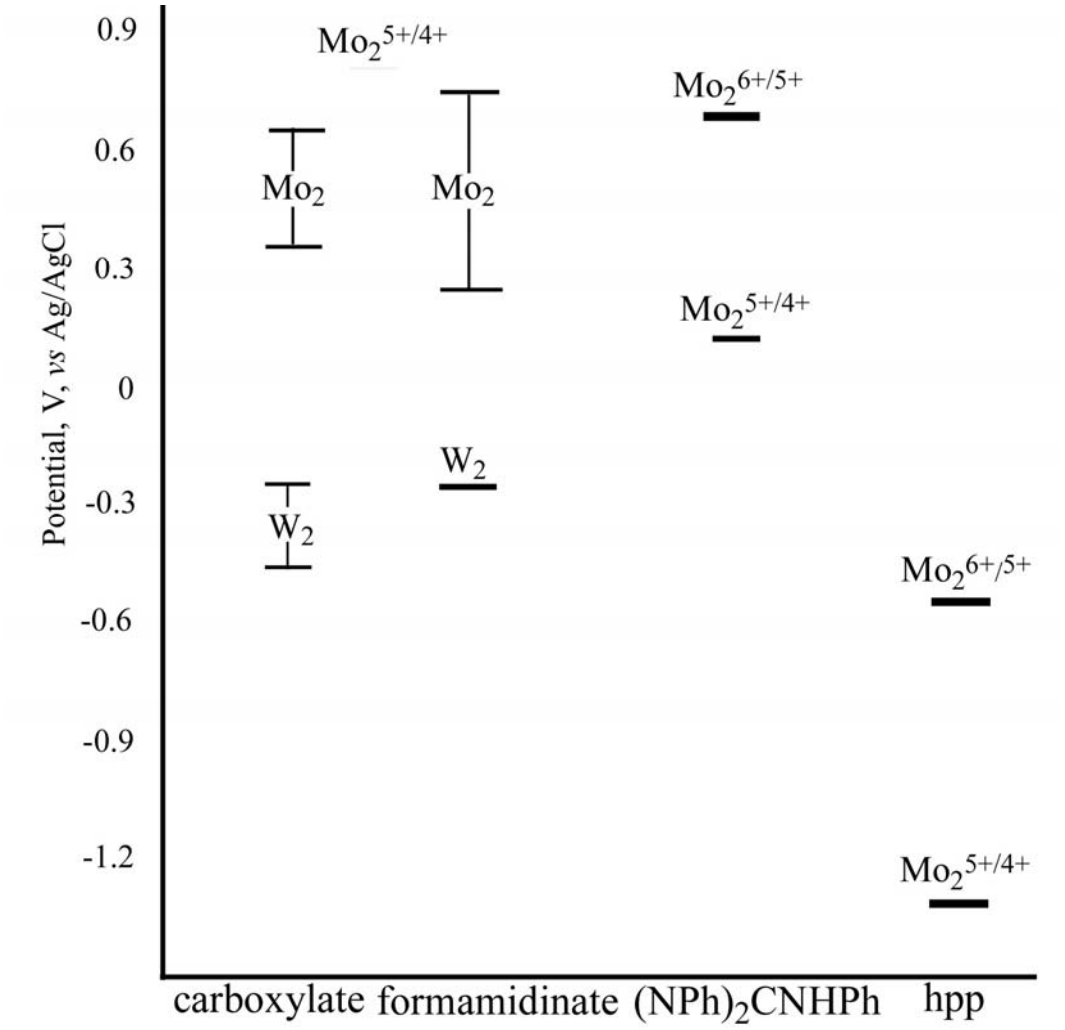

Figure 7. Variation in potentials as a function of ligand for paddlewheel complexes for the type M_2L_4, M = Mo, W. The data were compiled as follows: For carboxylates from reference 40, for formamidinates from reference 46, for $(HPh)_2CNHPh$ from reference 37, and for hpp the data are from this work.

guanidinate core, CN_3, especially for those of the hpp ligand. Here the $E_{½}$ for the process:

$$Mo_2(hpp)_4^+ + 1e \longrightarrow Mo_2(hpp)_4$$

is *ca* 1.5 V apart from that of the corresponding process for the tetraformamidinate having anisyl groups (*p*-C_6H_4OMe) and almost 2.0 V from that of *p*-$C_6H_4CF_3$. Thus, such an enormous shift in the electrode potential is what allows the observation of an electrochemical wave for the process corresponding to:

$$Mo_2^{5+} \longrightarrow Mo_2^{6+} + 1e$$

The reduction potential at –0.444 V (Figure 5) indicates that even the oxidation of $Mo_2(hpp)_4^+$ is far easier than that of any of the neutral tetraformamidinate or tetracarboxylate species, Mo_2L_4. This great ability of the guanidinate-type ligands to stabilize higher oxidation numbers places them in a unique new category among the ligands that have revolutionalized the chemistry of metal–metal compounds. These allow another quantum jump and the creation of a category of highly oxidized paddlewheel dimetal units.

The increased stability of higher oxidation number given to dimetal units by hpp is further supported by the isolation of other M_2^{6+} compounds, e.g., M = W,[12a] Re,[47] Ru,[10] Os,[12b] Ir,[21] Pd[20] and Pt.[12b] There are other signs that this generality does exist. For example, it has been reported[10] that $Ru_2(hpp)_4^{2+}$ can be reversibly oxidized to $Ru_2(hpp)_4^{3+}$, the only known case of Ru_2^{6+} to Ru_2^{7+}. In addition, we have recently prepared and characterized the first Os_2^{7+} species, $Os_2(hpp)_4(BF_4)_3$ as well as the first Re_2^{7+} species, $[Re_2(hpp)_4Cl_2]PF_6$.[48,49]

It appears that one of the reasons for this behavior is the presence of the guanidinate skeleton with the partial C–N double bond character of each of the three bonds as shown by the short distances (*vide supra*). However, important differences between hpp and $(NPh_2)_2CNHPh$ also indicate that it is likely that electronic effects from substituents must play a role (e.g., changes in basicity). The rigidity imposed by the fusion of the two rings in the hpp ligand could also be important.

To evaluate the relative importance of various factors it will be necessary to create new ligands of the guanidinate type; those having additional arms will be particularly appealing because they should also increase solubility of the dinuclear units. Efforts to develop the necessary synthetic chemistry are currently underway in our laboratory.

Comproportionation Constant, K_C. From the electrochemical data provided above, and using the $\Delta E_{½}$ values, measured by the method of Richardson and Taube,[50] it is possible to calculate the comproportionation constant for the process

$$Mo_2(hpp)_4 + Mo_2(hpp)_4^{2+} \rightleftharpoons 2Mo_2(hpp)_4^{+}$$

The equilibrium constant at 298 K, K_C, is given by the expression:[51]

$K_C = e^{\Delta E_{1/2}/25.69}$ where $\Delta E_{½}$ is the separation for successive one-electron processes in millivolts.

Thus for E_1 of –0.444V and E_2 of –1.271 V, the $\Delta E_{½}$ is 827 millivolts and K_C is 9.56×10^{13}, indicating that the equilibrium strongly favors the monooxidized species. This is not due to the lack of stability of the $Mo_2(hpp)_4^{2+}$ species but to the apparently disfavored $Mo_2(hpp)_4$ complex, a phenomenon observed now for the first time in quadruply-bonded Mo_2^{4+} species.

Because of the large value of K_C, it should be no surprise that the cation $Mo_2(hpp)_4^+$ forms even by reaction of $Mo_2(hpp)_4$ with CH_2Cl_2 at room temperature. A cyclic voltammogram of the solvent CH_2Cl_2 (1 mM in Bu_4NBF_4·3toluene) shows a chemically and electrochemically irreversible reduction wave at −1.114 V. At this potential, CH_2Cl_2 is able to oxidize $Mo_2(hpp)_4$ to the corresponding monocation.

CHAPTER III

HOMOLOGS OF Hhpp WITH SMALLER RINGS (Htbo AND Htbn) AND THEIR DIMOLYBDENUM COMPLEXES

Introduction

In this chapter the preparation of Htbo (**XIII**) and Htbn (**XIV**) is discussed. The reaction to produce these compounds proceeds via sequential ring closures as evidenced by the isolated intermediate (**XV**). Paddlewheel complexes $Mo_2(tbo)_4$ (**XVI**) and $Mo_2(tbn)_4$ (**XVII**) have been prepared by reaction of $Mo_2(O_2CCF_3)_4$ with Li(tbo) and Li(tbn), respectively. The oxidation of these paddlewheel compounds has also been accomplished through the use of various oxidizing agents. Table 3 provides a list of the compounds to be discussed.

Table 3. Listing of Compounds to be Discussed In Chapter III.

Compound	Formula	Number
1-(2-Aminoethyl)-2-imidazolidinethione (**XV**)	$C_5H_{11}N_3S$	**6**
Htbo (**XIII**)	$C_5H_9N_3$	**7**
Htbn (**XIV**)	$C_6H_{11}N_3$	**8**
$Mo_2(tbo)_4$ (**XVI**)	$Mo_2(C_5H_8N_3)_4$	**9**
$Mo_2(tbo)_4Cl$	$Mo_2(C_5H_8N_3)_4Cl$	**10**
$Mo_2(tbn)_4$ (**XVII**)	$Mo_2(C_6H_{10}N_3)_4$	**11**
$Mo_2(tbn)_4PF_6$	$Mo_2(C_6H_{10}N_3)_4PF_6$	**12**
$Mo_2(tbn)_4Cl_2$	$Mo_2(C_6H_{10}N_3)_4Cl_2$	**13**

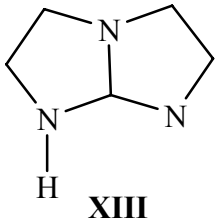

XIII

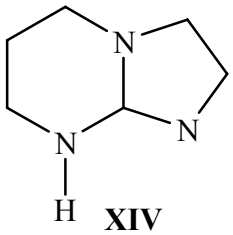

XIV

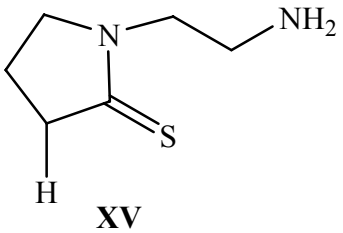

XV

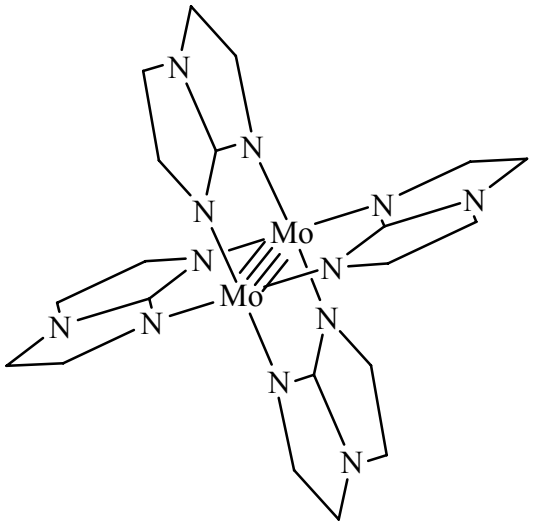

XVI

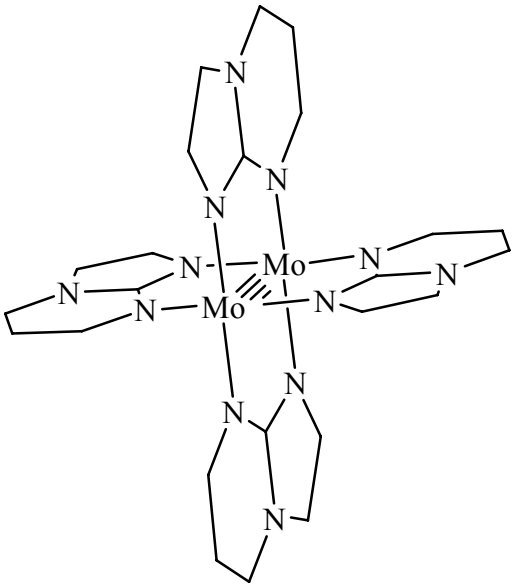

XVII

Experimental Section

General Procedures. All procedures were performed under a nitrogen atmosphere unless otherwise noted and all glassware was oven-dried prior to use. Diethylenetriamine, carbon disulfide, *p*-toluenesulfonic acid monohydrate and (2-aminoethyl)-1,3-propanediamine, were purchased from Aldrich and used as received.

Hexanes and *p*-xylene were purchased from Aldrich and dried over 3 Å molecular sieves prior to use for organic synthesis. The solvents THF, CH_2Cl_2, benzene and hexanes were also purchased from Aldrich and purified using a Contour Glass solvent system. Lead(II) acetate was purchased from Strem and used as received. Evolution of H_2S in the synthesis of **6**, **7** and **8** was monitored by passing the reaction exhaust through test strips of filter paper wetted with aqueous lead(II) acetate. BuLi (1.6 M in hexanes) was purchased from Acros and stored at -20 °C until used. $Mo_2(O_2CCF_3)_4$ and was prepared according to a published procedure.[52]

Physical Measurements. IR spectra were recorded using a Perkin Elmer 16PC FT-IR spectrometer or a Bruker Tensor 27 spectrometer. UV-Vis spectra were recorded on a Shimadzu UV-2501 PC spectrometer. ^{1}H NMR spectra were recorded on a Unity Plus 300 NMR spectrometer, using solvent peaks to reference chemical shifts (δ). Cyclic voltammetry and differential pulse voltammetry were recorded using a CH Instruments electrochemical analyzer with a 2 mm Pt disk working electrode, Ag/AgCl reference electrode, and Pt wire auxillary electrode. Potentials are reported versus Ag/AgCl. The magnetic susceptibility was measured using a Johnson Matthey Mark II magnetic susceptibility balance. Elemental analysis was performed by Robertson Microlit Laboratories, Inc., Madison, NJ, USA. Mass Spectroscopy data (electrospray ionization) were recorded at the Laboratory for Biological Mass Spectroscopy at Texas A&M University, using an MDS Qstar Pulsar with a spray voltage of 5 kV.

X-ray Crystallography. Single crystals of **6**, **7**, **8**, **9**, **9**·THF, **10**, **11**, **13**, **13**·$2CH_2Cl_2$, **13**·$3CHCl_3$ and $[H_2tbn][HCO_3]$ were placed on a cryoloop using a

minimum of silicone grease. Data for **6** were collected at 213 K on a Nonius FAST area detector. For the others, data were collected at 213 K (except for **8** which were collected at 193 K and **13** which were collected at 110 K) on a Bruker SMART area detector using the SMART and SAINT programs.[27,28] The crystal structures were solved via direct methods and refined using SHELXL-97.[29] Hydrogen atoms were placed at calculated positions. Non-hydrogen atoms were refined with anisotropic displacement parameters. Cell parameters and refinement results for organic compounds are summarized in Table 4 while those for inorganic compounds are found in Table 5.

Table 4. Crystallographic Parameters for **6**, **7**, **8**, and $[H_2tbn][HCO_3]$.

Compound	**6**	**7**	**8**	$[H_2tbn][HCO_3]$
Empirical Formula	$C_5H_{11}N_3S$	$C_5H_9N_3$	$C_6H_{11}N_3$	$C_7H_{13}N_3O_3$
Formula Weight	145.23	111.15	125.18	187.20
Space Group	$P2_1/n$	$P2_1/c$	$C2/c$	$P\bar{1}$
a (Å)	6.300(3)	7.067(3)	18.670(7)	7.240(2)
b (Å)	9.491(2)	10.294(4)	7.600(3)	8.252(3)
c (Å)	12.321(4)	7.596(3)	10.008(3)	8.350(3)
α (°)	90	90	90	110.375(5)
β (°)	94.71(3)	101.075(6)	103.192(7)	106.701(5)
γ (°)	90	90	90	96.033(5)
V (Å^3)	734.2(4)	542.3(3)	1382.6(8)	436.1(2)
Z	4	4	8	2
d_{calc} (g/cm^3)	1.314	1.361	1.203	1.426
μ (mm^{-1})	0.357	0.090	0.078	0.112
T (K)	213(2)	213(2)	193(2)	213(2)
R1[a]	0.0482	0.0497	0.0625	0.0454
wR2[b]	0.1182	0.1286	0.1623	0.1242

[a] $R1 = \Sigma \| F_o | - | F_c \| / \Sigma | F_o |$

[b] $wR2 = [\Sigma[w(F_o^2 - F_c^2)^2] / \Sigma w(F_o^2)^2]^{1/2}$, $w = 1/[\sigma^2(F_o^2) + (aP)^2 + bP]$, where $P = [\max(0 \text{ or } F_o^2) + 2(F_c^2)]/3$

Table 5. Crystallographic Parameters for **9**·THF, **9**, **10**, **11**, **13**, **13**·2CH_2Cl_2, and **13**·3$CHCl_3$.

Compound	**9**·THF	**9**	**10**	**11**	**13**	**13**·2CH_2Cl_2	**13**·3$CHCl_3$
Empirical Formula	$C_{24}H_{40}Mo_2N_{12}O$	$C_{20}H_{32}Mo_2N_{12}$	$C_{20}H_{32}ClMo_2N_{12}$	$C_{24}H_{40}Mo_2N_{12}$	$C_{24}H_{40}Cl_2Mo_2N_{12}$	$C_{26}H_{44}Cl_6Mo_2N_{12}$	$C_{27}H_{43}Cl_{11}\ Mo_2N_{12}$
Formula Weight	704.56	632.46	667.91	688.56	759.46	929.31	1117.56
Space Group	*P2₁/n*	$P\bar{1}$	*I2/a*	$P\bar{1}$	*I4/m*	$P\bar{1}$	*P1*
a (Å)	10.604(2)	7.324(1)	15.636(5)	8.088(2)	9.592(4)	8.494(2)	9.602(2)
b (Å)	24.081(5)	8.334(2)	8.318(3)	8.858(2)	9.592(4)	10.113(2)	10.036(2)
c (Å)	11.473(2)	10.641(2)	19.924(6)	11.076(3)	15.48(1)	11.014(3)	13.051(2)
A(°)	90	105.957(3)	90	74.167(4)	90	99.517(4)	102.568(3)
B(°)	109.097(3)	105.308(3)	102.311(5)	70.104(4)	90	106.371(4)	97.518(3)
γ(°)	90	98.391(3)	90	72.188(4)	90	92.737(4)	116.077(3)
V (Å^3)	2768.6(9)	585.4(2)	2531.7(1)	697.7(3)	1423.8(1)	890.8(4)	1065.1(3)
Z	4	1	4	1	2	1	1
d_{calc} (g/cm^3)	1.690	1.794	1.752	1.639	1.772	1.732	1.742
μ (mm^{-1})	0.949	1.108	1.132	0.937	1.109	1.193	1.317
T (K)	213(2)	213(2)	213(2)	213(2)	110(2)	213(2)	213(2)
R1[a]	0.0271	0.0306	0.0320	0.0377	0.0635	0.0404	0.0652
wR2[b]	0.0653	0.0687	0.0800	0.0956	0.1611	0.0929	0.1821

[a] $R1 = \Sigma \| F_o | - | F_c \| / \Sigma | F_o |$

[b] $wR2 = [\Sigma[w(F_o^2 - F_c^2)^2]/\Sigma w(F_o^2)^2]^{1/2}$, $w = 1/[\sigma^2(F_o^2) + (aP)^2 + bP]$, where $P = [\max(0 \text{ or } F_o^2) + 2(F_c^2)]/3$

Preparation of 1-(2-Aminoethyl)-2-imidazolidinethione, 6. The compound was prepared by a modification of an existing procedure.[53] Carbon disulfide (7.60 g, 100 mmol) was added to a solution of diethylenetriamine (10.3 g, 100 mmol) in 150 mL of *p*-xylene, which immediately formed a white precipitate. The mixture was heated to reflux and the solid dissolved while H_2S evolved. The solution was refluxed for 24 h and then the solvent was removed under vacuum, leaving a white solid. The solid was purified by sublimation, resulting in colorless crystals suitable for X-ray diffraction. Yield: 11.2 g (77 mmol, 77%). IR (KBr, cm^{-1}): 3413 (w), 3327 (s), 3264 (s), 3090 (s), 3018 (s), 2939 (s), 2865 (s), 2803 (s), 2767 (s), 2677 (s), 2374 (m), 1655 (m), 1597 (s), 1524 (s), 1500 (s), 1475 (s), 1457 (s), 1445 (s), 1415 (s), 1361 (s), 1316 (s), 1281 (s), 1258 (s), 1214 (s), 1161 (s), 1094 (s), 1024 (s), 994 (s), 969 (s), 947 (s), 880 (s), 836 (s), 733 (m), 641 (s), 525 (s), 483 (m). ^{1}H NMR ($CDCl_3$, ppm): 6.17 (br s, 1H (NH)), 3.80 - 3.58 (mult., 6H (CH_2)), 2.95 (t, 2H (CH_2)), 1.21 (br s, 2H (NH_2)). Mass Spectrum (ESI^+): Calculated ($M+H^+$): 146 amu; found 146 amu. The melting point (110.0 - 110.5 °C) is in agreement with reported values which are 110.0 - 110.5 °C.[54]

1,4,6-Triazabicyclo(3.3.0)oct-4-ene (Htbo), 7. This compound was prepared according to the patent literature.[53] Carbon disulfide (7.60 g, 100 mmol) was added to a solution of diethylenetriamine (10.3 g, 100 mmol) in 150 mL of *p*-xylene which immediately formed a white precipitate. The mixture was heated to boiling and the solid dissolved. The solution was refluxed until evolution of H_2S ceased (*ca* 10 days) and then the solvent was removed under vacuum, leaving a yellow-white solid. This was purified by sublimation, resulting in colorless crystals suitable for X-ray diffraction.

Yield: 6.87 g (62 mmol, 62%). IR (KBr, cm^{-1}): 3310 (m), 3158 (m), 3111 (s), 3048 (s), 2955 (s), 2835 (s), 2372 (m), 2291 (w), 1750 (s), 1596 (s), 1545 (m), 1479 (s), 1447 (s), 1421 (s), 1341 (m), 1298 (s), 1268 (s), 1241 (s), 1202 (s), 1177 (m), 1117 (m), 1092 (s), 1059 (m), 990 (s), 933 (m), 897 (w), 875 (m), 815 (m), 771 (m), 726 (s), 708 (s), 672 (m), 623 (m), 454 (w). ^{1}H NMR ($CDCl_3$, ppm): 4.51 (br s, 1H (NH)), 3.08 (t, 4H, 2(CH_2)), 3.14 (t, 4H, 2(CH_2)). Mass spectrum (ESI^+): Calculated ($M+H^+$): 112 amu; found: 112 amu. The melting point (158 - 159 EC) is in good agreement with literature values of 158.5 - 159.5 °C.[55]

1,4,6-Triazabicyclo(3.4.0)-non-4-ene (Htbn), 8. This known compound[56] was synthesized by a modification of a reported procedure.[53] Carbon disulfide (12.8 mL, 16.2 g, 213 mmol) was added slowly to a solution of N-(2-aminoethyl)-1,3-propanediamine (25 g, 210 mmol) in 150 mL of *p*-xylene resulting in the formation of a white precipitate. As the mixture was heated to reflux under nitrogen, the solid transformed into a green oil which dissolved to give a colorless solution as refluxing progressed. The reaction was continued for about 10 days, until the evolution of H_2S ceased. The solvent was then removed leaving behind a yellow-white solid. The solid was purified by sublimation, resulting in colorless crystals suitable for X-ray diffraction. Yield: 22.7 g (182 mmol, 85%). IR (KBr, cm^{-1}): 3278 (m), 3172 (m), 3127 (m), 3052 (m), 2930 (s), 2843 (s), 1650 (s), 1501 (s), 1477 (s), 1438 (s), 1372 (m), 1320 (s), 1268 (s), 1198 (m), 1175 (m), 1147 (s), 1101 (m), 1032 (m), 974 (m), 941 (m), 842 (m), 754 (m), 722 (m), 692 (m), 543 (w), 471 (m). ^{1}H NMR ($CDCl_3$, ppm): 3.43 (td, 2H (CH_2)), 3.29-3.23 (mult, 4H (CH_2)), 3.10 (t, 2H (CH_2)), 1.92 (p, 2H (CH_2)). Mass spectrum

(ESI^+): Calculated ($M+H^+$): 126 amu; found: 126 amu. Crystals of (H_2tbn)(HCO_3), suitable for X-ray diffraction, were prepared by the slow evaporation in air of a solution in 90% v/v ethanol/water.

$Mo_2(tbo)_4$, 9. A Schlenk flask was charged with Htbo (**2**) (0.689 g, 6.21 mmol) and THF (20 mL). To the resulting suspension, BuLi (3.90 mL, 6.24 mmol) was added and the mixture was stirred for 30 min. A solution of $Mo_2(O_2CCF_3)_4$, (1.00 g, 1.55 mmol) in THF (20 mL) was then added and the mixture stirred for 1 h. The solution rapidly darkened, and a light red precipitate of **9** was observed. The mixture was filtered and the solid was washed with 20 mL THF. Orange block crystals of **9**·THF were prepared by placing a saturated THF solution in a freezer at -20 ºC for one week. Red plate crystals of **9** (no interstitial solvent) were grown by layering a saturated benzene solution of **9** with hexanes. Yield: 0.778 g (1.23 mmol, 79%). IR (KBr, cm^{-1}): 3367 (w), 2956 (s), 2835 (s), 1686 (s), 1655 (m), 1625 (s), 1496 (s), 1464 (s), 1431 (s), 1339 (w), 1288 (m), 1270 (m), 1228 (m), 1198 (s), 1143 (m), 1108 (m), 1078 (s), 1023 (s), 933 (w), 914 (w), 851 (w), 804 (m), 785 (m), 729 (w), 670 (w), 521 (w), 485 (m). ^1H NMR (C_6D_6, ppm): 3.38 (t, 16H, 8(CH_2)), 2.45 (t, 16H, 8(CH_2)). UV-Vis (THF) λ_{MAX}, nm; (ε_M, L/mol·cm): 486.5 (1,800), 355.0 (4,400). Mass spectrum (ESI^+): Calculated ($M+H^+$): 633 amu; found: 633 amu.

$Mo_2(tbo)_4Cl$, 10. Dichloromethane (20 mL) was added to a Schlenk flask containing red $Mo_2(tbo)_4$ (0.100 g, 0.158 mmol) and the resulting brown suspension was stirred for 1 h. Hexanes (60 mL) were added and the mixture was filtered. The solid was washed with hexanes (20 mL) and briefly dried under vacuum. Crystals were

prepared by layering a saturated CH_2Cl_2 solution of **10** with hexanes. The diffusion was complete after 2 weeks at which time the crystals were collected. Yield: 0.085 g (0.127 mmol, 80%). IR (KBr, cm^{-1}): 3358 (m), 2963 (s), 2861 (m), 1654 (s), 1560 (m), 1543 (m), 1508 (s), 1474 (m), 1440 (m), 1342 (w), 1262 (s), 1199 (s), 1089 (s), 1021 (s), 924 (m), 864 (m), 800 (s), 720 (m), 623 (w), 516 (w), 475 (w). UV-Vis (CH_2Cl_2) λ_{MAX}, nm; (ε_M, L/mol·cm): 587 (shoulder), 497 (shoulder), 376 (shoulder), 348 (4,000). Magnetism: 1.68 μ_B, g = 1.94. Elemental Analysis: Calculated for $Mo_2(tbo)_4Cl{\cdot}0.33CH_2Cl_2$, C: 35.08, H: 4.73, N: 24.14; Found C: 35.30, H: 4.96, N: 24.58.

$Mo_2(tbn)_4$, 11. A Schlenk flask was charged with Htbn (**3**) (1.00 g, 8.00 mmol) and THF (10 mL). To the resulting solution BuLi (5.00 mL, 8.00 mmol) was added and the solution was stirred for 10 min. This pale yellow solution was then layered onto a brilliant yellow solution of $Mo_2(O_2CCF_3)_4$ (1.29 g, 2.00 mmol) in THF (10 mL) forming a dark interface. The flask was shaken once and left standing overnight. The next day a yellow-orange microcrystalline precipitate was observed. The mixture was filtered and the solid was washed with THF (10 mL). Yield: 0.991 g (1.44 mmol, 72%). Crystals, as yellow-orange plates suitable for X-ray diffraction, were grown by diffusion of hexanes into a saturated THF solution over the course of 2 weeks. The crystals were collected, washed with hexanes and dried under vacuum. IR (KBr, cm^{-1}): 3405 (w), 2921 (s), 2816 (s), 1686 (m), 1655 (m), 1624 (m), 1575 (s), 1496 (s), 1468 (s), 1438 (s), 1375 (m), 1319 (m), 1270 (s), 1246 (m), 1198 (s), 1167 (s), 1119 (m), 1098 (m), 1058 (m), 983 (w), 938 (w), 899 (w), 803 (w), 776 (w), 710 (w), 655 (w), 553 (w), 523 (w), 431 (w). ^1H NMR

(C_6D_6, ppm): 3.86 (mult., 8H), 3.65 (mult., 8H), 3.19 (mult., 8H), 2.88 (mult., 8H), 1.92 (mult., 8H). UV-Vis (THF) λ_{MAX}, nm; (ε_M, L/mol·cm): 455.5 (1,100), 351.0 (8,900), 318.0 (12,000), 277.5 (16,000), 258.0 (23,000). Mass spectrum (ESI^+): Calculated ($M+H^+$): 689 amu; found: 689 amu.

$Mo_2(tbn)_4(PF_6)$, 12. A deep blue solution of (Cp_2Fe)(PF_6) (0.050 g, 0.15 mmol) in 20 mL MeCN was added to an orange solution of 11 (0.100 g, 0.15 mmol) in THF (20 mL). The resulting orange-brown solution was stirred for 30 min and the solvent removed under vacuum. The residue was then washed with 40 mL of hexanes to remove Cp_2Fe. The remaining solid was dried under vacuum and collected. Yield: 0.101 g (85%). IR (KBr, cm^{-1}): 3158 (m), 2963 (s), 1675 (s), 1619 (s), 1559 (s), 1483 (m), 1439 (m), 1372 (m), 1323 (m), 1262 (s), 1204 (m), 1099 (s), 1022 (s), 842 (s), 556 (m), 478 (w). Magnetism: 1.70 μ_B, g = 1.95. Mass Spectrum (ESI^+): Calculated: 688 amu; found 688 amu. UV-Vis (CH_2Cl_2) λ_{MAX}, nm; (ε_M, L/mol·cm): 486 (900), 380 (sh), 324 (sh). Single crystals have not yet been isolated.

$Mo_2(tbn)_4Cl_2$, 13. A dichloromethane solution (20 mL) of **11** (0.100 g, 0.145 mmol) was briefly exposed to air (60 s). The flask was then evacuated and back-filled with N_2 three times, and the solution was layered with hexanes. Brown block–crystals of **13**·$2CH_2Cl_2$ were harvested after 2 weeks. Yield: 0.087 g (79%). Crystals of **13** (no interstitial solvent) were prepared by vapor diffusion of ether into a CH_2Cl_2 solution. Crystals of **13**·$3CHCl_3$ were prepared by vapor diffusion of hexanes into a $CHCl_3$ solution. IR (KBr, cm^{-1}): 3853 (w), 3743 (m), 3435 (w), 2932 (m), 2854 (s), 2370 (w), 1689 (s), 1621 (s), 1551 (s), 1446 (s), 1370 (s), 1322 (m), 1277 (s), 1203 (s), 1119 (s),

1049 (m), 940 (m), 800 (s), 727 (m), 430 (w). ^{1}H NMR ($CDCl_3$, ppm): 4.16 (mult., 2H), 3.93 (m, 2H), 3.78 (m, 2H), 3.57 (m, 2H), 2.03 (m, 2H). UV-Vis (CH_2Cl_2) λ_{MAX}, nm; (ε_M, L/mol·cm): 523 (shoulder), 411 (28,000), 335 (18,000). Elemental Analysis: Calculated for **13**·0.5CH_2Cl_2: C: 36.70, H: 5.15, N: 20.96; found: C: 36.33, H: 5.44, N: 20.75.

Results and Discussion

Ligand Syntheses. The preparation of the ligands Htbo and Htbn were accomplished by reacting the appropriate triamine with carbon disulfide in a 1:1 ratio using *p*-xylene as solvent, according to the patent literature.[53] This method is also used to prepare Hhpp and is the most direct synthetic route available, although all three compounds have been prepared by an alternative route.[54,55,56]

The initial reaction of polyamines with one equivalent of carbon disulfide produces a zwitterionic dithiocarbamate.[57] This reactive intermediate, which is not isolated, then forms the rings of the ligands in a stepwise fashion as evidenced by the intermediate (**6**) which can be isolated by stopping the reaction before the complete evolution of H_2S. The synthesis of Htbn also shows a similar monocyclic intermediate as evidenced by a peak at 160 amu in the mass spectrum (ESI^+, $M+H^+$). Thus, the reaction pathway to produce the bicyclic guanidines Htbo and Htbn by reaction of a triamine with carbon disulfide can be summarized as:

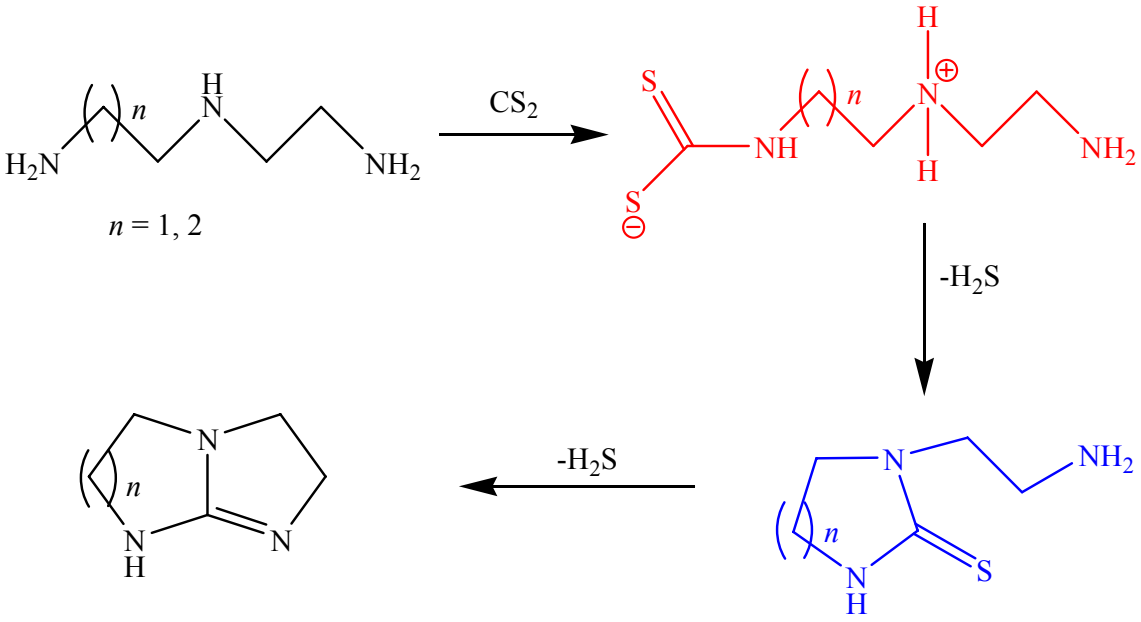

The presumed intermediate is in red and the isolable intermediate (n = 1, **6**) is in blue.

The ligands, **7** and **8**, are readily purified by sublimation and both give clean ^{1}H NMR spectra and show the appropriate parent ion peak in the mass spectrum. The melting points of the ligands are also in agreement with previously prepared samples whose purity had been confirmed by elemental analysis.[55,56]

Syntheses of Dimolybdenum Compounds. The quadruply bonded, paddlewheel species, $Mo_2(tbo)_4$ and $Mo_2(tbn)_4$, were prepared in the same manner as $Mo_2(hpp)_4$.[58] By reacting $Mo_2(O_2CCF_3)_4$ with the lithium salt of the ligand in THF the compounds $Mo_2(tbo)_4$ and $Mo_2(tbn)_4$ were isolated in good yields as red and orange powders, respectively. Crystalline samples were prepared by layering THF or benzene solutions with hexanes or placing THF solutions in a freezer at -20 °C.

Preparation of the Mo_2^{5+} complex of tbo, **10**, was accomplished by dissolving the Mo_2^{4+} precursor in CH_2Cl_2. Crystals of $Mo_2(tbo)_4Cl$ were then isolated by layering the dichloromethane solution with hexanes. $Mo_2(tbn)_4(PF_6)$, **12**, was prepared by reacting **11** with a stoichiometric amount of $(Cp_2Fe)(PF_6)$ in a mixture of MeCN and THF. Synthesis of $Mo_2(tbn)_4Cl_2$, **13**, was accomplished by exposing a dichloromethane solution of $Mo_2(tbn)_4$, **11**, to air for a brief period (60 s). Care must be taken not to expose the solution to air for an extended period of time. The compound is hygroscopic and decomposes in the presence of water. The solution was then purged of air and layered with hexanes to produce brown needle–crystals. Isolation of a $Mo_2(tbo)_4^{2+}$ species has been attempted with a variety of oxidizing agents and has consistently resulted in isolation of colorless needles corresponding to a protonated salt of the ligand (i.e. if $[Cp_2Fe][PF_6]$ was used then $[H_2tbo][PF_6]$ was isolated).

Attempts to obtain satisfactory elemental analysis for **9** and **11** were unsuccessful due to their extreme sensitivity to oxygen and water. Immediately upon exposure to air, the solid Mo_2^{4+} compounds begin to darken, and after a short time form a thick paste. Thermogravimetric analysis of a sample of $Mo_2(hpp)_4$, a compound which behaves very similar to **9** and **11**, exposed to air shows a mass gain due to the absorption of oxygen and water of approximately 20% within 90 seconds. This shows that even small exposure to air would cause considerable error in the values found for elemental analysis. The elemental analysis values of compound **12** are in agreement for the presence of 0.5 molecules of CH_2Cl_2 per molecule of **12** due to incomplete solvent loss from the crystals of **12**·$2CH_2Cl_2$. In the case of **10**, we have seen previously that

crystallization of similar compounds is dependant upon conditions such as temperature and even the choice of layering solvent.[59] When dichloromethane is used as a solvent, the solvated crystals obtained typically contain more than one molecule of solvent (typically two or four molecules are present).[58,59] While conditions used to grow crystals of **10** favor a nonsolvated form, the presence of a few solvated crystals would account for an overall formula of **10**·0.33CH_2Cl_2. For all four compounds, the appropriate parent ion peak is observed in the mass spectrum.

Crystallographic Studies. Sublimed samples of **6**, **7** and **8** produced crystals suitable for X-ray diffraction. Htbn, **8**, however, is endoscopic and crystals rapidly form a solution upon exposure to moist air. Therefore the crystal was suspended in silicone oil, mounted on a cryoloop and placed on the diffractometer with a N_2 stream set at 193 K in order to freeze the oil. Alternatively, an ethanol solution of **8** was allowed to absorb water and CO_2 from the atmosphere. Slow evaporation produced crystals of [H_2tbn][HCO_3] suitable for X-ray studies.

Figure 8 shows the thermal ellipsoid plot of **6** and the caption provides selected bond distances and angles. All of the C–C distances and angles are typical for the carbon atoms found in their respective environments. The C–N and C–S bond distances lie between that expected of a single bond or a double bond. The N–C–S angles are 125° and 126° and the N–C–N angle is 109°; the sum is 360º, suggesting an sp^2-hybridized carbon at C(3).

Thermal ellipsoid plots of **7** and **8** are shown in Figure 9 and selected bond distances are given in Table 6. Again, the C–C bond distances are typical for single

bonds. All of the C–N distances fall between the expected values for single and double bonds, indicating the delocalized nature of the guanidine core. The environment around C(3) is essentially planar, suggesting sp^2-hybridization.

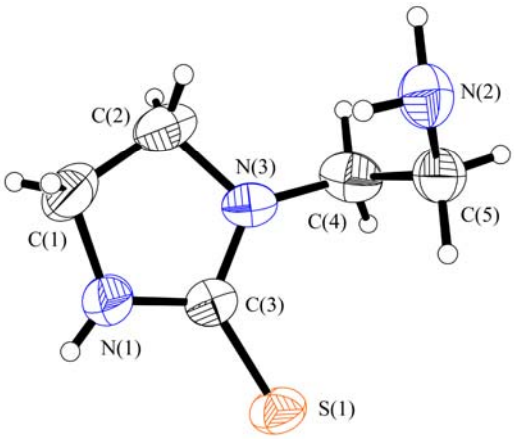

Figure 8. Thermal ellipsoid plot of **6**. Ellipsoids are drawn at the 50% probability level. C(3)–N(1) = 1.331(3) Å, C(3)–N(3) = 1.337(3) Å, C(3)–S(1) = 1.687(2) Å, N(1)–C(3)–N(3) = 109.2(2)°, N(1)–C(3)–S(1) = 124.8(2)°, N(3)–C(3)–S(1) = 126.1(2)°.

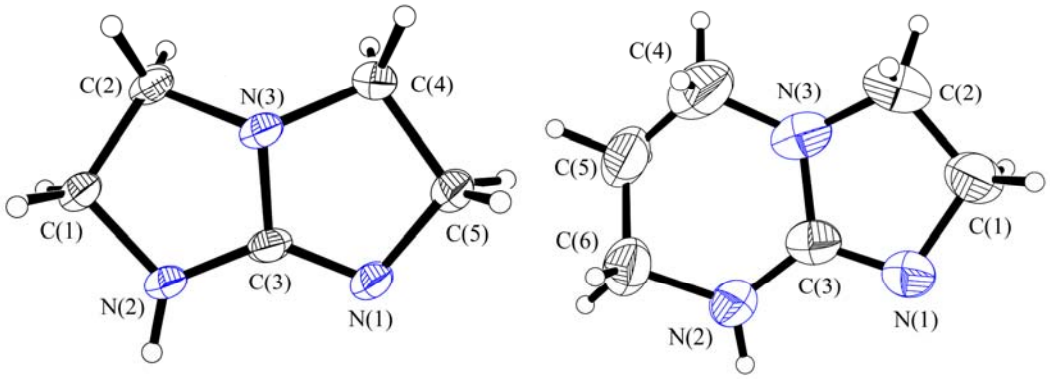

Figure 9. Thermal ellipsoid plots of **7** and **8**. Ellipsoids are drawn at the 50% probability level.

Table 6. Selected Bond Distances for Htbo (**7**), Htbn (**8**) and [H_2tbn][HCO_3].			
Compound	C(3)–N(1) (Å)	C(3)–N(2) (Å)	C3–N(3) (Å)
Htbo	1.346(2)	1.297(2)	1.391(2)
Htbn	1.290(3)	1.347(3)	1.383(3)
[H_2tbn][HCO_3]	1.335(3)	1.315(3)	1.336(3)

The structure of [H_2tbn][HCO_3] is shown in Figure 10 and selected bond distances and angles are also found in Table 6. In this case, the C–N bond lengths are nearly equivalent, as in a nearly ideal guanidinium cation. Each $[H_2tbn]^+$ unit is hydrogen-bonded to a bicarbonate anion as shown by an N–O distance of 2.80 Å which is shorter than the sum of van der Waals radii by 14%.[60]

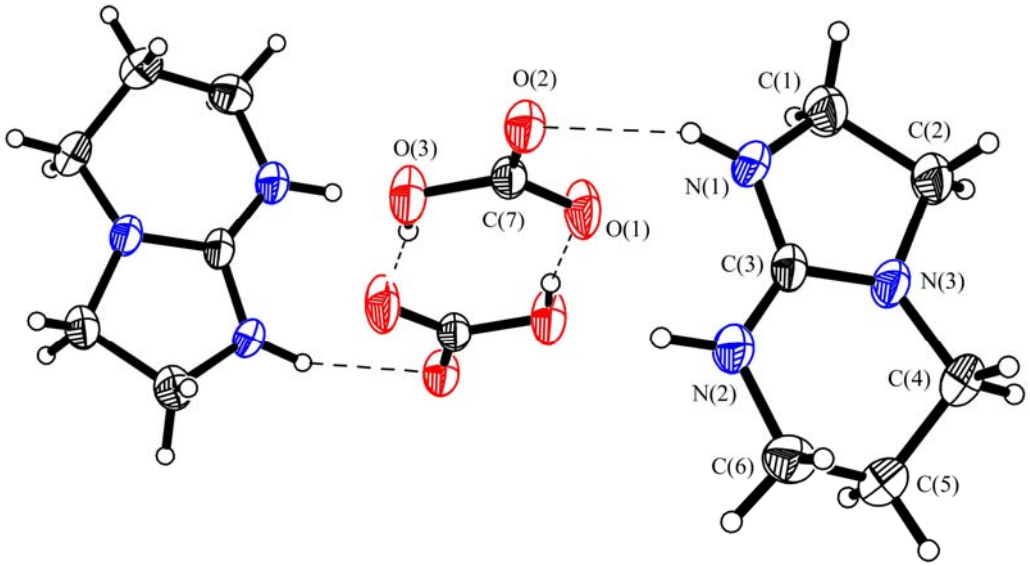

Figure 10. Thermal ellipsoid plot of [H_2tbn][HCO_3]. Ellipsoids are drawn at the 50% probability level.

The thermal ellipsoid plots of the Mo_2^{4+} tbo compounds **9** and **9**·THF are shown in Figure 11. Selected interatomic distances and angles are provided in the caption. Both structures show a long Mo–Mo distance and that of 2.1453(4) Å in **9**·THF is the longest distance recorded for a Mo_2^{4+} unit embraced by four ligands in a tetragonal lantern arrangement (i.e. Mo_2L_4 complexes where L is a bridging ligand).[61] Compared to the short Mo–Mo distance in $Mo_2(hpp)_4$ (2.067(1) Å)[12a] the Mo–Mo distance in **9** and **9**·THF is longer by 0.065 Å and 0.078Å, respectively. Such a drastic increase is attributable to the large divergent bite angle (*ca* 23°) of the ligand.

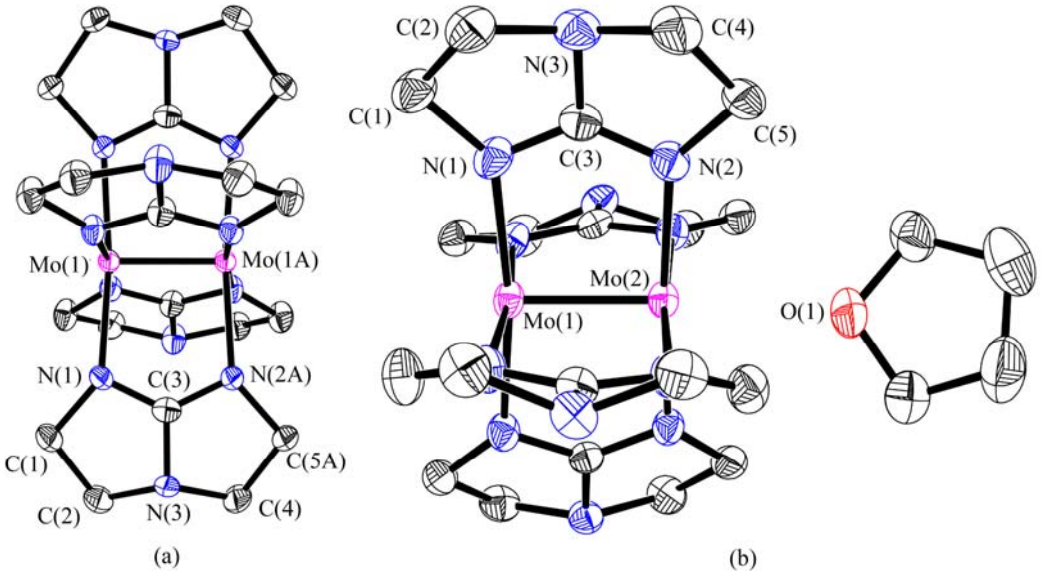

Figure 11. Thermal ellipsoid plots of **9** (a) and **9**·THF (b). Selected values for **9** are Mo(1)–Mo(1A) = 2.1321(7) Å, Mo–N(av) = 2.160[6] Å, Mo–Mo–N(av) = 93.2[2]°. Selected values for **9**·THF are Mo(1)–Mo(2) = 2.1453(4) Å, Mo–N(av) = 2.165[5] Å, Mo(2)–O(1) = 2.588(2) Å, Mo(1)–Mo(2)–O(1) = 175.66(5)°, Mo–Mo–N(av) = 92.9[2]°. Ellipsoids are drawn at the 50% probability level. Hydrogen atoms are removed for clarity.

As shown in Figure 12(a), the tbo ligand in **9** is puckered into a boat conformation. The drawing in Figure 12(b) shows the value expected for the Mo–Mo distance based on geometric considerations. Figure 12(b) assumes regular geometries (i.e. a regular pentagon with 108° angles), but the geometry found in the tbo ligand of **9** is not regular, as revealed by Figure 12(a). The geometry shown in Figure 12(c) incorporates values found in the crystal structure. The angle of divergence has decreased from 36° to 23° and the distance expected has been reduced from 3.63 Å to 3.17 Å. This value is still far greater than the distance found in a quadruply bonded dimolybdenum unit, or a dimolybdenum unit in any known oxidation state.[61] Despite this obstacle a paddlewheel compound still forms, revealing the resiliency of both the dimetal unit and the ligand. The interaction of the nitrogen orbitals with the dimolybdenum unit is increased by the puckering of the ligand into a boat conformation and the elongation of the Mo–Mo distance.

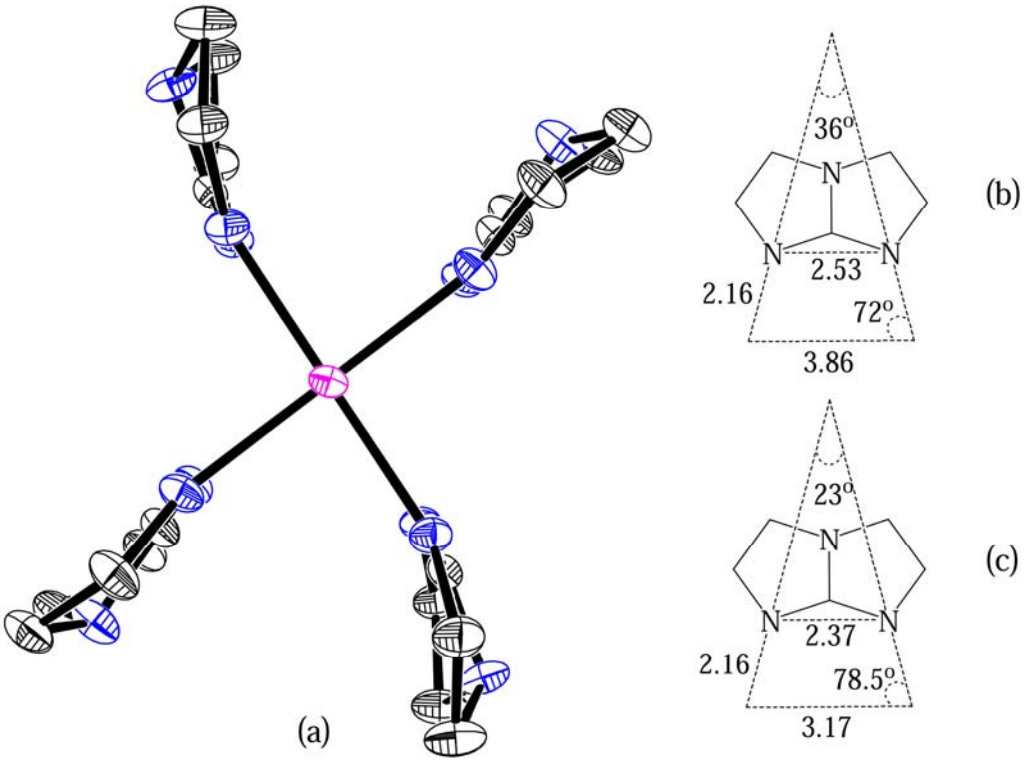

Figure 12. (a) A view of **9** along the Mo–Mo axis, showing the boat conformation adopted by the tbo ligand. (b) The value expected for the Mo–Mo distance based on purely geometric considerations. (c) The value expected for the Mo–Mo distance based on the geometric values found in the crystal structure. All distances are in Angstroms.

The structure of $Mo_2(tbo)_4Cl$, **10**, is shown as a thermal ellipsoid plot in Figure 13 and selected bond distances and angles are given in the caption. Again, the Mo–Mo distance of 2.2305(8) Å is extremely long. The resulting increase in Mo–Mo distance (0.099 Å) relative to $Mo_2(tbo)_4$ is more than twice that found between $Mo_2(hpp)_4Cl$ and $Mo_2(hpp)_4$ (0.049 Å) and similar to the increase when two electrons are removed from

$Mo_2(hpp)_4$ to form $Mo_2(hpp)_4Cl_2$ (0.107 Å).[12a,59] The Mo–Cl distance (2.7947(9) Å) is too long to consider the Cl^- ion as making a significant bonding contribution.

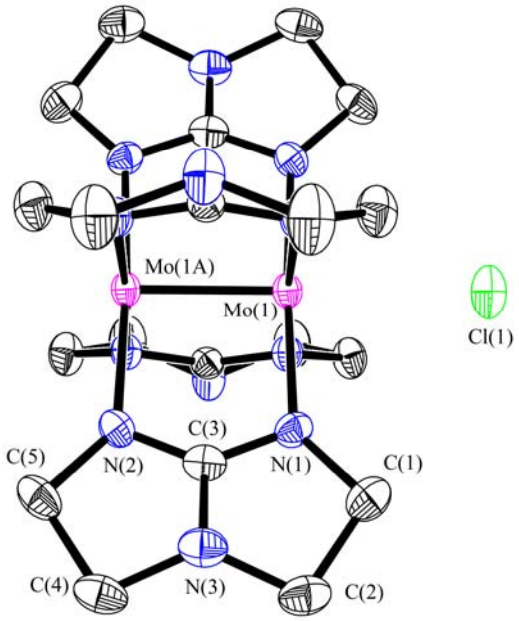

Figure 13. Thermal ellipsoid plot of **10**. Ellipsoids are drawn at the 50% probability level. Mo(1)–Mo(1A) = 2.2305(8) Å, Mo–N(av) = 2.121[8] Å, Mo(1)–Cl(1) = 2.7947(9) Å, Mo(1A)–Mo(1)–Cl(1) = 177.64(3)°, Mo–Mo–N(av) = 91.7[2]°.

The structure of $Mo_2(tbn)_4$, **11**, is shown in Figure 14 as a thermal ellipsoid plot, with selected interatomic distances and angles found in the caption. The Mo–Mo distance (2.082(1) Å) is typical of dimolybdenum units and longer than the distance in $Mo_2(hpp)_4$ by 0.015 Å. As with **10**, the longer distance is attributable to the ligand bite angle which, by purely geometric considerations, is divergent 18° but not as divergent as tbo (36°). Because of the asymmetry of the tbn ligand, the structure of **11** shows

disorder in all positions except for the dimolybdenum unit, making approximations of the bite angle in the crystal structure unreliable.

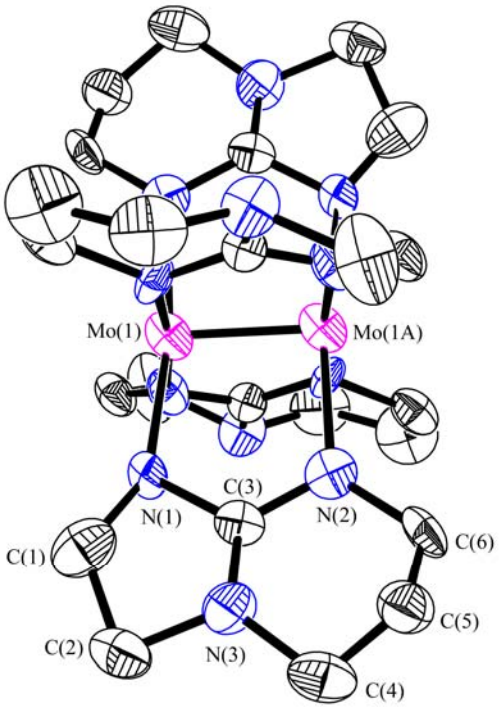

Figure 14. Thermal ellipsoid plot of **11**. Ellipsoids are drawn at the 50% probability level. Hydrogen atoms are removed for clarity. Disorder of the ligands is not shown. Mo(1)–Mo(1A) = 2.082(1) Å, Mo–N(1)(av) = 2.14[3] Å, Mo–N(2)(av) = 2.18[3] Å, Mo–Mo–N(1)(av) = 92.6[1]°, Mo–Mo–N(2)(av) = 93.6[1]°.

It is instructive to contrast the structure of **11** to that of $Mo_2(azin)_4$ (azin = the anion of 7-azaindole, **XVIII**), since the bicyclic system of azin is structurally similar to tbn. The structures of $Mo_2(azin)_4 \cdot 2THF$ and $Mo_2(azin)_4 \cdot 2acetone$ have been previously observed and have Mo–Mo distances of 2.1239(9) Å and 2.135(1) Å, respectively.[62]

These distances are considerably longer than that for **11**, and longer than average for Mo_2^{4+} paddlewheel compounds in general.[61] The explanation for the longer distances in the azin compounds has been discussed in terms of ligand geometry, ligand basicity and incorporation of interstitial solvent molecules.[62]

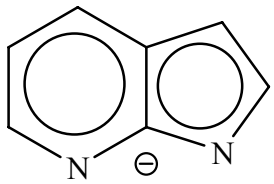

XVIII

Figure 15 displays the thermal ellipsoid plot of **13**. Selected bond distances and angles for **13**, as well as the solvated forms, **13**·$2CH_2Cl_2$ and **13**·$3CHCl_3$ are provided in Table 7. The paddlewheel structure in **13**·$2CH_2Cl_2$ and **13**·$3CHCl_3$ is well-ordered, with the ligands arranged around the dimetal unit in a centrosymmetric fashion. The non-solvated form, **13**, crystallized in the body-centered tetragonal space group *I4/m* with two molecules contained in the unit cell. The difficulties associated with the proper solution and refinement of such systems has been discussed previously. The molecule resides on a site of *4/m* symmetry, resulting in disorder of the ligand set. The Mo–Mo distances (average 2.230[3] Å) are increased by *ca* 0.148 Å from the distance in $Mo_2(tbn)_4$. This increase is greater than that of 0.108 Å found between $Mo_2(hpp)_4$ and

$Mo_2(hpp)_4Cl_2$.[12a,59] The Mo–Cl distances (*ca* 2.77–2.80 Å) are too long to consider the Cl^- ions as making a significant bonding contribution.

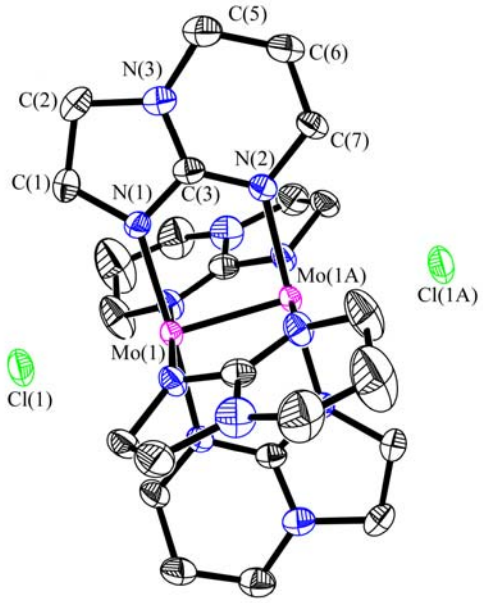

Figure 15. Thermal ellipsoid plot of $Mo_2(tbn)_4Cl_2$ in **13**. Ellipsoids are drawn at the 50% probability level. Hydrogen atoms are removed for clarity.

Table 7. Selected Bond Distances and Angles in $Mo_2(tbn)_4Cl_2$, **13**, Complexes.			
Distances and Angles	Compound		
	13	**13**·CH_2Cl_2	**13**·$3CHCl_3$
Mo–Mo (Å)	2.242(3)	2.2233(8)	2.224(1)
Mo–Cl (Å)	2.770(4)	2.771(1)	2.806(2)
Mo–N(1) (Å)	2.10(2)	2.082[4]	2.073[8]
Mo–N(2) (Å)	2.12(2)	2.119[4]	2.121[8]
Mo–Mo–Cl (°)	180.0	173.22(4)	177.5(5)
Mo–Mo–N(1) (°)	90.9(4)	89.6[1]	90.9[8]
Mo–Mo–N(2) (°)	91.8(4)	93.1[1]	92.1[8]

Electrochemistry. The CV and DPV of $Mo_2(tbo)_4$ and $Mo_2(tbn)_4$ were observed using THF solutions of approximately 1 mM concentration. The DPVs of these two compounds are depicted in Figure 16. The two peaks observed at -1.015 V and -0.564 V for $Mo_2(tbn)_4$ are related to successive one-electron oxidations corresponding to:

$$Mo_2^{4+} \xrightleftharpoons{-e^-} Mo_2^{5+}$$

$$Mo_2^{5+} \xrightleftharpoons{-e^-} Mo_2^{6+}$$

The first peak at -0.990 V observed for $Mo_2(tbo)_4$ is related to a one-electron oxidation of the paddlewheel compound. The second peak at -0.189 V is associated with an irreversible electron transfer. The current ratio in the CV (i_{pa}/i_{pc}) is less than 1 and varies with scan rate. This irreversibility is the most likely reason why no $Mo_2(tbo)_4^{2+}$ species has been isolated.

For each of these voltammograms, the Fc/Fc^+ couple was measured at 0.663 V under similar conditions. This places the potentials versus ferrocene at the values seen in Table 8, which also lists the potential versus ferrocene for $Mo_2(hpp)_4$. All three compounds have very large negative $E_{1/2}^{(1)}$ potentials.

Table 8. Redox Potential Values for $Mo_2(hpp)_4$, $Mo_2(tbo)_4$ and $Mo_2(tbn)_4$.

	$E_{1/2}^{(1)}$ (Mo_2^{4+}/Mo_2^{5+})		$E_{1/2}^{(2)}$ (Mo_2^{5+}/Mo_2^{6+})		
	Ag/AgCl	Fc/Fc^+	Ag/AgCl	Fc/Fc^+	Ref
$Mo_2(hpp)_4$[a]	-1.271	-1.795	-0.444	-0.968	58
$Mo_2(tbo)_4$[b]	-0.990	-1.653	-0.189	-0.852	this work
$Mo_2(tbn)_4$[b]	-1.015	-1.678	-0.564	-1.227	this work

[a] $Bu_4NBF_4 \cdot 3$toluene
[b] THF/Bu_4NBF_4 (0.1 M)

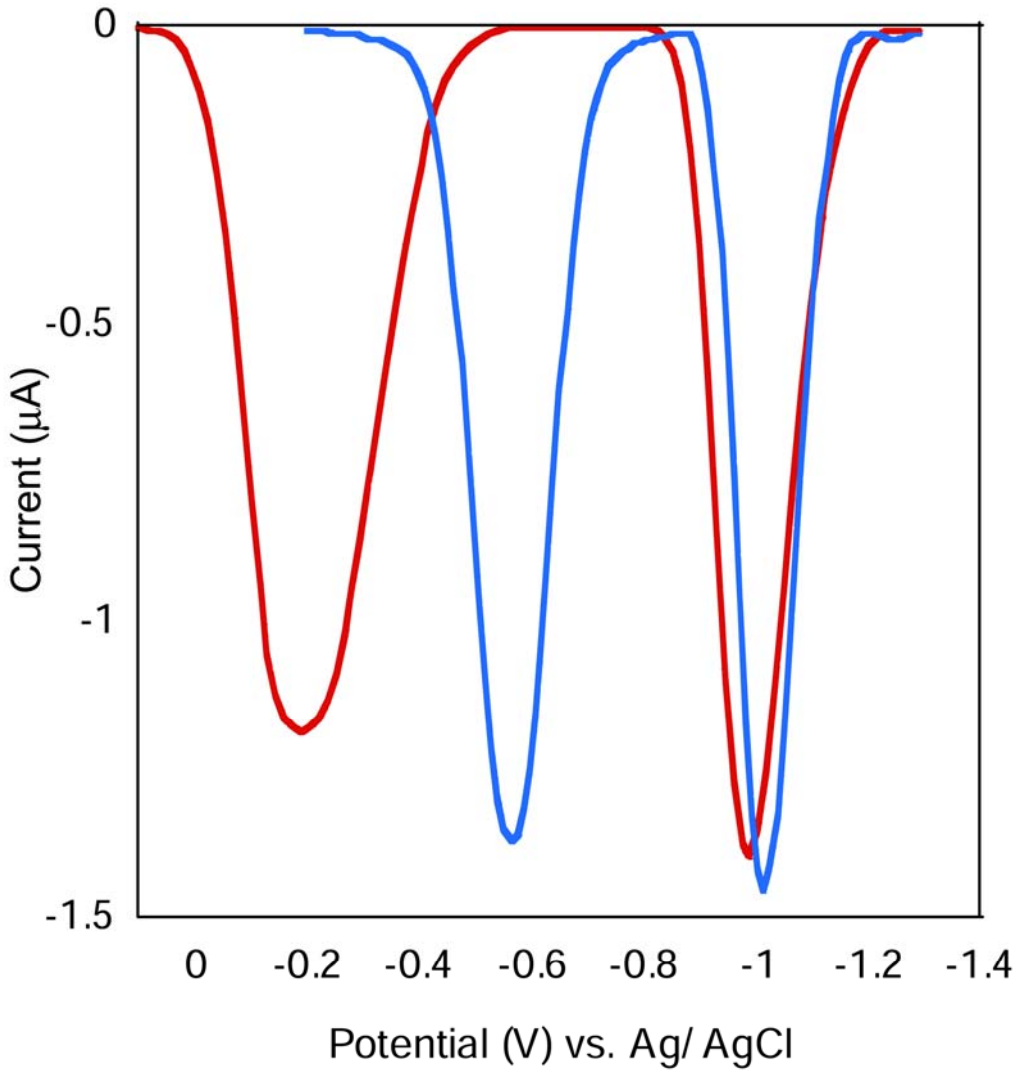

Figure 16. Differential pulse voltammograms of $Mo_2(tbo)_4$ (red) and $Mo_2(tbn)_4$ (blue).

These negative potentials mean that simple dissolution in CH_2Cl_2 leads to the formation of Mo_2^{5+} species (the reduction potential of CH_2Cl_2 has previously been measured at -1.638 V versus ferrocene).[58] The $E_{1/2}^{(2)}$ for **11** also shows that oxidation to the Mo_2^{6+} state is quite easy and may be accomplished by O_2 or other oxidizing agents.

The $\Delta E_{1/2}$ values defined as $E_{1/2}^{(2)} - E_{1/2}^{(1)}$ of both compounds allow for the calculation of the conproportionation constant[50] $K_C = \exp(\Delta E_{1/2}/25.69)$ for the process

$$Mo_2^{6+} + Mo_2^{4+} \rightleftharpoons Mo_2^{5+}$$

The $\Delta E_{1/2}$ for the $Mo_2(tbn)_4$ system is 451 mV and the K_C is 3.48×10^{13}. For the $Mo_2(tbo)_4$ system, the $\Delta E_{1/2}$ is 801 mV and the K_C is 1.51×10^{31}, although this can only be considered an approximation because of the irreversibility of the oxidation leading to the $Mo_2(tbo)_4^{2+}$ species. As with the $Mo_2(hpp)_4$ system ($K_C = 9.56 \times 10^{13}$) the large values are not due to the instability of the Mo_2^{6+} species (although this may play a greater role for $Mo_2(tbo)_4^{2+}$), but the greater reactivity of the Mo_2^{4+} species toward even very mild oxidizing agents such as CH_2Cl_2.[58]

Magnetic Behavior. While both $Mo_2(tbo)_4$ and $Mo_2(tbn)_4$ are only sparingly soluble in common NMR solvents, their ^1H spectra have been observed in very dilute C_6D_6 solutions, though for $Mo_2(tbo)_4$ the signal is only slightly above the background to be detected. However, both compounds give clean spectra. The signals of $Mo_2(tbn)_4$ are slightly stronger, but the presence of isomers results in overlapping peaks, making for a spectrum that cannot be easily interpreted. Because all of the signals are in the normal regions and of normal sharpness, it may be concluded that both compounds are diamagnetic as expected for a $\sigma^2\pi^4\delta^2$ configuration.

The singly oxidized species **10** and **12** show the expected single unpaired electron as evidenced by the measurements taken on an Gouy balance. The *g* value calculated from this measurement is 1.94 for **10** and 1.95 for **12**, essentially the same as

that found for $Mo_2(hpp)_4Cl$,[58] and is less than 2.00 due to spin-orbit coupling associated with the molybdenum atoms.

The ^1H NMR spectrum of $Mo_2(tbn)_4Cl_2$ reveals this compound to be diamagnetic. The spectrum also reveals a complex pattern of signals suggesting the presence of isomers in the bulk sample, even though the crystals of **13**·$2CH_2Cl_2$ and **13**·$3CHCl_3$ analyzed by X-ray diffraction show a well-ordered structure of the *cis* isomer.

Supplemental Information. A table of information for the LMSB crystallographic database and selected NMR and UV-Vis spectra are found in Appendix A.

CHAPTER IV

HOMOLOGS OF Hhpp WITH ALKYL SUBSTITUENTS (HTMhpp AND HTEhpp) AND THEIR DIMOLYBDENUM COMPLEXES

Introduction

This chapter concerns the development of derivatives of Hhpp that contain alkyl substituents, namely 3,3,9,9-tetramethyl-1,5,7-triazabicyclo[4.4.0]dec-4-ene (HTMhpp, **XIX**) and 3,3,9,9-tetraethyl-1,5,7-triazabicyclo[4.4.0]dec-4-ene (HTEhpp, **XX**). The preparation of these compounds follows the strategy of reacting the appropriate triamine with carbon disulfide in a 1:1 ratio. However, the requisite triamines are not commercially available and must be prepared by modifications of procedures found in the patent literature. The intermediates in this process have been characterized by a variety of methods including X-ray crystallography. The dimolybdenum paddlewheel complexes **XXI** and **XXII** are prepared by reacting $Mo_2(O_2CCF_3)_4$ with the lithium salt of the appropriate ligand. The compounds to be discussed in this chapter are listed in Table 9.

Table 9. Listing of Compounds to be Discussed In Chapter IV.		
Compound	Formula	Number
N,N-bis(2,2-dimethyl-3-iminohydroxypropyl)amine	$C_{10}H_{21}N_3O_2$	**14**
N,N-bis(3-amino-2,2-dimethyl-propyl)amine	$C_{10}H_{25}N_3$	**15**
HTMhpp (**XIX**)	$C_{11}H_{21}N_3$	**16**
N,N-bis(2,2-diethyl-3-iminohydroxypropyl)amine	$C_{14}H_{29}N_3O_2$	**17**
N,N-bis(3-amino-2,2-diethyl-propyl)amine	$C_{14}H_{33}N_3$	**18**
HTEhpp (**XX**)	$C_{15}H_{29}N_3$	**19**
$Mo_2(TMhpp)_4$ (**XXI**)	$Mo_2(C_{11}H_2N_3)_4$	**20**
$Mo_2(TMhpp)_4(TFPB)$	$[Mo_2(C_{11}H_2N_3)_4][B(C_8H_3F_6)_4]$	**21**
$Mo_2(TMhpp)_4(TFPB)_2$	$[Mo_2(C_{11}H_2N_3)_4][\ B(C_8H_3F_6)_4]_2$	**22**
$Mo_2(TEhpp)_4$ (**XXII**)	$Mo_2(C_{15}H_{28}N_3)_4$	**23**
$Mo_2(TEhpp)_4(TFPB)$	$[Mo_2(C_{15}H_{28}N_3)_4][\ B(C_8H_3F_6)_4]$	**24**
$Mo_2(TEhpp)_4(TFPB)_2$	$[Mo_2(C_{15}H_{28}N_3)_4][\ B(C_8H_3F_6)_4]_2$	**25**

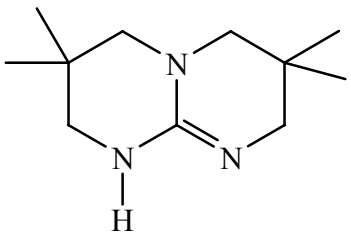

XIX

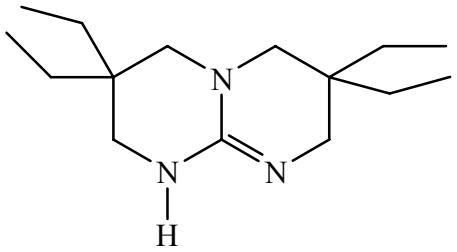

XX

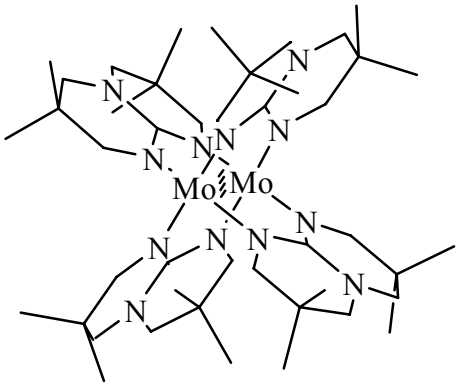

XXI

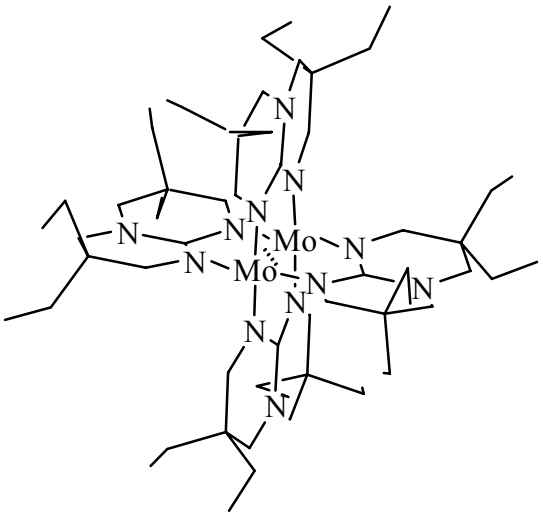

XXII

Experimental Section

General Procedures. All procedures were performed under a nitrogen atmosphere unless otherwise noted and all glassware was oven-dried prior to use. Ammonium hydroxide, carbon disulfide, *p*-toluenesulfonic acid monohydrate, isobutyraldehyde, paraformaldehyde, ammonium chloride, hydroxylamine hydrochloride, 2-ethylbutyraldehyde and sodium hydroxide were purchased from Aldrich and used as received. Lead(II) acetate, cadmium nitrate trihydrate and Raney nickel were purchased from Strem and used as received. Ether, ethanol, *p*-xylene, methanol, hexanes and acetonitrile were purchased from Aldrich and dried over 3 Å molecular sieves prior to use. Anhydrous DMSO was provided as a gift from ACROS. The solvents THF, CH_2Cl_2, benzene, toluene and hexanes were also purchased from Aldrich and purified using a Contour Glass solvent system. Evolution of H_2S in the synthesis of **16** and **19** was monitored by passing the reaction exhaust through test strips of filter paper wetted with aqueous lead(II) acetate. BuLi (1.6 M in hexanes) was purchased from Acros and stored at -20 °C until used. $Mo_2(O_2CCF_3)_4$, potassium tetra[3,5-bis(trifluoro-methyl)phenyl]borate (K(TFPB)) and Ag(TFPB) were prepared according to published procedures.[52,63]

Physical Measurements. IR spectra were recorded using a Perkin Elmer 16PC FT-IR spectrometer or a Bruker Tensor 27 spectrometer. UV-Vis spectra were recorded on a Shimadzu UV-2501 PC spectrometer. ^{1}H NMR spectra were recorded on a Unity Plus 300 NMR spectrometer, using solvent peaks to reference chemical shifts (δ). Cyclic voltammetry and differential pulse voltammetry were recorded using a CH

Instruments electrochemical analyzer with a 2 mm diameter Pt disk working electrode, Ag/AgCl reference electrode, and Pt wire auxillary electrode. Potentials are reported versus Ag/AgCl. Magnetic susceptibility was measured using a Johnson Matthey Mark II magnetic susceptibility balance. Elemental analysis was performed by Robertson Microlit Laboratories, Inc., Madison, NJ, USA. Mass Spectroscopy data (electrospray ionization) were recorded at the Laboratory for Biological Mass Spectroscopy at Texas A&M University, using an MDS Qstar Pulsar with a spray voltage of 5 kV.

X-ray Crystallography. Single crystals of **14**, **14**·HCl, Cd(**15**)$_2$(NO$_3$)$_2$·H$_2$O, [H$_2$TMhpp][HCO$_3$], **17**·HCl, Cd(**18**)$_2$(NO$_3$)$_2$·EtOH, **19**, **20**, **21**, **21**·CH$_2$Cl$_2$, **22**, **23** and **24**·2DMSO were placed in a cryoloop with a minimum of silicone grease. Data were collected at 213 K on a Bruker SMART area detector using the SMART and SAINT programs.[27, 28] The crystal structures were solved via direct methods and refined using SHELXL-97.[29] Hydrogen atoms were placed at calculated positions. Non-hydrogen atoms were refined with anisotropic displacement parameters. Cell parameters and refinement results for organic compounds are summarized in Table 10 while those for inorganic compounds are found in Table 11.

Table 10. Crystallographic Parameters for **14**·HCl, **14**, Cd(**15**)$_2$(NO$_3$)$_2$·H$_2$O, [H$_2$TMhpp][HCO$_3$], **17**·HCl, Cd(**18**)$_2$(NO$_3$)$_2$·EtOH and **19**.

Compound	**14**·HCl	**14**	Cd(**15**)$_2$(NO$_3$)$_2$·H$_2$O	[H$_2$TMhpp][HCO$_3$]	**17**·HCl	Cd(**18**)$_2$(NO$_3$)$_2$·EtOH	**19**
Empirical Formula	$C_{10}H_{22}ClN_3O_2$	$C_{10}H_{21}N_3O_2$	$C_{20}H_{52}CdN_8O_7$	$C_{12}H_{23}N_3O_3$	$C_{14}H_{32}ClN_3O_3$	$C_{30}H_{72}CdN_8O_7$	$C_{15}H_{29}N_3$
Formula Weight	251.76	215.30	629.10	257.33	325.88	769.36	251.41
Space Group	*Cmca*	*P4$_2$/n*	*Cc*	*P2$_1$/c*	*Pnma*	$P\bar{1}$	$P\bar{1}$
a(Å)	18.835(2)	19.424(2)	14.898(1)	13.853(3)	12.5762(9)	10.351(2)	5.833(2)
b(Å)	8.1735(7)	19.424(2)	20.009(1)	15.973(4)	21.295(4)	12.056(3)	10.569(3)
c(Å	17.420(2)	6.843(1)	9.9762(7)	13.067(3)	6.6890(7)	16.131(4)	12.505(4)
α(°)	90	90	90	90	90	78.651(5)	93.964(5)
β(°)	90	90	97.611(1)	99.038(4)	90	77.981(6)	96.108(5)
γ(°)	90	90	90	90	90	84.069(6)	97.355(5)
V (Å^3)	2681.7(4)	2581.8(6)	2947.6(4)	2856(1)	1791.4(4)	1926.4(8)	757.5(4)
Z	8	8	4	8	4	2	2
d_{calc}(g/cm^3)	1.247	1.108	1.418	1.197	1.208	1.326	1.102
μ(mm^{-1})	0.278	0.078	0.791	0.086	0.227	0.618	0.066
T (K)	213(2)	213(2)	213(2)	213(2)	213(2)	213(2)	213(2)
$R1$[a]	0.0380	0.0595	0.0148	0.0604	0.0406	0.0318	0.0495
$wR2$[b]	0.0836	0.1561	0.0392	0.1218	0.1049	0.0885	0.1493

[a] $R1 = \Sigma \| F_o | - | F_c \| / \Sigma | F_o |$
[b] $wR2 = [\Sigma[w(F_o^2 - F_c^2)^2] / \Sigma w(F_o^2)^2]^{1/2}$, $w = 1/[\sigma^2(F_o^2) + (aP)^2 + bP]$, where $P = [\max(0 \text{ or } F_o^2) + 2(F_c^2)]/3$

Table 11. Crystallographic Parameters for **20**, **21**, **21**·CH_2Cl_2, **22**, **23** and **24**·2DMSO.

Compound	**20**	**21**	**21**·CH_2Cl_2	**22**	**23**	**24**·2DMSO
Empirical Formula	$C_{44}H_{80}Mo_2N_{12}$	$C_{76}H_{92}BF_{24}Mo_2N_{12}$	$C_{77}H_{94}BCl_2F_{24}Mo_2N_{12}$	$C_{108}H_{104}B_2F_{48}Mo_2N_{12}$	$C_{60}H_{112}Mo_2N_{12}$	$C_{96}H_{136}BF_{24}Mo_2N_{12}O_2S_2$
Formula Weight	969.08	1832.31	1917.23	2695.53	1193.50	2212.98
Space Group	*I2/m*	$P\bar{1}$	$P\bar{1}$	$P\bar{1}$	$P\bar{1}$	*P4/n*
a(Å)	10.206(2)	12.015(2)	12.020(4)	14.506(2)	11.262(2)	21.287(1)
b(Å)	15.864(3)	14.213(2)	14.276(5)	14.554(3)	14.365(2)	21.287(1)
c(Å)	15.607(3)	27.980(5)	28.22(1)	15.193(3)	20.885(4)	23.846(2)
α(°)	90.00	88.823(3)	90.799(7)	86.936(3)	97.180(3)	90
β(°)	105.716(3)	88.470(3)	90.432(6)	87.882(3)	100.508(3)	90
γ(°)	90.00	65.487(3)	114.659(6)	62.453(3)	103.563(3)	90
V (Å^3)	2432.4(8)	4346(1)	4400(3)	2839.5(8)	3179.5(9)	10805(1)
Z	2	2	2	1	2	4
d_{calc}(g/cm^3)	1.323	1.400	1.447	1.576	1.247	1.360
μ(mm^{-1})	0.558	0.387	0.444	0.353	0.440	0.363
T (K)	213	213	213	213	213	213
R1[a]	0.0368	0.1048	0.1050	0.0534	0.0438	0.0732
wR2[b]	0.0835	0.2323	0.2660	0.1390	0.0889	0.1783

[a] $R1 = \Sigma \| F_o | - | F_c \| / \Sigma | F_o |$

[b] $wR2 = [\Sigma[w(F_o^2 - F_c^2)^2] / \Sigma w(F_o^2)^2]^{1/2}$, $w = 1/[\sigma^2(F_o^2) + (aP)^2 + bP]$, where $P = [\max(0 \text{ or } F_o^2) + 2(F_c^2)]/3$

Preparation of *N,N*-bis(2,2-dimethyl-3-iminohydroxypropyl)amine hydrochloride, 14·HCl. The synthesis follows a slightly modified procedure in the patent literature.[64] A mixture of NH_4Cl (33.44 g, 625 mmol), isobutyraldehyde (127 mL, 100.0 g, 1.39 mol), paraformaldehyde (45.00 g, 1.50 mol), 20.0 mL water, and 1.0 mL of 12 M HCl in a 2000 mL flask was refluxed under nitrogen for 4.5 h. During this time the paraformaldehyde dissolved, resulting in an exothermic reaction which caused the reflux to become vigorous. While the viscous solution was boiling, 1.3 L EtOH, 400 mL H_2O and 100.0 g (1.43 mol) $NH_2OH·HCl$ were added stepwise. A colorless precipitate formed, and redissolved as the solution was refluxed for 20 min. The solution was then cooled to room temperature and allowed to stand overnight. The next day, colorless needle–crystals of **14**·HCl were collected by filtration and washed with 100 mL of ether. The solvent was removed from the filtrate using a rotary evaporator and the residue was recrystallized from 300 mL of hot 75% v/v EtOH/H_2O, giving a second crop of colorless needles. Yield: 115 g (73%). The crystals produced were suitable for X-ray diffraction. IR (KBr, cm^{-1}): 3212 (s), 2973 (m), 2713 (w), 1648 (w), 1567 (w), 1540 (w), 1444 (s), 1413 (m), 1377 (w), 1317 (m), 1290 (m), 1230 (w), 1168 (w), 10061 (w), 979 (s), 929 (w), 855 (w), 777 (m), 690 (m), 580 (w), 484 (w). ^1H NMR (DMSO-d_6, ppm): 10.81 (s, 2H (CH)), 8.00 (br s, 2H (OH)), 7.34 (s, 2H (NH_2)), 3.07 (t, 4H (CH_2)), 1.16 (s, 12H (CH_3)). Mass spectrum (ESI^+): Calculated ($M+H^+$): 216 amu; found: 216 amu. Crystals of **14**, suitable for X-ray diffraction, were prepared by making a hot 75% v/v EtOH/H_2O solution basic with NaOH and then placing the solution in a refrigerator at 10 °C overnight.

***N,N*-bis(3-amino-2,2-dimethyl-propyl)amine, 15.** The procedure is modified from the patent literature.[64] Compound **14**·HCl (10.0 g, 39.8 mmol) was dissolved in a mixture of hot 75% v/v EtOH/H_2O (100 mL) and made basic with NaOH. The solvent was then removed using a rotary evaporator and the colorless solid washed with water to remove NaCl. The solid was then placed in the glass liner of a Parr high-pressure reactor and dissolved in 100 mL of ethanol and 50 mL of 14.8 M ammonium hydroxide. An aliquot (*ca* 0.5 mL) of Raney Ni slurry was added and the vessel was then placed in the reactor which was subsequently assembled. The reactor was flushed briefly with H_2 gas and then charged to a pressure of 1100 psi of H_2. The mixture was heated at 100 °C and stirred for 4 h, then cooled to room temperature before the reactor was disassembled. The mixture was filtered to remove Raney Ni and the solution was concentrated to a colorless oil (*ca* 5 mL) on a rotary evaporator. Methanol (50 mL) was added and the solution was once more concentrated to a viscous oil (*ca* 5 mL) using a rotary evaporator to remove traces of water through the formation of a H_2O/MeOH azeotrope. The residue was then vacuum distilled and the colorless oil **15** collected and stored under nitrogen. Yield: 5.017 g (26.8 mmol, 68%). IR (NaCl plates, cm^{-1}): 3370 (m), 3296 (m), 2950 (s), 2867 (s), 1598 (m), 1471 (s), 1388 (m), 1362 (m), 1311 (w), 1273 (w), 1227 (w), 1119 (s), 1065 (m), 1021 (m), 918 (m), 839 (m), 757 (m), 731 (m), 600 (w), 517 (w). ^1H NMR (C_6D_6, ppm): 2.44 (br s, 4H (CH_2)), 2.29 (s, 4H (CH_2)), 1.42 (br s, 5 H (NH_2/NH)), 0.78 (s, 12H (CH_3)). Mass Spec. (ESI^+): Calculated ($M+H^+$): = 188 amu; found: 188 amu. Crystals of Cd(**15**)$_2$(NO_3)$_2$·H_2O suitable for X-ray diffraction were

produced by reacting **15** with $Cd(NO_3)_2 \cdot 3H_2O$ in a 2:1 ratio in ethanol and crystallizing the product from ethanol and water.

3,3,9,9-tetramethyl-1,5,7-triazabicyclo[4.4.0]dec-4-ene (HTMhpp), 16. The procedure is modified from the patent literature.[53] Compound **15** (2.0 g, 10.7 mmol) was dissolved in 150 mL of *p*-xylene and CS_2 (0.65 mL, 0.823 g, 10.8 mmol) and *p*-toluenesulfonic acid monohydrate (0.103 g, 0.541 mmol) were added. Initially a white precipitate formed. The solution was heated to reflux under nitrogen causing the precipitate to rapidly redissolve. The solution was refluxed until all of the H_2S evolved (*ca* 3 days). While still hot, the solution was decanted away from any solid or oily residue in the flask and the solution was allowed to cool to room temperature under nitrogen. The solvent was then removed under vacuum and the resulting colorless microcrystalline powder was washed with acetonitrile (20 mL) and hexanes (5 mL). The solid was then placed in an oven at 100 °C for 1 h. Yield: 1.618 g (8.30 mmol, 78 %) IR (KBr, cm^{-1}): 3260 (w), 3188 (m), 3114 (m), 3064 (m), 3034 (m), 2950 (s), 2899 (s), 2858 (s), 1656 (s), 1572 (w), 1517 (s), 1478 (m), 1464 (m), 1442 (m), 1387 (m), 1360 (m), 1310 (m), 1297 (m), 1257 (s), 1212 (w), 1167 (s), 1113 (w), 1057 (m), 1023 (w), 1007 (w), 934 (w), 814 (w), 744 (w), 715 (w), 635 (w), 561 (w), 481 (w). ^1H NMR (C_6D_6, ppm): 2.94 (s, 4H (CH_2)), 2.78 (s, 4H (CH_2)), 1.03 (s, 12 H (CH_3)). Mass Spectrum (ESI^+): Calculated ($M+H^+$): 196 amu; found 196 amu. Crystals of the bicarbonate salt, $[H_2TMhpp][HCO_3]$, suitable for X-ray diffraction, were produced by the slow evaporation in air of a solution of **15** in 90% v/v $EtOH/H_2O$.

***N,N*-bis(2,2-diethyl-3-iminohydroxypropyl)amine hydrochloride monohydrate, 17·HCl·H_2O.** The synthesis was modified from a procedure in the patent literature.[64] A mixture of NH_4Cl (4.90 g, 92 mmol), 2-ethylbutyraldehyde (25.0 mL, 20.4 g, 204 mmol), paraformaldehyde (6.60 g, 220 mmol), 5.0 mL water, and 60 mL of MeCN was refluxed under nitrogen for 4.5 h. During this time, the paraformaldehyde dissolved resulting in an exothermic reaction which caused the reflux to become vigorous. The volatile components were removed using a rotary evaporator and the pasty residue was dissolved in 100 mL of 75% v/v EtOH/H_2O. Hydroxylamine hydrochloride (14.5 g, 209 mmol) was added and a colorless precipitate formed, but then dissolved as the temperature of the solution was raised to boiling. The solution was refluxed for 20 min then cooled to room temperature and allowed to stand overnight. The next day, crystals of **17**·HCl·H_2O in the form of colorless plates were collected by filtration and washed with 20 mL of ether. Yield: 9.87 g (30%). The crystals produced were suitable for X-ray diffraction. IR (KBr, cm^{-1}): 3395 (s), 3356 (s), 3271 (s), 3232 (s), 3148 (s), 3067 (s), 2972 (s), 2941 (s), 2882 (s), 2853 (s), 2752 (m), 2711 (m), 1617 (m), 1529 (m), 1441 (s), 1390 (m), 1331 (s), 1290 (s), 1179 (w), 1154 (w), 1074 (w), 1044 (w), 1026 (w), 1005 (w), 966 (s), 909 (w), 886 (w), 844 (w), 788 (w), 709 (s), 667 (m), 574 (w), 542 (m), 522 (m). ^{1}H NMR (DMSO-d_6, ppm): 10.92 (s, 2H (CH)), 7.80 (br s, 2H (OH)), 7.32 (s, 2H (NH_2)), 3.12 (t, 4H (CH_2)), 1.55 (q, 8H (-C$H_2$$CH_3$)), 0.81 (t, 12H (-$CH_2CH_3$)). Mass spectrum ($ESI^+$): Calculated ($M+H^+$): 272 amu; found: 272 amu.

***N,N*-bis(3-amino-2,2-diethyl-propyl)amine, 18.** The procedure was modified from the patent literature.[64] Compound **17**·HCl·H_2O (10.0 g, 39.8 mmol) was dissolved in hot 75% v/v EtOH/H_2O and the solution was made basic with NaOH. The solvent was then removed using a rotary evaporator and the colorless solid was washed with water to remove NaCl. The solid was then placed in the glass liner of a Parr high-pressure reactor and dissolved in 100 mL ethanol and 50 mL of 14.8 M ammonium hydroxide. An aliquot (*ca* 0.5 mL) of Raney Ni slurry was added and the vessel then placed in the reactor. The reactor was flushed briefly with H_2 gas and then charged with $H_2$to a pressure of 1100 psi. The mixture was heated at 100 °C and stirred for 4 h, then cooled to room temperature before the reactor was disassembled. The mixture was filtered to remove Raney Ni and the filtrate was concentrated (*ca* 2 mL) to a viscous oil on a rotary evaporator. Methanol (50 mL) was added and the solution was once more concentrated to a colorless oil (*ca* 2 mL) using a rotary evaporator to remove traces of water through the formation of an MeOH/H_2O azeotrope. The residue was then vacuum distilled and the colorless oil **18** collected and stored under nitrogen. Yield: 2.087 g (8.6 mmol, 57%). IR (NaCl plates, cm^{-1}): 3372 (m), 3299 (m), 2958 (s), 2937 (s), 2920 (s), 2877 (s), 1599 (m), 1463 (s), 1379 (m), 1297 (m), 1230 (w), 1120 (m), 1073 (m), 1031 (m), 988 (m), 823 (s), 785 (s), 729 (m), 637 (w), 600 (w), 532 (w). ^{1}H NMR (C_6D_6, ppm): 2.50 (br s, 4H (CH_2)), 2.35 (s, 4H (CH_2)), 1.24 (q, 8H (-C*H*$_2$CH$_3$)), 0.77 (t, 12H (-CH$_2$C*H*$_3$)). Mass spectrum (ESI^+): Calculated ($M+H^+$): 244 amu; found: 244 amu. Crystals of Cd(**18**)$_2$(NO_3)$_2$·EtOH suitable for X-ray diffraction were produced by

reacting **18** with $Cd(NO_3)_2 \cdot 3H_2O$ in a 2:1 ratio in ethanol and crystallizing the product from ethanol and water.

3,3,9,9-tetraethyl-1,5,7-triazabicyclo[4.4.0]dec-4-ene (HTEhpp), 19. The procedure was modified from the patent literature.[61] Compound **18** (2.0 g, 8.2 mmol) was dissolved in 150 mL *p*-xylene and CS_2 (0.48 mL, 0.62 g, 8.2 mmol) and *p*-toluenesulfonic acid monohydrate (0.078 g, 0.41 mmol) were added. Initially a white precipitate formed, which rapidly dissolved as the solution was heated to reflux under nitrogen. The solution was refluxed until evolution of H_2S ceased. While still hot, the solution was decanted away from any solid or oily residue in the flask and allowed to cool to room temperature under nitrogen. The solvent was removed under vacuum and the resulting colorless microcrystalline powder was washed with acetonitrile (20 mL) and hexanes (5 mL). The solid was then dried in an oven at 100 °C for 1 h. Yield: 0.89 g (3.6 mmol, 44%) IR (KBr, cm^{-1}): 3272 (w), 3197 (m), 3145 (m), 3071 (m), 3039 (m), 2965 (s), 2935 (s), 2861 (s), 2807 (s), 1650 (s), 1578 (w), 1520 (s), 1484 (m), 1461 (s), 1447 (s), 1375 (s), 1310 (m), 1292 (m), 1265 (m), 1232 (m), 1193 (w), 1153 (m), 1115 (w), 1069 (m), 1029 (w), 1005 (w), 941 (w), 914 (w), 804 (w), 770 (w), 736 (w), 711 (w), 679 (w), 651 (w), 566 (w), 528 (w). ^1H NMR (C_6D_6, ppm): 2.89 (s, 4H (CH_2)), 2.42 (s, 4H (CH_2)), 1.35 - 1.16 (m, 8H (-C*H*$_2$CH$_3$)), 0.69 (t, 12H (-CH$_2$C*H*$_3$)). Mass Spectrum (ESI^+): Calculated ($M+H^+$): 251 amu; found 251 amu. Colorless plate crystals, suitable for X-ray diffraction, were produced by slow evaporation of a *p*-xylene solution of **19** under vacuum.

$Mo_2(TMhpp)_4$, 20. A Schlenk flask was charged with HTMhpp, **16**, (1.00 g, 5.13 mmol) and THF (20 mL). To the solution BuLi (3.30 mL, 5.28 mmol) was added and the solution was stirred for 10 min. The pale yellow solution was then transferred to a flask containing a brilliant yellow THF solution (20 mL) of $Mo_2(O_2CCF_3)_4$ (0.826 g, 1.28 mmol). The solution immediately darkened and was stirred for 10 min. The solvent was removed under vacuum and toluene (40 mL) was added. The residue was shaken from the sides of the flask in an ultrasonic bath and the mixture was filtered through Celite. The orange filtrate was evaporated under vacuum and the residue was collected as an orange powder. Yield: 0.921 g (0.951 mmol, 74%). Crystals, as orange plates, suitable for X-ray diffraction were prepared by placing a saturated THF solution in a freezer at -20 °C for 1 week. IR (KBr, cm^{-1}): 3398 (w), 2959 (s), 2904 (m), 2869 (s), 2836 (m), 2371 (w), 2046 (w), 1689 (s), 1638 (m), 1597 (m), 1561 (m), 1524 (s), 1487 (s), 1476 (s), 1443 (s), 1397 (s), 1369 (m), 1303 (m), 1289 (m), 1208 (s), 1179 (s), 1142 (s), 1052 (s), 1024 (m), 838 (m), 803 (s), 773 (m), 724 (m), 668 (w), 606 (w), 523 (w), 489 (w). ^1H NMR (C_6D_6, ppm): 3.42 (s, 16H), 2.70 (s, 16H), 1.17 (s, 48H). UV-Vis (THF) λ_{MAX}, nm; (ε_M, L/mol·cm): 475.0 (500), 378.0 (3,000), 306.5 (4,000). Mass Spectrum (ESI^+): Calculated ($M+H^+$): 969 amu; found 969 amu.

$Mo_2(TMhpp)_4(TFPB)$, 21. A Schlenk flask was charged with $Mo_2(TMhpp)_4$ (0.100 g, 0.103 mmol) and 20 mL CH_2Cl_2. The solution was stirred for 10 min. and then K(TFPB) (0.095 g, 0.105 mmol) in 20 mL ether was added. A colorless precipitate formed and the mixture was stirred for 10 min. The mixture was filtered through Celite and the filtrate evaporated to dryness. The residue was dissolved in 20 mL CH_2Cl_2 and

layered with hexanes. Brown plate crystals of **21**·CH_2Cl_2 and **21** (no interstitial solvent), suitable for X-ray diffraction, were collected after 1 week. Yield: 0.122 g (65%). IR (KBr, cm^{-1}): 2964 (m), 2877 (m), 2845 (m), 1646 (w), 1525 (s), 1485 (m), 1445 (m), 1400 (m), 1355 (s), 1279 (s), 1167 (s), 1125 (s), 1051 (w), 886 (w), 839 (w), 812 (w), 772 (w), 714 (w), 682 (w), 669 (w). UV-Vis (CH_2Cl_2) λ_{MAX}, nm; (ε_M, L/mol·cm): 768 (800), 512 (600), 399 (12,000), 342 (8,500). Elemental Analysis: Calculated for $Mo_2(TMhpp)_4(TFPB)\cdot CH_2Cl_2$: C: 48.24, H: 4.94, N: 8.77; found C: 47.92, H: 4.84, N: 8.58. Magnetism: 1.65 μ_B, g = 1.91.

$Mo_2(TMhpp)_4(TFPB)_2$, 22. An orange-brown dichloromethane solution (20 mL) of **20** (0.050 g, 0.052 mmol) was briefly exposed to air (60 s). The flask was then purged and back-filled (3x) with nitrogen and an ether solution (10 mL) of K(TFPB) (0.100 g, 0.111 mmol) was then added. The solution was concentrated to *ca* 10 mL, filtered through Celite, and layered with hexanes. Crystals, as brown blocks suitable for X-ray diffraction, were collected after 2 weeks. Yield: 0.107 g (78%). Mass Spectrum (ESI^+): Calculated $(M - 2(TFPB))^{2+}$: 484 amu; found 484 amu. ^1H NMR (CD_2Cl_2, ppm): 7.71 (m, o, 16H), 7.56 (m, p, 8H), 3.05 (s, 16H), 2.12 (s, 16H), 1.10 (s, 48H). IR (KBr, cm^{-1}): 2969 (m), 2876 (w), 1681 (s), 1548 (s), 1473 (m), 1315 (s), 1281 (s), 1105 (s), 1050 (m), 884 (m), 841 (s), 801 (s), 770 (m), 657 (m), 602 (w). UV-Vis (CH_2Cl_2) λ_{MAX}, nm; (ε_M, L/mol·cm): 617 (100), 473 (sh), 455 (sh), 350 (3,000).

$Mo_2(TEhpp)_4$, 23. A Schlenk flask was charged with HTEhpp (1.00 g, 3.98 mmol) and 10 mL THF. To the solution, BuLi (2.50 mL, 4.00 mmol) was added and the solution stirred for 10 min. The pale yellow solution was added to a brilliant yellow

solution of $Mo_2(O_2CCF_3)_4$ (0.645 g, 1.00 mmol) in 5 mL THF. The solution, which immediately darkened, was shaken briefly and placed in a freezer at -20 °C for 3 days. The solution was then decanted away from the resulting orange precipitate and the solid washed with 5 mL of THF. Yield: 90% (1.07 g, 0.897 mmol). Crystals, as orange plates, suitable for X-ray diffraction were grown from a saturated THF solution layered with acetonitrile. IR (KBr, cm^{-1}): 3303 (m), 3223 (m), 3156 (w), 2950 (s), 2936 (s), 2878 (s), 1686 (s), 1638 (s), 1542 (s), 1459 (s), 1383 (s), 1282 (s), 1202 (s), 1134 (s), 1061 (m), 1033 (m), 938 (w), 901 (m), 801 (s), 764 (s), 742 (s), 721 (s), 521 (w), 473 (w). Mass spectrum (ESI^+): Calculated ($M+H^+$): 1193 amu; found: 1193 amu. Elemental analysis: Calculated for $Mo_2(TEhpp)_4O$: C: 59.48, H: 9.48, N: 13.87; Found C: 59.59, 9.42, 13.74. NMR (C_6D_6, ppm): 3.53 (s, 16H), 2.78 (s, 16H), 1.73 (m, 16H), 1.51 (m, 16H), 0.94 (t, 48H). UV-Vis (THF) λ_{MAX}, nm; (ε_M, L/mol·cm): 500 (200), 409 (1500), 376 (sh), 339 (sh), 303 (sh).

$Mo_2(TEhpp)_4(TFPB)$, 24. A flask was charged with 0.400 g (0.336 mmol) **23** and 20 mL CH_2Cl_2. After stirring for 5 min the solution was transferred to a flask containing 0.310 g (0.344 mmol) K(TFPB). Within 5 min a colorless precipitate of KCl formed and the mixture was stirred for an additional 30 min. The mixture was filtered through Celite and the solvent removed under vacuum. Yield 0.603 g (87%). Brown block crystals of **24**·2DMSO, suitable for X-ray diffraction, were prepared by layering a CH_2Cl_2 solution with DMSO. IR (KBr, cm^{-1}): 2971 (s), 2928 (m), 2886 (m), 2862 (m), 1610 (w), 1530 (s), 1487 (m), 1468 (m), 1443 (m), 1386 (m), 1355 (s), 1276 (s), 1159 (s), 1124 (s), 1063 (w), 886 (w), 809 (w), 786 (w), 712 (w), 675 (w). Magnetism: 1.66

$\mu_{B,}$ g = 1.92. Mass Spectrum (ESI^+): main peak 1192 amu $(M - (TFPB))^+$. UV-Vis (CH_2Cl_2) λ_{MAX}, nm; (ε_M, L/mol·cm): 771 (500), 527 (800), 400 (20,000), 351 (17,000), 300 (sh).

$Mo_2(TEhpp)_4(TFPB)_2$, 25. A flask was charged with 0.100 g (0.084 mmol) **23** and 20 mL CH_2Cl_2. The solution was stirred for 30 min and transferred to a flask containing 0.165 g (0.170 mmol) Ag(TFPB). Within 5 min a precipitate was observed and the mixture was stirred for an additional 30 min. The mixture was filtered through Celite and the solvent removed under vacuum. Yield 0.204 g (83%). IR(KBr,cm^{-1}): 3306 (m), 3219 (m), 2973 (s), 2880 (m), 1646 (s), 1544 (m), 1466 (m), 1356 (s), 1279 (s), 1124 (s), 934 (w), 889 (m), 838 (m), 803 (m), 743 (m), 712 (m), 677 (m). ^1H NMR (CD_2Cl_2, ppm): 7.71 (m, o, 16H), 7.56 (m, p, 8H), 3.08 (s, 16H), 3.01 (s, 16H), 1.38 (q, 32H), 0.85 (t, 48H). Mass spectrum (ESI^+): Calculated $(M-2(TFPB))^{2+}$: 596 amu; found 596 amu. UV-Vis (CH_2Cl_2) λ_{MAX}, nm; (ε_M, L/mol·cm): 404 (sh), 352 (sh). Single crystals have not yet been obtained.

Results and Discussion

Organic Syntheses. The preparation of hpp has been previously described in the patent literature by the reaction of 3,3′-diaminopropylamine and carbon disulfide in a 1:1 ratio.[61] This synthetic strategy has also been used to prepare derivatives of hpp which replace either one or both 6-membered rings with 5-membered rings. The reaction seems quite general and should be able to produce any desired derivative of hpp as long as the appropriate triamine is available. However, the availability of triamines with

desirable alkyl substituents are not commercially available and preparations from the journal literature are often complex and result in derivatives with undesirable substituents. We therefore turned our attention once again to the patent literature.

The preparation of the triamines used to produce HTMhpp and HTEhpp begins with a Mannich reaction. Normally, Mannich reactions must be carefully controlled in order to avoid production of amines which are more substituted than desired.[65] The alkyl substituents, however, provide enough steric hinderance to limit substitution and results exclusively in a disubstituted amine as seen below. Isolated intermediates are shown in blue.

Mannich reactions are also very sensitive to a number of conditions which can affect the resulting product even if a reaction occurs.[65,66] The choice of solvent can be crucial to the success of a Mannich reaction. For example, in the production of **14**, a simple solvent-free reaction (with only enough water present to dissolve the ammonium chloride) results in a successful reaction. This strategy also works for producing **17**, but the yield is poor (about 10%). The yield of **17** improves considerably (to about 30% yield) if acetonitrile is used as the reaction solvent.

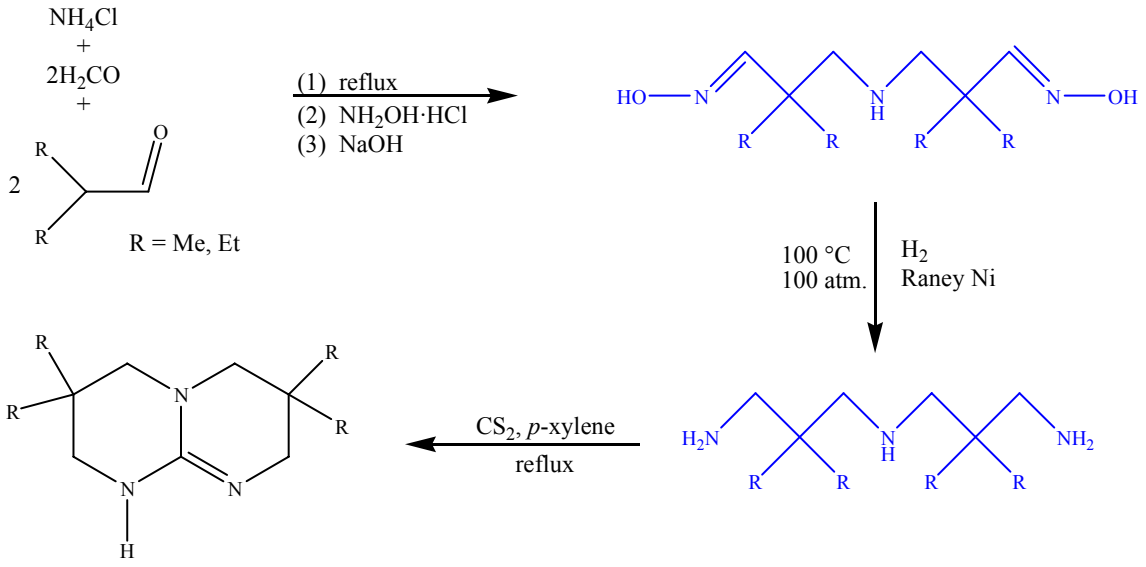

The choice of formaldehyde source is also an important consideration. In general, there are five different types of formaldehyde reagents available from commercial sources. Often these five types are described ambiguously or even interchangeably.[66] Thus, when paraformaldehyde purchased from Aldrich was used the reaction was successful. When paraformaldehyde purchased from Acros was used no reaction occurred.

The dialdehyde from the Mannich reaction may be isolated, but the product is a viscous oil that is difficult to work with. Addition of a slight excess of hydroxylamine hydrochloride to the crude reaction mixture results in conversion of the aldehyde groups into oxime groups, with the product isolated as its HCl salt in crystalline form. Neutralization with one equivalent of NaOH provides the free oxime.

Hydrogenation of the oxime then produces the desired triamine in good yield. The patent, however, only describes in vague detail the conditions used to accomplish

the hydrogenation.[64] A wide range of temperatures and pressures were suggested, as well as a variety of catalysts and no mention was made of the solvent used. Eventually, the proper conditions hinted at in the patent were discovered, along with an appropriate choice of solvent.

Primary amines formed during the hydrogenation are often susceptible to further reaction under the conditions used. One method of countering these side reactions is to perform the reaction under acidic conditions, trapping the amine as its salt as soon as it is formed.[67] Acidic conditions would require additional steps to isolate the free amine, however. Another common strategy is to perform the reaction in the presence of ammonia, thereby shifting the equilibrium of the side reactions in favor of the primary amine.[68] Thus, the hydrogenation was carried out in a mixture of ethanol and aqueous ammonia resulting in isolation of **15** and **18** in good yields.

Conversion of the triamines to bicyclic guanidines is accomplished by reaction with 1 equivalent of CS_2 in *p*-xylene. The guanidines do not sublime, as do Hhpp or its ring-size derivatives, but they are insoluble in acetonitrile and any impurities generated in the reaction may be washed away by this solvent.

Both of these alkyl derivatives, **16** and **19**, are soluble in the same solvents that Hhpp is. However, while HTMhpp shows only a slight improvement in solubility, the effect of the ethyl groups on the solubility of HTEhpp is quite pronounced. Large quantities of the compound dissolve in small volumes of common solvents such as benzene and THF. Even solvents not capable of dissolving Hhpp, namely hexanes and ether, are capable of dissolving HTEhpp.

Inorganic Syntheses. Both ligands readily form paddlewheel complexes with dimolybdenum units through reaction of their lithiated salts with $Mo_2(O_2CCF_3)_4$ in THF. The improvement in solubility afforded by these ligands is immediately apparent, as the solution rapidly darkens but no precipitate forms. The product is isolated by placing the reaction mixture in a freezer at -20 ºC for 1 week and then decanting the THF solution away from the resulting solid. Another method used was the removal of the THF solvent under vacuum followed by addition of toluene to the resulting solid, filtration of the mixture through Celite to separate the dissolved compound from the insoluble LiO_2CCF_3 and removal of the solvent under vacuum. X-ray quality crystals of $Mo_2(TMhpp)_4$ were isolated by placing a saturated THF solution of **20** in a freezer at -20 ºC for 1 week, whereas crystals of $Mo_2(TEhpp)_4$ were prepared by layering a THF solution of **23** with acetonitrile. Diffusion of the layers was complete after 2 weeks and the crystals were then isolated.

The Mo_2^{4+} species are readily oxidized to Mo_2^{5+} by dissolution in CH_2Cl_2. Layering CH_2Cl_2 solutions of $Mo_2(TMhpp)_4Cl$ with hexanes results in complete diffusion with no precipitate formed. Therefore, the CH_2Cl_2 solution was treated with 1 equivalent of K(TFPB) to provide a large anion which would better pack with the paddlewheel cation. Within 5 min a colorless precipitate of KCl was observed and the mixture was filtered through Celite. The solution was layered with hexanes and crystals of $Mo_2(TMhpp)_4(TFPB)$, **21**, and **21**·CH_2Cl_2, were observed the next day. These crystals were isolated after 1 week in good yield.

The preparation of $Mo_2(TMhpp)_4(TFPB)_2$, **22**, was effected in a similar manner. $Mo_2(TMhpp)_4$ was dissolved in CH_2Cl_2 and briefly exposed to air. After purging the flask of air and the placing the solution under a nitrogen atmosphere, 2 equivalents of K(TFPB) were added. Within 5 min a colorless precipitate of KCl formed and the mixture was filtered through Celite. The solution was then layered with hexanes and the resulting crystals harvested after 2 weeks.

Preparation of the oxidized forms of $Mo_2(TEhpp)_4$ has also been performed using similar strategies as for the oxidation of $Mo_2(TMhpp)_4$. These compounds have proven to be exceedingly soluble in most solvents. Crystals of **24**·2DMSO were prepared by layering a CH_2Cl_2 solution of **24** with DMSO. A crystalline sample of **26** has not yet been obtained.

Crystallographic Studies. Compounds **14** and **17**, as their HCl salts, both readily form crystals suitable for X-ray diffraction. Their structures are shown in Figure 17. The interatomic distances and angles are typical for the atoms found in their respective environments. The presence of the Cl^- ion proves the ionic nature of the compound, and hydrogen bonding is present between the Cl^- ion and the hydrogen atoms on the oxime groups. This is confirmed by the Cl–O distance, 3.054(1) Å for **14**·HCl and 3.098(1) Å for **17**·HCl which is shorter than the sum of the van der Waals radii by 6.5% and 5%, respectively.[60] Crystals of the neutral oxime, **14**, are also suitable for X-ray diffraction. The structure is identical to the organic portion of **14**·HCl. Table 12 provides a listing of interatomic distances.

Table 12. Selected Interatomic Distances in **14**, **14**·HCl and **17**·HCl.				
Compound	N(1)–C(1)	N(2)–C(3)	N(2)–O(1)	O(1)–Cl(1)
14	1.449[4]	1.261[4]	1.416[4]	–
14·HCl	1.502(2)	1.261(2)	1.405(2)	3.054(1)
17·HCl	1.503(2)	1.258(2)	1.409(2)	3.098(1)

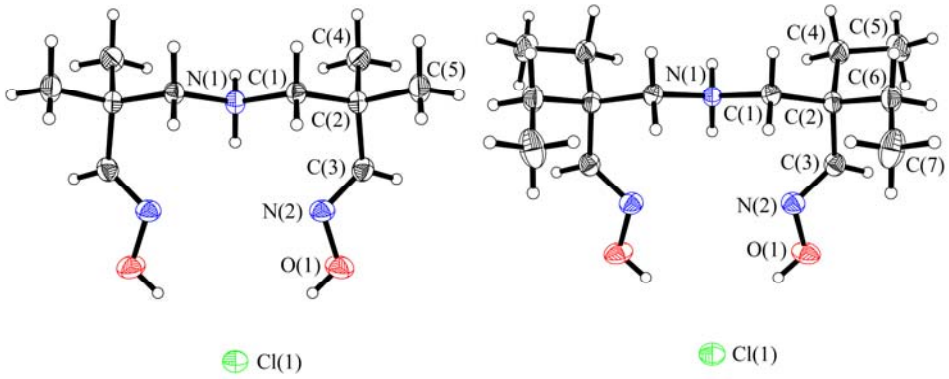

(a) (b)

Figure 17. Thermal ellipsoid plots of **14**·HCl (a) and **17**·HCl·H_2O (b). Ellipsoids are drawn at the 50% probability level. Solvent molecules are omitted for clarity.

The triamines **15** and **18**, although they are liquids, readily form crystals through reaction with $Cd(NO_3)_2$. Two triamines chelate the Cd^{2+} cation in a slightly distorted octahedron as seen in Figure 21. For the triamines, the interatomic distances and angles are typical for the atoms found in their respective environments.

This is not the first time $Cd(NO_3)_2$ has been used to obtain the structure of a triamine. The structures of (3-aminopropyl)-1,3-propanediamine, (2-aminoethyl)-1,3-propanediamine, and diethylene triamine, the triamines used to prepare Hhpp, Htbn and

Htbo respectively, have been studied in this manner.[69] The structures are similar to the two shown in Figure 18. Table 13 provides a list of Cd–N distances.

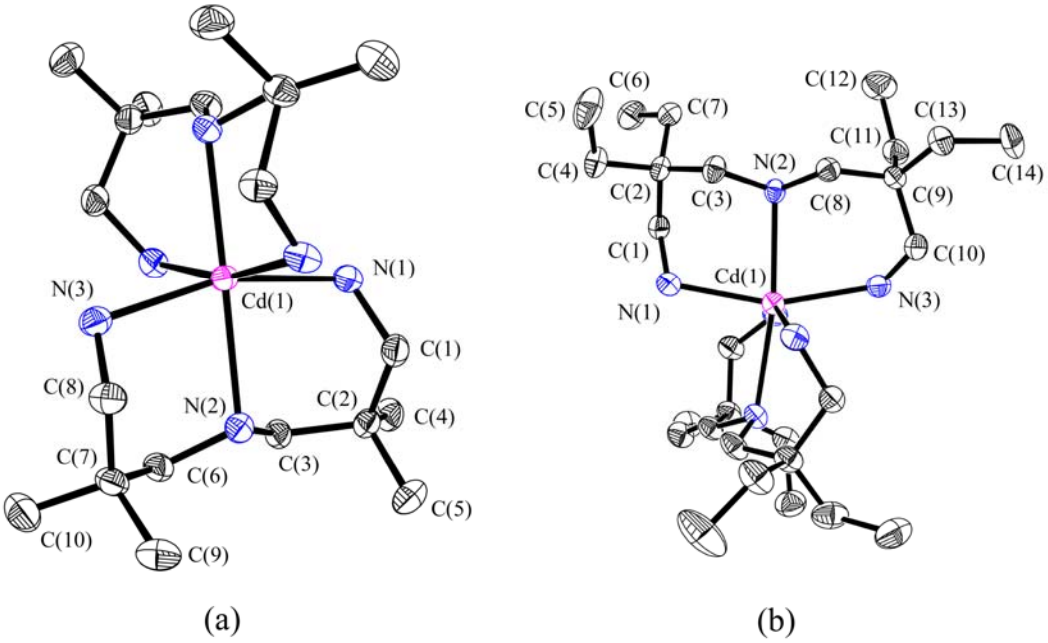

Figure 18. Thermal ellipsoid plots of Cd(**15**)$_2$(NO$_3$)$_2$ (a) and Cd(**18**)$_2$(NO$_3$)$_2$·EtOH (b). Ellipsoids are drawn at the 50% probability level. Solvent molecules and hydrogen atoms omitted for clarity.

Table 13. Cd–N Distances in Cd(**X**)$_2^{2+}$ Complexes.

X	Cd–N(1)	Cd–(N2)	Cd–N(3)	Ref
(3-aminopropyl)-1,3-propanediamine	2.351[5]	2.394[5]	2.385[4]	69
(2-aminoethyl)-1,3-propanediamine	2.339[6]	2.406[8]	2.375[4]	69
ethylenediamine	2.340(2)	2.431(2)	2.336(2)	69
15	2.375[4]	2.456[3]	2.357[4]	this work
18	2.331[3]	2.490[3]	2.343[3]	this work

Evaporation of a *p*-xylene solution of **16** results in microcrystalline needles unsuitable for X-ray diffraction. Therefore, an ethanol solution of **16** was allowed to evaporate in air. During this evaporation, **16** reacted with components of the atmosphere (H_2O and CO_2) and plate crystals of $[H_2TMhpp][HCO_3]$, suitable for X-ray diffraction studies, formed. The structure is shown in Figure 19. The C–C distances and angles are typical and the C(4)–N distances are approximately 1.33 Å which is longer than a typical C–N double bond, but shorter than a typical C–N single bond. Hydrogen bonding exists between the H_2TMhpp^+ cation and the bicarbonate anion as well as between bicarbonate atoms.

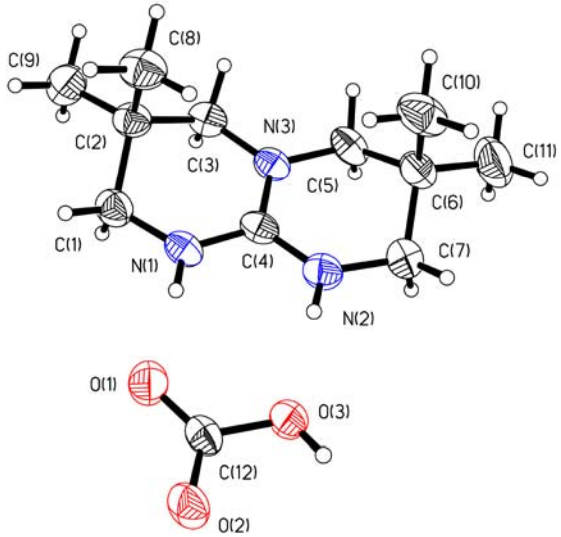

Figure 19. Thermal ellipsoid plot of $[H_2TMhpp][HCO_3]$. Ellipsoids are drawn at the 50% probability level. N(1)–C(4) = 1.334(2) Å, N(2) –C(4) = 1.335(2) Å, N(3) –C(4) = 1.333(2) Å. N(1) –C(4) –N(2) = 118.3(2)°, N(1) –C(4) –N(3) = 121.0(2)°, N(2) –C(4) –N(3) = 120.6(2)°.

The thermal ellipsoid plot of **19** is shown in Figure 20. Again, the C–C distances and angles are typical and the C(4)–N distances lie between the values for a C–N double bond and C–N single bond. The sum of the N–C(4)–N angles is 360° indicating sp^2-hybridization. The HTEhpp molecules, **19**, form centrosymmetric dimers through hydrogen bonding.

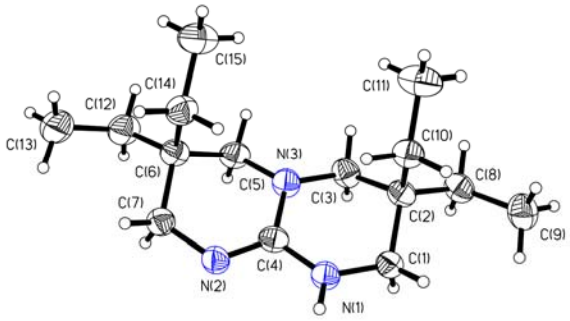

Figure 20. Thermal ellipsoid plot of **19**. Ellipsoids are drawn at the 50% probability level. N(1)–C(4) = 1.355(2) Å, N(2) –C(4) = 1.299(2) Å, N(3) –C(4) = 1.382(2) Å. N(1) –C(4) –N(2) = 118.2(1)°, N(1) –C(4) –N(3) = 117.3(1)°, N(2) –C(4) –N(3) = 124.4(1)°.

Figure 21 shows the thermal ellipsoid plot of $Mo_2(TMhpp)_4$, **20**, with selected bond distances and angles found in the caption. The Mo–Mo distance (2.0627(7) Å) is slightly shorter than that found in $Mo_2(hpp)_4$ (2.067(1) Å).[12a] The carbon atoms in the outer periphery of the ligand have typical C–C bond distances and angles. The atoms of the guanidine core have C–N distances that suggest delocalization. However, the planarity of the core is distorted as can be easily seen when the compound is viewed along the Mo–Mo axis as in Figure 24(b). The bridgehead nitrogen atom in the

guanidine core, N(3), is out of the plane of the other guanidine core atoms by approximately 0.298 Å.

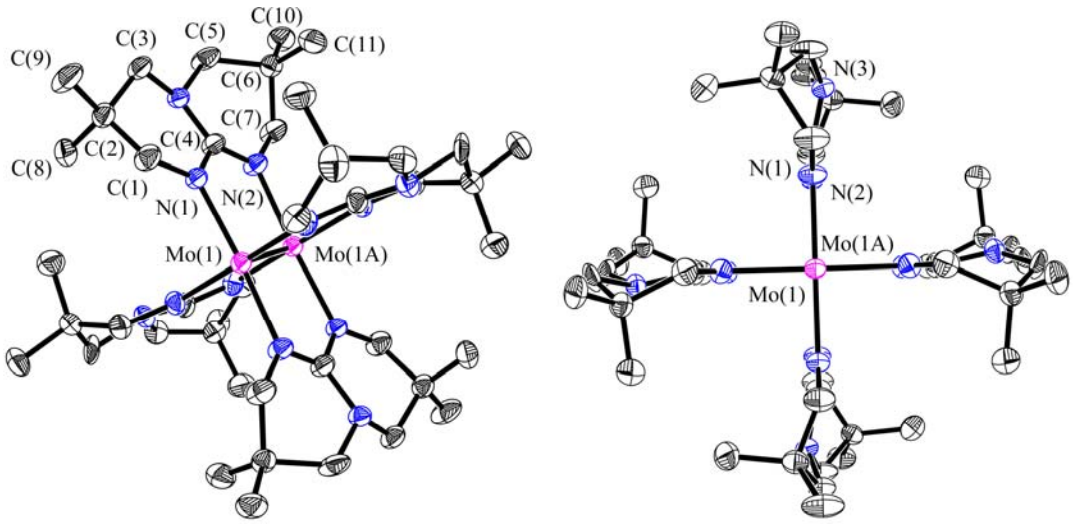

Figure 21. Thermal ellipsoid plot of **20** (left) and a view along the Mo–Mo axis (right). Ellipsoids are drawn at the 50% probability level. Hydrogen atoms have been removed for clarity. Mo(1)–Mo(1A) = 2.0627(7) Å, Mo–N(av) = 2.145[5] Å. Mo–Mo–N(av) = 92.9[1]°.

One consequence of this deviation is the disorder found in the ligands, generated by a two-fold axis that runs along the Mo–Mo axis and a mirror plane that is perpendicular to the Mo–Mo axis. While disorder of the carbon atoms in the outer periphery of hpp is commonly encountered, disorder of the planar guanidine core is not. The non-planar nature of the guanidine core in $Mo_2(TMhpp)_4$ gives rise to disorder of each bridgehead nitrogen over two positions.

Figure 22 shows an overlay of the hpp ligand of $Mo_2(hpp)_4$ and the TMhpp ligand of $Mo_2(TMhpp)_4$. The disorder of the TMhpp ligand in **20** makes the conformation of the ligand uncertain, but if a chair conformation is assumed, which is the typical conformation of hpp in dimetal complexes, then Figure 22 suggests the top nitrogen is not only out of the plane of the rest of the guanidine core, it is also twisted by approximately 18° such that the p-orbital where the lone pair of the nitrogen atom resides is not as readily available for interaction with the rest of the core.

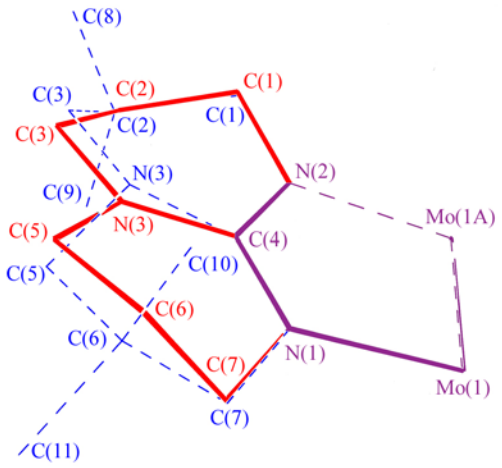

Figure 22. An overlay of the ligands in $Mo_2(hpp)_4$ and $Mo_2(TMhpp)_4$. Bonds belonging exclusively to the hpp ligand are in red while those belonging to TMhpp are in blue. Bonds which were deliberately overlapped to generate a common plane are in purple.

The structure of $Mo_2(TMhpp)_4(TFPB)$, from **21**·CH_2Cl_2, is shown as a thermal ellipsoid plot in Figure 23. The compound crystallized in space group $P\bar{1}$ with two crystallogaphically independent well-ordered paddlewheels, each residing on a center of

inversion. The Mo–Mo distances found in each paddlewheel cation are not very different (2.097(2) Å and 2.106(2) Å). The average Mo–Mo distance (2.102[3] Å) shows an increase of 0.039 Å from the distance in $Mo_2(TMhpp)_4$. This increase is slightly less than that found between $Mo_2(hpp)_4Cl$ and $Mo_2(hpp)_4$ (0.049 Å).[66] The guanidine core of the ligand is still distorted from planarity but only by approximately 0.10 Å. The +1 charge of the cation is offset by the presence of a TFPB anion, also commonly referred to as BArF. The closest interaction between a fluorine atom and a molybdenum atom is 3.555(9) Å, too long to imply a bonding interaction. The dichloromethane molecule is disordered over two positions and the fluorine atoms of the TFPB anion are highly disordered, resulting in higher than usual figures of merit (*R*1 and *wR*2).

Another crystal, harvested from the same reaction batch, was analyzed by X-ray diffraction and solved as **21** (without interstitial solvent). The only significant difference between this structure and **21**·CH_2Cl_2 is the presence or absence of a dichloromethane molecule. The two independent Mo–Mo distances in the well-ordered paddlewheels are identical with a value of 2.092(2) Å. This is slightly shorter (0.010 Å) than the average value observed in **21**·CH_2Cl_2 and is an increase of only 0.029 Å from the Mo–Mo distance in **20.** This crystal also has considerable disorder of the fluorine atoms in the TFPB anion,resulting again in higher than usual figures of merit, similar to those observed in **21**·CH_2Cl_2.

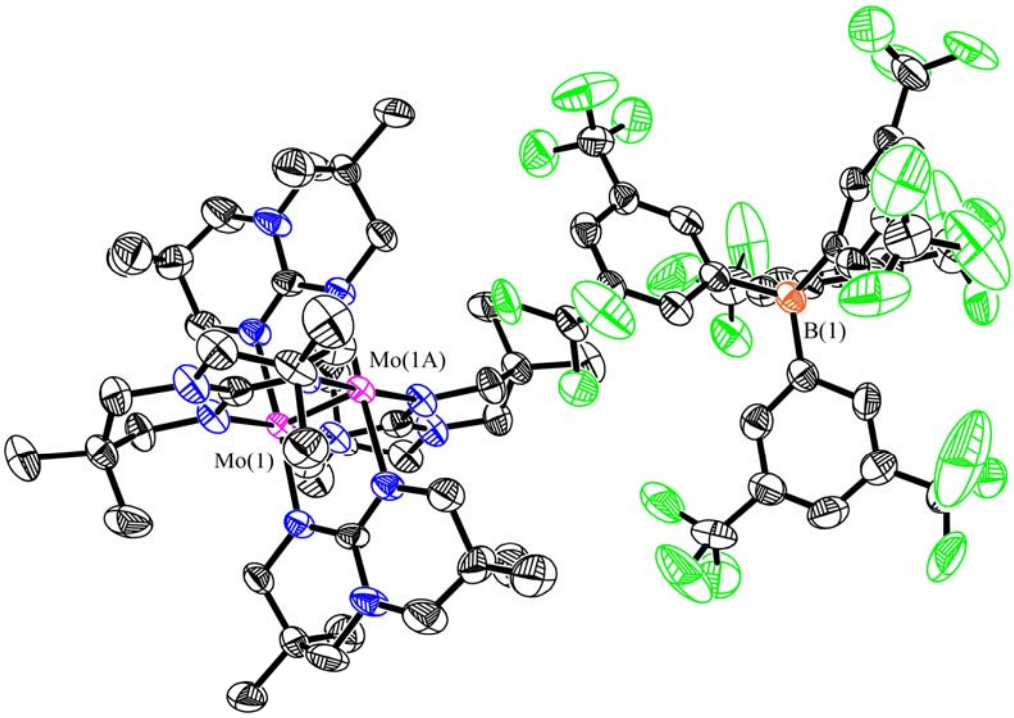

Figure 23. Thermal ellipsoid plot of **21**·CH_2Cl_2. Ellipsoids are drawn at the 50% probability level. Solvent molecules and hydrogen atoms are removed for clarity. Mo(1)–Mo(1A) = 2.097(2) Å, Mo(2)–Mo(2A) = 2.106(2) Å, Mo(1)–N(av) = 2.12[2] Å, Mo(2)–N(av) = 2.11[2] Å. Mo–Mo–N(av) = 92.6[8]°.

The structure of $Mo_2(TMhpp)_4(TFPB)_2$, **22**, is shown as a thermal ellipsoid plot in Figure 24 with selected bond distances and angles found in the caption. The Mo–Mo distance (2.1222(7) Å) shows an increase from the distance in $Mo_2(TMhpp)_4$ of 0.059 Å. As with the change in distance between **20** and **21**, this change is considerably smaller than the change in distance found between $Mo_2(hpp)_4Cl_2$ and $Mo_2(hpp)_4$ (0.107 Å).[66] The guanidine core has returned to an essentially planar configuration, the bridgehead nitrogen atom deviating from the plane of the other guanidine core atoms by only 0.041

Å. The fluorine atoms of the TFPB anion are again disordered, but the closest Mo–F distance is only 3.237(6) Å.

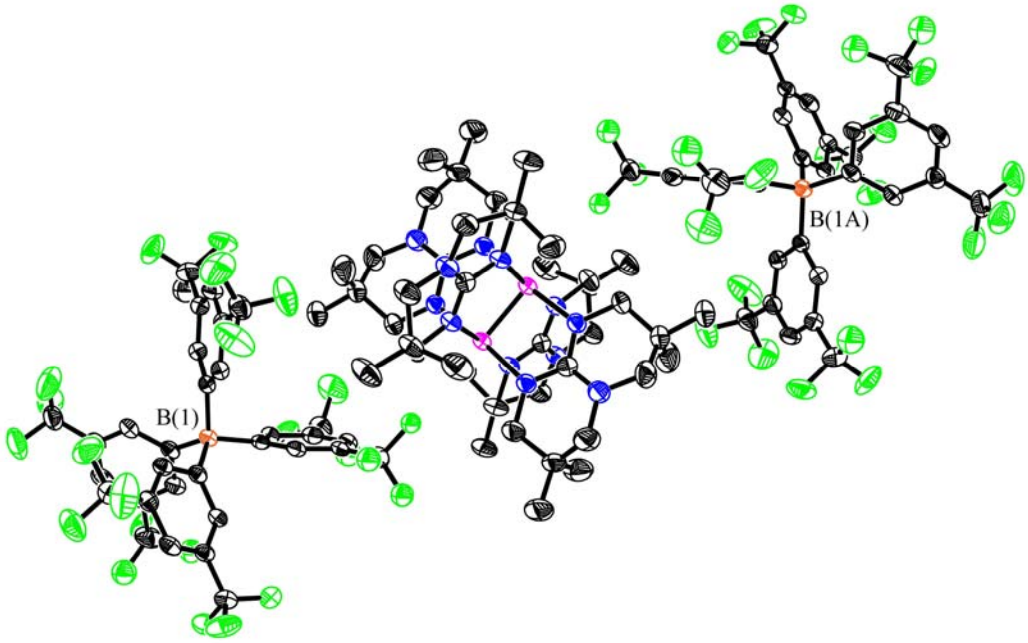

Figure 24. Thermal ellipsoid plot of **22**. Ellipsoids are drawn at the 50% probability level. Hydrogen atoms are removed for clarity. Mo(1)–Mo(1A) = 2.1222(7) Å, Mo–N(av) = 2.081[6] Å. Mo–Mo–N(av) = 92.43[6]°.

The thermal ellipsoid plot of $Mo_2(TEhpp)_4$, **23**, is shown in Figure 25. Unlike $Mo_2(TMhpp)_4$ the structure is well ordered with the ligands adopting a boat conformation. Like the structure of $Mo_2(TMhpp)_4$, though, the guanidine core is distorted from planarity. In this case the bridgehead nitrogen atom is out of the plane of the rest of the guanidine core by 0.097 Å. The Mo–Mo distance is 2.0599(5) Å, just at the threshold of 2.06 Å established as the shortest Mo–Mo distance found in

paddlewheel complexes.[61] Despite the non-planarity of the guanidine core, the structure is well ordered with two molecules contained in the unit cell and related by an inversion center.

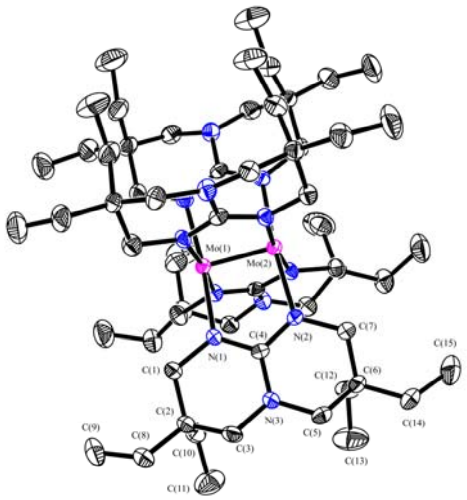

Figure 25. Thermal ellipsoid plot of **23**. Ellipsoids are drawn at the 50% probability level. Hydrogen atoms removed for clarity. Mo(1)–Mo(2) = 2.0599(5) Å, Mo–N(av) = 2.151[8] Å. Mo–Mo–N(av) = 92.9[2]°.

The thermal ellipsoid plot of $Mo_2(TEhpp)_4(TFPB)$ from **24**·2DMSO is shown in Figure 26. There are two crystallographically independent paddlewheels, one residing on a 4-fold axis and the other residing on a $\bar{4}$ axis. The two independent Mo–Mo distances are not significantly different (2.115(2) Å and 2.116(2) Å). The dimetal core and bicyclic system of the paddlewheels are well ordered. However, most of the ethyl substituents are disordered over two positions. The two crystallographically independent TFPB anions also reside on special positions. This results in disorder of each anion over

two positions. The commonly encountered disorder of the fluorine atoms among two orientations in the CF_3 units is also observed, which makes the fluorine atoms disordered over a total of four positions. Two disordered DMSO molecules are located along the Mo–Mo axis with the shortest Mo–O distance at 2.882(1) Å. The Mo–Mo distance is increased from that in **23** by 0.057 Å which is comparable to the change in distance observed between $Mo_2(hpp)_4Cl$ and $Mo_2(hpp)_4$ (0.061 Å),[58] but is longer than the change in distance observed between $Mo_2(TMhpp)_4(TFPB)$ and $Mo_2(TMhpp)_4$ (0.029 Å).

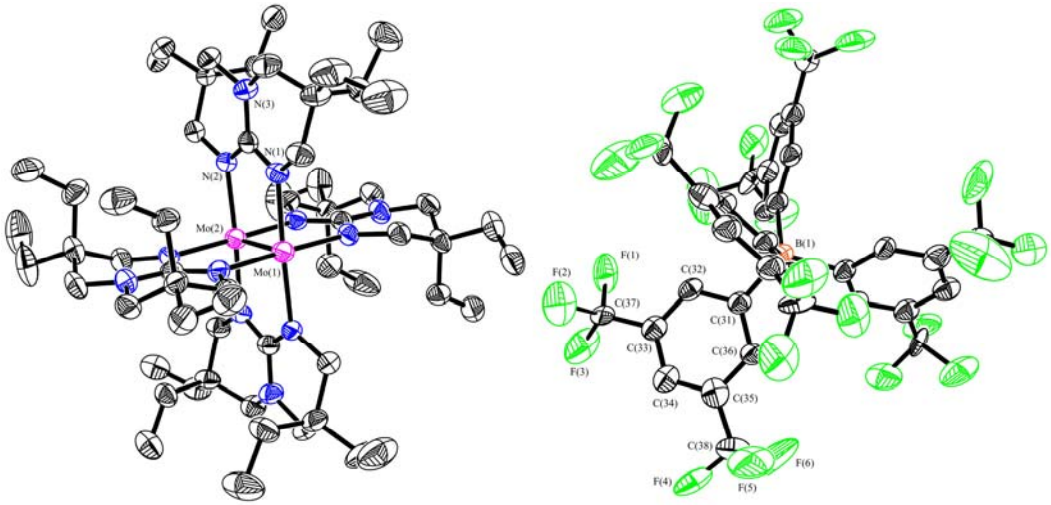

Figure 26. Thermal ellipsoid plot of **24** from **24**·2DMSO. Ellipsoids are drawn at the 30% probability level. Hydrogen atoms and solvent molecules are removed for clarity. Disorder is not shown. Mo(1)–Mo(2) = 2.115(2) Å, Mo(3)–Mo(3A) = 2.116(2) Å, Mo–N(av) = 2.13[1] Å, Mo(1)–O(1) = 2.882(1) Å, Mo(2)–O(2) = 3.604(1) Å, Mo(3)–O(3) = 3.086(1) Å. Mo–Mo–N(av) = 92.3[2]°.

Planarity of the Guanidine Core. Table 14 provides a listing of relevant interatomic distances for compounds **20**-**24** and $Mo_2(hpp)_4$. One might initially assume the deviation from planarity seen for **20** and **23** is due to steric hinderence which might be caused by the hydrogen atoms of the alkyl groups and the hydrogen atoms on the rings of the ligands. If this were indeed the case the distortion would persist regardless of changes in the dimetal core, as such changes should not significantly affect the structure of the outer periphery of the bicyclic ring system. As can be seen in Table 12, however, the deviation from planarity decreases as the oxidation state increases in the $Mo_2(TMhpp)_4^{n+}$ (n = 0, 1, 2) series. This suggests the distortion may be associated with the ligand's degree of interaction with the δ-orbital of the dimolybdenum unit, since this is the orbital from which electrons are removed during oxidation.

Table 14. Mo–Mo Distances and Deviation of the Guanidine Core from Planarity for Various Compounds.

Compound	Mo–Mo (Å)[a]	bond order	charge n for Mo_2^{n+}	planar deviation (Å)
$Mo_2(hpp)_4$	2.067(1)	4	4	0.022
$Mo_2(TMhpp)_4$	2.063(1)	4	4	0.298
$Mo_2(TMhpp)_4(TFPB)$	2.092(2)	3.5	5	0.082
$Mo_2(TMhpp)_4(TFPB)_2$	2.122(1)	3	6	0.041
$Mo_2(TEhpp)_4$	2.060(1)	4	4	0.097
$Mo_2(TEhpp)_4(TFPB)\cdot 2DMSO$	2.116(2)	3.5	5	0.093

[a] Distances rounded to the third decimal place.

DFT calculations for $Mo_2(hpp)_4$ show the hpp ligand interacts with the δ-orbital of the dimolybdenum unit very strongly, contributing about 40% of the electron

density.[70,71] The calculation shows the guanidine core as the sole contributor of the ligand interaction. Similar calculations on the paddlewheel compounds using the alkyl derivative ligands are too cumbersome, so calculations have been carried out on the TMhpp anion by itself.[71] These calculations show that the methyl groups contribute about 5% of the electron density found in the orbital which would interact with the dimolybdenum unit's δ orbital.

The smaller increase in Mo–Mo bond lengths upon oxidation of $Mo_2(TMhpp)_4$ to $Mo_2(TMhpp)_4^{2+}$ compared to those found in the analogous $Mo_2(hpp)_4^{0/2+}$ pair is attributable to the presence of axial chlorine atoms in the latter case.

Electrochemistry. The CV and DPV of $Mo_2(TMhpp)_4$ and $Mo_2(TEhpp)_4$ were observed using THF solutions of approximately 1 mM concentration. The DPVs of these two compounds are depicted in Figure 27. The two peaks observed at -1.076 V and -0.306 V for $Mo_2(TMhpp)_4$ and at -1.168 V and -0.388 V for $Mo_2(TEhpp)_4$ are related to successive one-electron oxidations corresponding to:

$$Mo_2^{4+} \overset{-e^-}{\rightleftharpoons} Mo_2^{5+}$$

$$Mo_2^{5+} \overset{-e^-}{\rightleftharpoons} Mo_2^{6+}$$

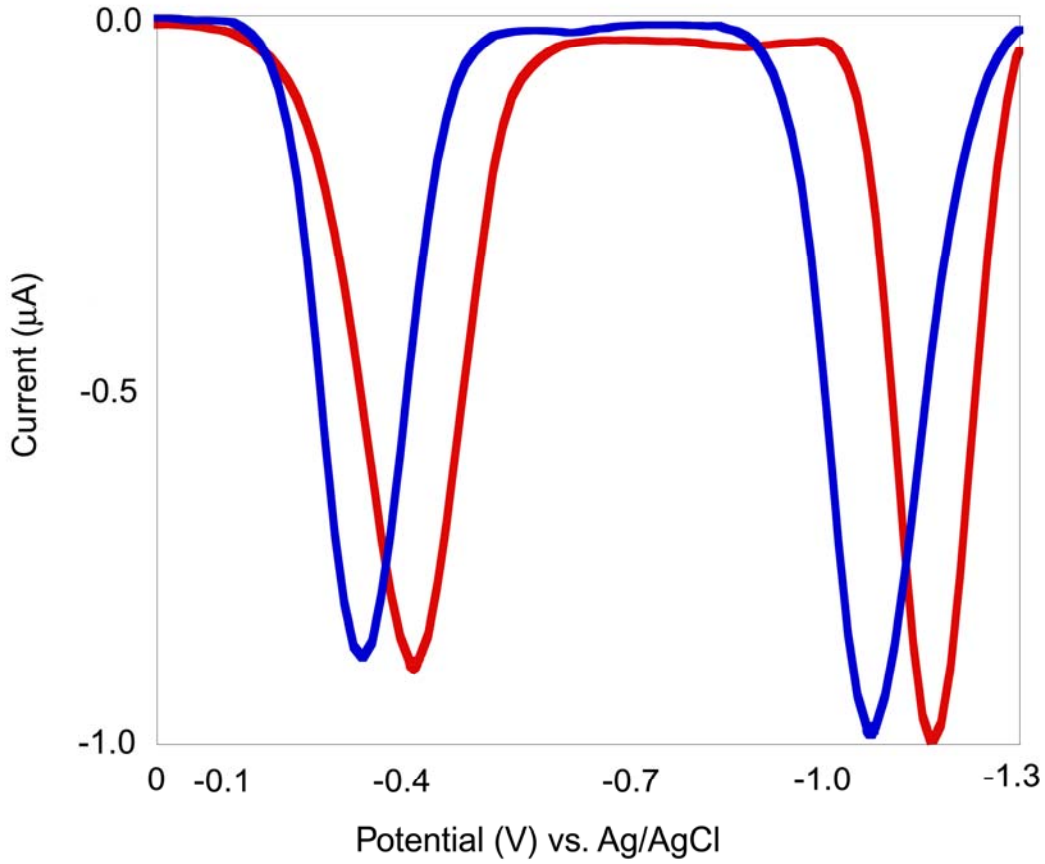

Figure 27. Differential pulse voltammograms of $Mo_2(TMhpp)_4$ (blue) and $Mo_2(TEhpp)_4$ (red).

For each of these voltammograms, the Fc/Fc^+ couple was measured at 0.663 V under similar conditions. This places the potentials versus ferrocene at the values seen in Table 15, which also lists the potential versus ferrocene for $Mo_2(hpp)_4$. All three compounds have extremely negative $E_{1/2}^{(1)}$ potentials. These negative potentials mean that simple dissolution in CH_2Cl_2 leads to the formation of Mo_2^{5+} species (the reduction

potential of CH_2Cl_2 has previously been measured at -1.638 V versus ferrocene).[13] The $E_{1/2}^{(2)}$ for **11** also shows that oxidation to the Mo_2^{6+} state is quite easy and may be accomplished by O_2 or other oxidizing agents.

Table 15. Redox Potential Values for $Mo_2(hpp)_4$, $Mo_2(TMhpp)_4$ and $Mo_2(TEhpp)_4$.

	$E_{1/2}^{(1)}$ (Mo_2^{4+}/Mo_2^{5+})		$E_{1/2}^{(2)}$ (Mo_2^{5+}/Mo_2^{6+})		
	Ag/AgCl	Fc/Fc^+	Ag/AgCl	Fc/Fc^+	reference
$Mo_2(hpp)_4$[a]	-1.271	-1.795	-0.444	-0.968	66
$Mo_2(TMhpp)_4$[b]	-1.076	-1.739	-0.306	-0.969	this work
$Mo_2(TEhpp)_4$[b]	-1.168	-1.831	-0.388	-1.051	this work

[a] Bu_4NBF_4·3toluene
[b] THF/Bu_4NBF_4 (0.1 M)

The $\Delta E_{1/2}$ values defined as $E_{1/2}^{(2)} - E_{1/2}^{(1)}$ of both compounds allow for the calculation of the conproportionation constant[50] $K_C = \exp(\Delta E_{1/2}/25.69)$ for the process

$$Mo_2^{6+} + Mo_2^{4+} \rightleftharpoons Mo_2^{5+}$$

The $\Delta E_{1/2}$ for the $Mo_2(TMhpp)_4$ system is 770 mV giving $K_C = 1.04 \times 10^{13}$. For the $Mo_2(TEhpp)_4$ system, the $\Delta E_{1/2}$ is 780 mV with $K_C = 1.53 \times 10^{13}$. As with the $Mo_2(hpp)_4$ system ($K_C = 9.56\times10^{13}$) the large values are not due to the instability of the Mo_2^{6+} species, but the great reactivity of the Mo_2^{4+} species toward even very mild oxidizing agents such as CH_2Cl_2.[66]

Magnetic Behavior. Both $Mo_2(TMhpp)_4$, **20**, and $Mo_2(TEhpp)_4$, **23**, are reasonably soluble in common NMR solvents, and their ^1H spectra have been observed in C_6D_6 solutions. The ^1H NMR spectra of the Mo_2^{6+} species **22** and **25** have also been observed in CD_2Cl_2 solutions. All of the compounds give clean spectra and because all

of the signals are in the normal regions and of normal sharpness, it may be concluded that all four compounds are diamagnetic.

The singly oxidized species **21** and **24** show the expected single unpaired electron as evidenced by measurements of magnetic susceptibility. The *g* values calculated from these measurements are 1.91 for **21** and 1.92 for **24**, similar to that found for $Mo_2(hpp)_4Cl$ ($g = 1.94$),[66] and are less than 2.00 due to spin-orbit coupling associated with the molybdenum atoms.

Supplemental Information. A table of information for the LMSB crystallographic database and selected NMR and UV-Vis spectra are found in Appendix B.

CHAPTER V

HOMOLOGS OF Hhpp WITH LARGER RINGS (Htbd AND Htbu) AND THEIR DIMOLYBDENUM COMPLEXES

Introduction

This chapter concerns the development of derivatives of Hhpp that contain 7-member rings, namely 1,5,6-Triazabicyclo[3.5.0]unadec-5-ene (Htbu, **XXIII**) and 1,4,6-Triazabicyclo[3.5.0]dec-4-ene (Htbd, **XXIV**). The strategy of reacting the appropriate triamine with carbon disulfide in a 1:1 ratio does not work well for the formation of 7-membered ring systems. An alternate synthetic route, which ensures the formation of the 7-membered ring is used. The intermediates in this process have been characterized by a variety of methods including X-ray crystallography. The dimolybdenum paddlewheel complexes **XXV** and **XXVI** are prepared by reacting $Mo_2(O_2CCF_3)_4$ with the lithium salt of the appropriate ligand. The compounds to be discussed in this chapter are listed in Table 16.

Table 16. Listing of Compounds to be Discussed in Chapter V.

Compound	Formula	Number
1,3-Diazacycloheptane-2-thione	$C_5H_{10}N_2S$	**26**
2-Methylmercapto-Δ^2-1,3-diazacycloheptane	$C_6H_{12}N_2S$	**27**
2-(γ-Hydroxypropylamino)-Δ^2-1,3-diazacycloheptene	$C_8H_{17}N_3O$	**28**
Htbu (**XXIII**)	$C_8H_{15}N_3$	**29**
2(β-Hydroxyethylamino)-Δ^2-1,3-diazacycloheptene	$C_7H_{15}N_3O$	**30**
Htbd(**XXIV**)	$C_7H_{13}N_3$	**31**
$Mo_2(tbd)_4$ (**XXV**)	$Mo_2(C_7H_{12}N_3)_4$	**32**
$Mo_2(tbd)_4Cl$	$Mo_2(C_7H_{12}N_3)_4Cl$	**33**
$Mo_2(tbd)_4Cl_2$	$Mo_2(C_7H_{12}N_3)_4Cl_2$	**34**
$Mo_2(tbu)_4$ (**XXVI**)	$Mo_2(C_8H_{15}N_3)_4$	**35**
$Mo_2(tbu)_4Cl$	$Mo_2(C_8H_{15}N_3)_4Cl$	**36**
$Mo_2(tbu)_4(TFPB)_2$	$[Mo_2(C_8H_{15}N_3)_4][B(C_8H_3F_6)_4]_2$	**37**

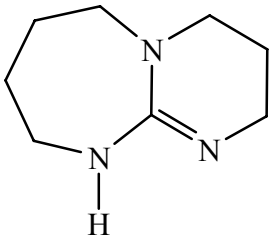

XXIII

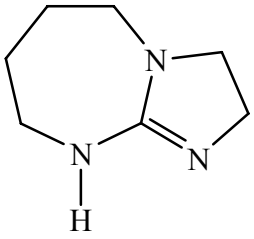

XIV

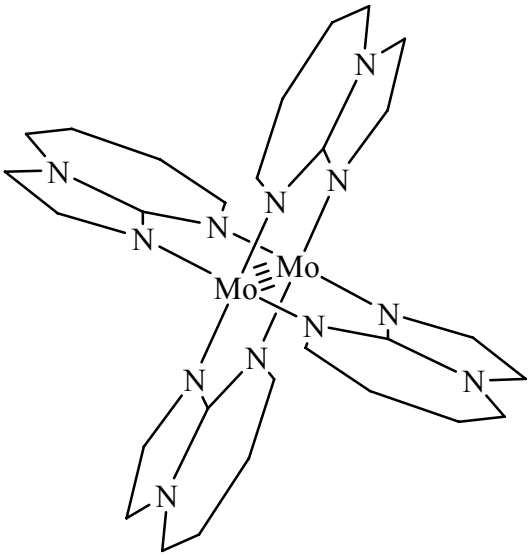

XV

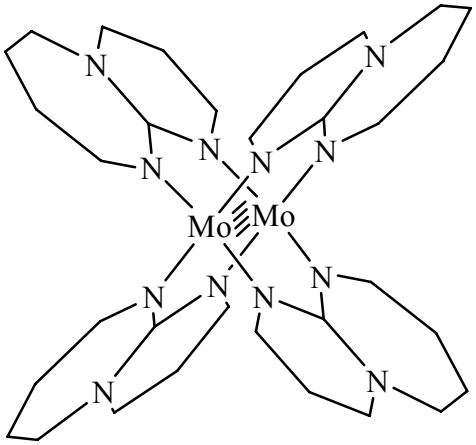

XVI

Experimental Section

General Procedures. All procedures were performed under a nitrogen atmosphere unless otherwise noted and all glassware was oven-dried prior to use. 1,4-diaminobutane, CS_2, aminoethanol, 3-amino-1-propanol, iodomethane, PBr_3, and KOH were purchased from Aldrich and used as received. Ether, ethanol, *p*-xylene, methanol, hexanes and acetonitrile were purchased from Aldrich and dried over 3 Å

molecular sieves prior to use. The solvents THF, CH_2Cl_2, benzene, toluene and hexanes were also purchased from Aldrich and purified using a Glass Contour solvent system. BuLi (1.6 M in hexanes) was purchased from Acros and stored at -20 °C until used. $Mo_2(O_2CCF_3)_4$ and potassium tetra[3,5-bis(trifluoromethyl)phenyl]borate (K(TFPB)) were prepared according to published procedures.[52,63]

Physical Measurements. IR spectra were recorded using a Perkin Elmer 16PC FT-IR spectrometer or a Bruker Tensor 27 spectrometer. UV-Vis spectra were recorded on a Shimadzu UV-2501 PC spectrometer. ^{1}H NMR spectra were recorded on a Unity Plus 300 NMR spectrometer, using solvent peaks to reference chemical shifts (δ). Elemental analysis was performed by Robertson Microlit Laboratories, Inc., Madison, NJ, USA. Cyclic voltammetry and differential pulse voltammetry were recorded using a CH Instruments electrochemical analyzer with a 2 mm diameter Pt disk working electrode, Ag/AgCl reference electrode, and Pt wire auxillary electrode. Potentials are reported versus Ag/AgCl. Magnetic susceptibility was measured using a Johnson Matthey Mark II magnetic susceptibility balance.

X-ray Crystallography. Single crystals of **26**, **27**·HI, **28**·HI, **29**, **31**, **33**·2CH_2Cl_2, **34**, **35** and **36** were placed on a cryoloop using a minimum of silicone grease. Data for 3**6** were collected at 110 K on a Bruker GADDS area detector. For the others, data were collected at 213 K on a Bruker SMART area detector using the SMART and SAINT programs.[27,28] The crystal structures were solved via direct methods and refined using SHELXL-97.[29] Hydrogen atoms were placed at calculated positions. Non-hydrogen atoms were refined with anisotropic displacement parameters.

Cell parameters and refinement results for organic compounds are summarized in Table 17 while those for inorganic compounds are found in Table 18.

Table 17. Crystallographic Parameters for **26**, **27**·HI, **28**·HI, **29** and **31**.

Compound	**26**	**27**·HI	**28**·HI	**29**	**31**
Empirical Formula	$C_5H_{10}N_2S$	$C_6H_{13}IN_2S$	$C_8H_{18}IN_3O$	$C_8H_{15}N_3$	$C_7H_{13}N_3$
Formula Weight	130.21	272.14	299.15	153.23	139.20
Space Group	$P2_1/m$	$P2_12_12_1$	$P\bar{1}$	$P2_1/c$	$P\bar{1}$
a(Å)	5.042(2)	8.924(3)	9.482(1)	16.595(3)	5.937(3)
b(Å)	8.429(4)	10.537(3)	9.613(1)	10.949(2)	8.520(5)
c(Å)	8.108(4)	11.061(3)	14.523(2)	9.846(2)	8.671(5)
α(°)	90	90	98.683(2)	90	67.410(9)
β(°)	104.748(8)	90	91.420(2)	103.995(3)	73.54(1)
γ(°)	90	90	115.187(2)	90	71.570(9)
V ($Å^3$)	333.2(3)	1040.2(5)	1178.3(3)	1735.9(5)	377.6(4)
Z	2	4	4	8	2
d_{calc}(g/cm^3)	1.298	1.738	1.686	1.173	1.224
μ(mm^{-1})	0.381	3.222	2.690	0.074	0.078
T (K)	213	213	213	213	213
R1[a]	0.0428	0.0184	0.0245	0.0504	0.0541
wR2[b]	0.1129	0.0457	0.0612	0.1439	0.1547

[a] $R1 = \Sigma \| F_o | - | F_c \| / \Sigma | F_o |$

[b] $wR2 = [\Sigma[w(F_o^2 - F_c^2)^2] / \Sigma w(F_o^2)^2]^{1/2}$, $w = 1/[\sigma^2(F_o^2) + (aP)^2 + bP]$, where $P = [\max(0 \text{ or } F_o^2) + 2(F_c^2)]/3$

Table 18. Crystallographic Parameters for **33**·$2CH_2Cl_2$, **34**, **35** and **36**.				
Compound	**33**·$2CH_2Cl_2$	**34**	**35**	**36**
Empirical Formula	$C_{30}H_{52}Cl_5Mo_2N_{12}$	$C_{28}H_{48}Cl_2Mo_2N_{12}$	$C_{32}H_{56}Mo_2N_{12}$	$C_{32}H_{56}ClMo_2N_{12}$
Formula Weight	949.97	815.56	800.77	836.22
Space Group	$P\bar{1}$	*I4/m*	*C2/c*	*P4/ncc*
a(Å)	11.826(1)	10.068(2)	20.211(3)	14.190(1)
b(Å)	12.512(1)	10.068(2)	8.963(1)	14.190(1)
c(Å)	16.337(2)	15.797(5)	19.641(3)	17.504(3)
α(°)	98.855(2)	90	90	90
β(°)	104.043(2)	90	91.168(3)	90
γ(°)	117.894(2)	90	90	90
V ($Å^3$)	1969.1(3)	1601.1(6)	3557.2(10)	3524.3(6)
Z	2	2	4	4
d_{calc}(g/cm^3)	1.602	1.692	1.495	1.576
μ(mm^{-1})	1.016	0.992	0.746	6.859
T (K)	213	213	213	110
R1[a]	0.0408	0.0366	0.0510	0.0362
wR2[b]	0.1098	0.0763	0.1292	0.0860

[a] $R1 = \Sigma \| F_o | - | F_c \| / \Sigma | F_o |$
[b] $wR2 = [\Sigma[w(F_o^2 - F_c^2)^2] / \Sigma w(F_o^2)^2]^{1/2}$, $w = 1/[\sigma^2(F_o^2) + (aP)^2 + bP]$, where $P = [\max(0 \text{ or } F_o^2) + 2(F_c^2)]/3$

Preparation of 1,3-Diazacycloheptane-2-thione, 26. A 1 L round-bottom flask was charged with 100 g of 1,4-diaminobutane, 64.6 mL (81.8 g) of CS_2, 400 mL of ethanol and 300 mL of water. The mixture was refluxed overnight, during which the colorless precipitate that had formed dissolved into a colorless solution. The next day the solution was cooled to room temperature and placed in a freezer overnight at -20 °C. The colorless plate crystals which formed were filtered and washed with 100 mL of ether. These crystals were suitable for X-ray diffraction. ^{1}H NMR (DMSO, ppm): 7.78

(br s, 2H), 3.06 (mult., 4H), 1.57 (mult., 4H). Mass Spectrum (ESI^+): Calculated ($M+H^+$): 130 amu; found 130 amu. IR (KBr, cm^{-1}): 3218 (s), 2946 (s), 2680 (m), 1533 (s), 1452 (s), 1353 (s), 1322 (s), 1215 (s), 1107 (m), 1082 (m), 1002 (m), 946 (w), 922 (w), 887 (w), 812 (m), 757 (m), 642 (m), 581 (w), 555 (w), 525 (m).

2-Methylmercapto-Δ^2-1,3-diazacycloheptane hydroiodide, 27·HI. A 250 mL round-bottom flask was charged with 26 g (0.200 mmol) of **26**, 100 mL ethanol and 13 mL iodomethane. As the mixture was heated the solid dissolved and the solution was refluxed for 1 h. The solution was cooled to room temperature, 120 mL ether added and the solution placed in a freezer at -20 °C overnight. The next day, yellow needle crystals, suitable for X-ray diffraction were harvested. In the typical course of synthesis, this compound was prepared and used in situ for the following steps. ^1H NMR (DMSO, ppm): 9.45 (br s, 2H), 3.44 (mult., 4H), 3.34(s, 3H), 1.75 (mult., 4H). Mass spectrum (ESI^+) Calculated $(M - I^-)^+$: 145 amu; found 145 amu. IR (KBr, cm^{-1}): 3449 (s), 2972 (m), 1611 (s), 1456 (m), 1383 (m), 1357 (m), 1329 (m), 1292 (m), 1229 (m), 1073 (w), 1046 (w), 996 (w), 916 (w), 803 (m), 748 (m), 633 (m), 525 (w).

2-(γ-Hydroxypropylamino)-Δ^2-1,3-diazacycloheptene, 28. To an ethanol solution of **27** prepared as above 15.3 mL of 3-amino-1-propanol was added and the solution refluxed overnight. The next day, 11.25 g of KOH was added and reflux continued for 1 h. During this time, a colorless precipitate of KI formed. The mixture was cooled to room temperature and filtered. The solution was evaporated to dryness using a rotary evaporator resulting in a colorless oil. ^1H NMR (DMSO, ppm): 7.45 (br s, 2H), 3.42-3.13 (mult., 8H), 1.63-1.52 (mult., 6H). Mass spectrum (ESI^+): calculated

($M+H^+$) 172 amu, found 172 amu. IR (NaCl plates, cm^{-1}): 3304 (s), 2930 (s), 1638 (s), 1541 (s), 1440 (s), 1360 (s), 1332 (s), 1282 (s), 1238 (m), 1160 (w), 1051 (s), 1005 (s), 926 (w), 880 (w), 732 (w), 644 (w). Crystals of **28**·HI, as colorless plates suitable for X-ray diffraction, were prepared by layering an ethanol solution with ether.

1,5,6-Triazabicyclo[3.5.0]unadec-5-ene (Htbu), 29. A 250 mL round-bottom flask was charged with 5.00 g of **28**, 60 mL of $CHCl_3$, and 1.5 mL of PBr_3. The mixture was refluxed overnight, during which a yellow-orange precipitate formed and coated the bottom of the flask. The next day, 100 mL of methanol and 2.67 g of KOH was added and the mixture refluxed for 2 h. The mixture was then cooled to room temperature, filtered and the solution evaporated to dryness using a rotary evaporator. The resulting colorless paste was sublimed, and colorless plates of **29** formed on the cold finger. These crystals were suitable for X-ray diffraction. IR (KBr, cm^{-1}): 3255 (s), 3183 (s), 3123 (s), 3067 (s), 2931 (s), 1644 (s), 1499 (s), 1436 (s), 1360 (s), 1316 (s), 1282 (s), 1206 (m), 1152 (m), 1125 (w), 1099 (m), 1072 (w), 1029 (w), 1005 (m), 963 (m), 885 (m), 846 (m), 813 (w), 742 (w), 698 (w), 654 (m), 573 (w), 499 (w), 428 (w). ^1H NMR (C_6D_6, ppm): 3.36 (t, 2H), 3.24 (br s, 1H), 2.75 (m, 4H), 2.60 (t, 2H), 1.49 (p, 2H), 1.19 (m, 4H). Mass spectrum (ESI^+): calculated ($M+H^+$) 154 amu, found 154 amu.

2(β-Hydroxyethylamino)-Δ^2-1,3-diazacycloheptene, 30. To a solution of **28** prepared as above 12.1 mL of ethanolamine was added and the solution refluxed overnight. The next day, 11.25 g of KOH was added and reflux continued for 1 h. During this time a colorless precipitate of KI formed. The mixture was cooled to room temperature and filtered. The solution was evaporated to dryness using a rotary

evaporator resulting in a colorless oil. Mass spectrum (ESI^+): calculated ($M+H^+$) 158 amu, found 158 amu. IR (NaCl plates, cm^{-1}): 3299 (s), 2943 (s), 1700 (m), 1640 (s), 1510 (m), 1442 (m), 1363 (m), 1331 (m), 1282 (m), 1237 (w), 1175 (w), 1114 (w), 1065 (m), 1008 (w), 718 (w).

1,4,6-Triazabicyclo[3.5.0]dec-4-ene (Htbd), 31. A 250 mL round-bottom flask was charged with 5.00 g of **30**, 60 mL of $CHCl_3$ and 1.5 mL of PBr_3. The mixture was refluxed overnight, during which a yellow-orange precipitate formed and coated the bottom of the flask. The next day 100 mL of methanol and 2.67 g of KOH was added and the mixture refluxed for 2 h. The mixture was then cooled to room temperature, filtered and the solution evaporated to dryness using a rotary evaporator. The resulting colorless paste was sublimed, and colorless needles of **31** formed on the cold finger. These crystals were suitable for X-ray diffraction. IR (KBr, cm^{-1}): 3415 (m), 3269 (s), 3190 (s), 3050 (s), 2927 (s), 2845 (s), 1654 (s), 1490 (s), 1432 (s), 1362 (s), 1333 (s), 1270 (s), 1181 (s), 1129 (s), 1057 (s), 1023 (s), 998 (s), 956 (m), 846 (s), 763 (m), 656 (m), 546 (m), 464 (w). ^1H NMR (C_6D_6, ppm): 4.55 (br s, 1H), 3.60 (t, 2H), 2.98 (t, 2H), 2.74 (t, 2H), 2.54 (t, 2H), 1.31 (mult., 4H). Mass spectrum (ESI^+): calculated 140 amu, found 140 amu.

$Mo_2(tbd)_4$, 32. A 10 mL THF solution containing 1.00 g (7.19 mmol) of Htbd was treated with BuLi (4.50 mL, 7.20 mmol) This solution was then added to a 5 mL of THF solution containing 1.16 g (1.80 mmol) of $Mo_2(O_2CCF_3)_4$, resulting in an immediate color change from deep yellow to dark red. The solution was then evaporated to dryness and 20 mL toluene added. The resulting mixture was filtered through Celite

and evaporated to dryness giving an orange powder. Yield: 0.960 g (72%). Single crystals have not been isolated. Mass Spectrum (ESI^+): Calculated ($M+H^+$): 745 amu; found 745 amu. IR (KBr, cm^{-1}): 3388 (w), 2962 (s), 2865 (m), 1681 (s), 1631 (m), 1517 (m), 1437 (m), 1339 (m), 1261 (s), 1210 (m), 1180 (m), 1095 (s), 1025 (s), 800 (s), 722 (w), 697 (w). UV-Vis (THF) λ_{MAX}, nm; (ε_M, L/mol·cm): 494 (758), 395 (sh), 303 (sh), 275 (sh). NMR (C_6D_6, ppm): 3.79-3.61 (m), 3.09-2.98 (m), 2.73-2.52 (m), 1.41-1.23 (m), 1.05-0.82 (m).

$Mo_2(tbd)_4Cl$, 33. A Schlenk flask was charged with 0.100 g (0.134 mmol) of $Mo_2(tbd)_4$ and 20 mL of CH_2Cl_2. The deep brown solution was layered with hexanes and crystals of **33**·$2CH_2Cl_2$, as brown blocks, were harvested after 2 weeks. Yield: 0.108 g (85%). IR (KBr, cm^{-1}): 3151 (w), 2921 (s), 1649 (m), 1529 (s), 1476 (s), 1422 (s), 1343 (s), 1265 (s), 1201 (m), 1142 (s), 1062 (m), 966 (w), 943 (w), 890 (m), 860 (m), 818 (m), 730 (m). UV-Vis (CH_2Cl_2) λ_{MAX}, nm; (ε_M, L/mol·cm): 501 (1,000), 372 (sh), 319 (sh). Magnetism: 1.68 μ_B, g = 1.94. Anal. Calcd for $C_{30}H_{52}Cl_5Mo_2N_{12}$: C, 37.93; H, 5.52; N, 17.69%. Found: C, 37.73; H, 5.26; N, 17.73%.

$Mo_2(tbd)_4Cl_2$, 34. A Schlenk flask was charged with 0.100 g (0.134 mmol) of $Mo_2(tbd)_4$ and 20 mL of CH_2Cl_2. The solution was then exposed to air for 60 s, then the flask was purged and back-filled with nitrogen. The solution was transferred to a Schlenk tube and layered with hexanes. Crystals, as brown blocks were harvested after 2 weeks. Yield: 0.077 g (71 %). IR (KBr, cm^{-1}): 3193 (w), 2926 (s), 2852 (s), 1693 (w), 1614 (s), 1520 (s), 1433 (s), 1366 (s), 1269 (s), 1197 (s), 1146 (s), 1097 (s), 1036 (s), 967 (w), 920 (m), 815 (m), 734 (s), 857 (w). ^1H NMR (CD_2Cl_2, ppm): 4.14-3.20

(m, 32 H), 2.05 (m, 8H), 1.71 (m, 8H). UV-Vis (CH_2Cl_2) λ_{MAX}, nm; (ε_M, L/mol·cm): 581(700), 396 (sh), 339 (sh). Anal. Calcd for $C_{28}H_{48}Cl_2Mo_2N_{12}$: C, 41.24; H, 5.93; N, 20.61%. Found: C, 40.85; H, 5.84; N, 20.26%.

$Mo_2(tbu)_4$, 35. A 10 mL THF solution containing 1.00 g (6.53 mmol) of Htbu was treated with BuLi (4.10 mL, 6.56 mmol). This solution was then added to a 5 mL THF solution containing 1.05 g (1.63 mmol) of $Mo_2(O_2CCF_3)_4$, resulting in an immediate color change from deep yellow to dark red. The solution was placed in a freezer at -20 °C for 1 week, and red-orange block crystals of $Mo_2(tbu)_4$ formed. These crystals were suitable for X-ray diffraction. Yield: 0.887 g (68%). IR (KBr, cm^{-1}): 3384 (w), 2921 (s), 2829 (s), 1692 (w), 1612 (w), 1518 (s), 1426 (s), 1334 (w), 1274 (m), 1163 (s), 1096 (m), 1030 (m), 970 (w), 920 (w), 838 (w), 699 (w), 592 (w), 556 (w), 526 (w), 470 (w). ^1H NMR (C_6D_6, ppm): 3.64 (m, 8H), 3.56 (m, 8H), 3.15 (m, 8H), 3.03 (m, 8H), 1.81 (m, 8H), 1.66 (m, 16H). UV-Vis(THF) λ_{MAX}, nm; (ε_M, L/mol·cm): 577 (400), 492 (800), 375 (sh), 337 (sh). Anal. Calcd for $C_{32}H_{56}Mo_2N_{12}$: C, 48.00; H, 7.05; N, 20.99%. Found: C, 48.29; H, 6.70; N, 20.60%. Mass spectrum (ESI^+): calculated ($M+H^+$) 801 amu, found 801 amu.

$Mo_2(tbu)_4Cl$, 36. A solution of $Mo_2(tbu)_4$ (0.100 g, 0.125 mmol) in 20 mL of CH_2Cl_2 was stirred for 30 min, the solvent removed under vacuum and the powder collected. Yield: 0.090 g (86%). A few small crystals, suitable for X-ray diffraction, were prepared by vapor diffusion of ether into a CH_2Cl_2 solution of **36**. IR (KBr, cm^{-1}): 3128 (s), 2928 (s), 1616 (s), 1518 (s), 1474 (m), 1438 (s), 1377 (s), 1318 (s), 1262 (s), 1209 (m), 1158 (m), 1100 (s), 1028 (s), 968 (w), 802 (s), 730 (m), 557 (w). UV-Vis

(CH_2Cl_2) λ_{MAX}, nm; (ε_M, L/mol·cm): 394 (sh), 314 (sh). Magnetism: 1.66 BM, g = 1.92. Mass Spectrum (ESI^+) Calculated $(M\text{-}Cl)^+$: 800 amu, found: 800 amu.

$Mo_2(tbu)_4(TFPB)_2$, 37. A solution of $Mo_2(tbu)_4$ (0.100 g, 0.125 mmol) in 20 mL of CH_2Cl_2 was transferred to a Schlenk flask containing 0.250 g (0.257 mmol) of Ag(TFPB). Within 5 min a precipitate was observed and the mixture was stirred for an additional 30 min. The mixture was filtered through Celite and the solvent removed under vacuum. Yield: 0.225 g (71%). IR (KBr, cm^{-1}): 3270 (w), 2962 (m), 2869 (m), 1613 (s), 1526 (m), 1444 (m), 1357 (s), 1279 (s), 1121 (s), 1024 (s), 954 (w), 888 (m), 837 (m), 799 (s), 712 (m), 676 (m). ^1H NMR (CD_2Cl_2, ppm): 7.70 (mult., ortho, 16H), 7.55 (mult., para, 8H), 4.10-3.20 (m, 8H), 1.92 (m, 8H), 1.69 (m, 8H). Mass Spectrum (ESI^+) Calculated $(M\text{-}2(TFPB))^{2+}$: 400 amu; found 400 amu. Single crystals have not been isolated.

Results and Discussion

Organic Syntheses. Patent literature[53] has described a simple and efficient way of making Hhpp and has been useful in producing a variety of derivatives. The patent mentions that the strategy is useful for producing 5–8 membered rings, though specific examples are only given for rings containing 5 and 6 members. Using this strategy of reacting a triamine with carbon disulfide in a 1:1 ratio the preparation of derivatives containing 7-membered rings was attempted. Spermidine and carbon disulfide were combined and refluxed in *p*-xylene for 3 weeks, until the evolution of H_2S ceased. The solvent was removed under vacuum resulting in a highly viscous oil. The mass spectrum

(ESI^+) of this oil revealed the major product was a cyclic thiourea (i.e. the intermediate to the bicyclic system). Mass spectrometry provides no structural information in this case so the intermediate having this mass could be either **XIV**(a) or **XIV**(b). Considering the ease with which 6-membered rings form compared to 7-membered rings, **XIV**(b) is the more likely structure.

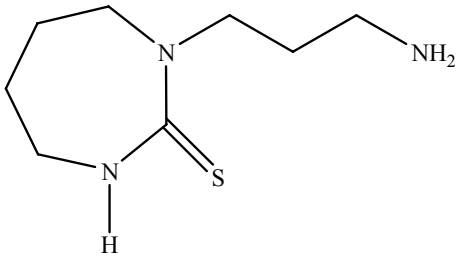

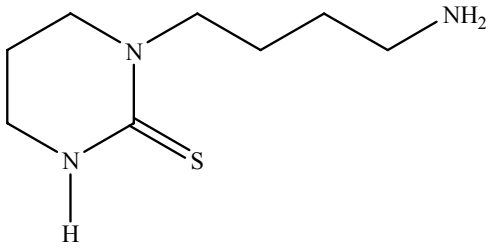

XIV

(a) (b)

In light of these results another strategy was applied to form homologs of hpp containing 7-membered rings as shown below. Presumed intermediates are in red while isolable intermediates are in blue.

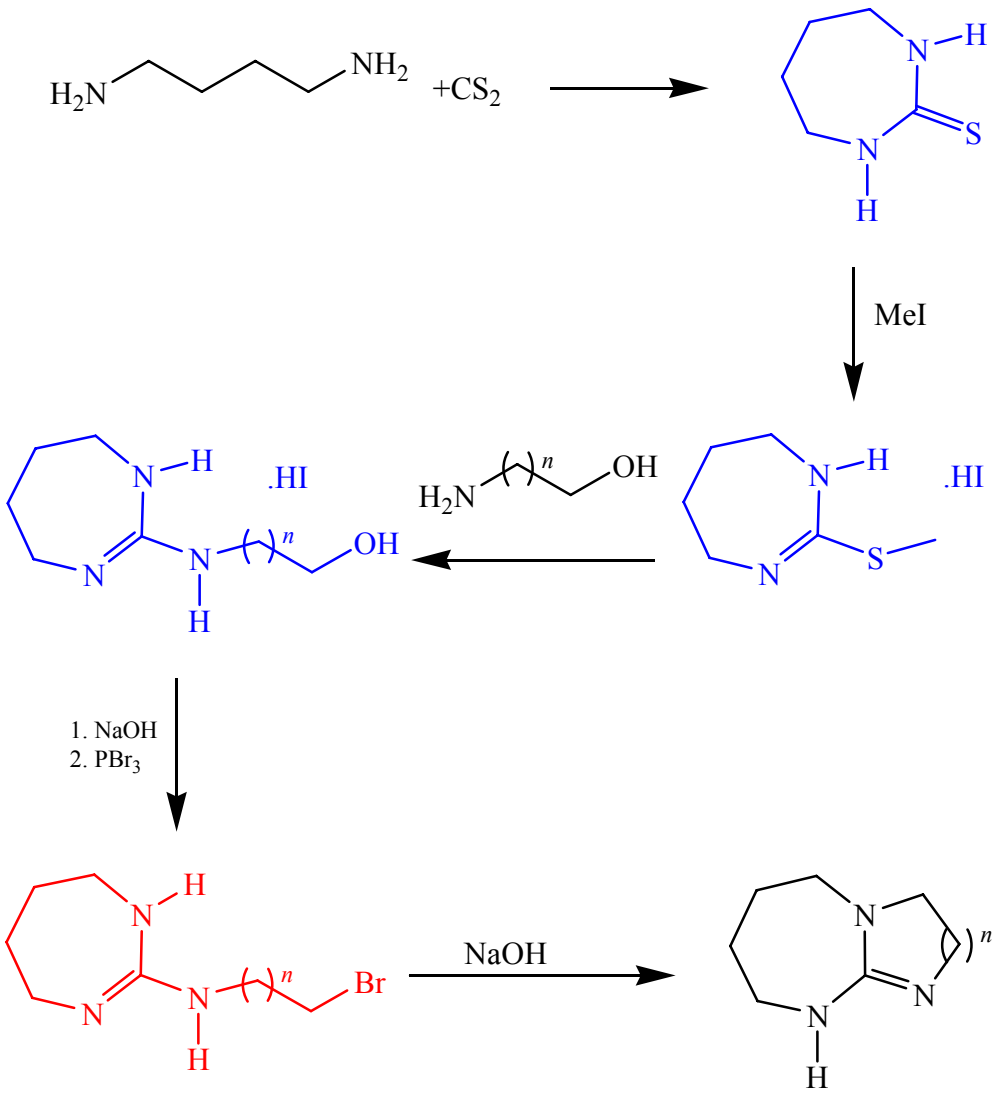

This strategy involves reacting 1,4-diaminobutane with carbon disulfide in a 1:1 ratio such that the 7-membered ring is formed as a cyclic thiourea first.[54,55] Next, the sulfur is made into the more reactive methylmercapto group by the use of iodomethane. The methylmercapto group is then displaced by an aminoalcohol resulting in the formation of a guanidine core.[54,55] The alcohol group is next converted to a bromo

group by the use of PBr_3. Dehydrohalogenation with KOH causes cyclization which results in the bicyclic guanidine.[54,55]

Both Htbd and Htbu were prepared through this route and the crude products obtained readily purified by sublimation. Both give clean ^1H NMR spectra, though they are complicated due to the asymmetry of the compounds. The mass spectrum also shows the expected parent ion. Htbu shows to be pure by elemental analysis and Htbd has a melting point in agreement with previously reported values for samples which are pure by elemental analysis.[55]

Inorganic Syntheses. The Mo_2^{4+} compounds were readily prepared by reacting $Mo_2(O_2CCF_3)_4$ with 4 equivalents of the lithiated ligand in THF. Crystals of $Mo_2(tbu)_4$, **35**, were formed by placing the THF solution in a freezer at -20 °C for 1 week. The powder of $Mo_2(tbd)_4$ was isolated by removing the THF solvent under vacuum, adding toluene to the residue, filtering the mixture though Celite to remove LiO_2CCF_3 and removing the toluene under vacuum.

$Mo_2(tbd)_4Cl$, **33**, and $Mo_2(tbu)_4Cl$, **36**,were prepared by dissolving the Mo_2^{4+} compounds in CH_2Cl_2. Layering the solution of **33** with hexanes afforded crystals of **33**·$2CH_2Cl_2$. Crystals of **36** were prepared by vapor diffusion of ether into a CH_2Cl_2 solution. Compound **34** was prepared by exposing a dichloromethane solution of **32** to air for a brief period (*ca* 60 s). Care must be taken not to overexpose the solution to air. The product is hygroscopic and decomposes upon prolonged exposure. Crystals of **34** were obtained by layering the CH_2Cl_2 solution with hexanes.

Crystallographic Studies. The reaction pathway for the formation of Htbd and Htbu is confirmed by the intermediates which may be isolated in crystalline form at each step. The first intermediate is the cyclic thiourea **26**, which has been previously described in the literature,[56,57] whose thermal ellipsoid plot is shown in Figure 28. From this structure it is quite obvious that a 7-membered ring is formed. The C–C distances and angles are typical for the atoms in their environment. The C–S distance is reasonable for a double bond, and the N–C(5)–N and N–C(5)–S angles add up to 360° indicating sp^2-hybridization.

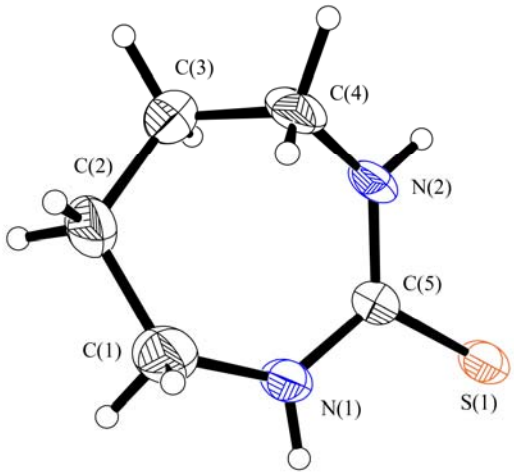

Figure 28. Thermal ellipsoid plot of **26**. Ellipsoids are drawn at the 50% probability level. N(1)–C(5) = 1.332(6) Å, N(2)–C(5) = 1.336(6) Å, S(1)–C(5) = 1.711(2) Å, N(1)–C(5)–N(2) = 120.6(3)°, N(1)–C(5)–S(1) = 116.3(6)°, N(2)–C(5)–S(1) = 123.1(6)°.

The intermediate **27**·HI is prepared by reacting **26** with iodomethane and readily forms yellow needle crystals.[56] The thermal ellipsoid plot of **27**·HI is shown in Figure

29. The 7-membered ring is structurally similar to that found in **26**. The C–S distance has increased to a value consistent with a single bond due to the addition of a methyl group to the sulfur atom. The N–C(5)–N and N–C(5)–S angles still total 360° proving that the sp^2-hybridization has been maintained. An iodide ion is present giving evidence of the ionic nature of this intermediate.

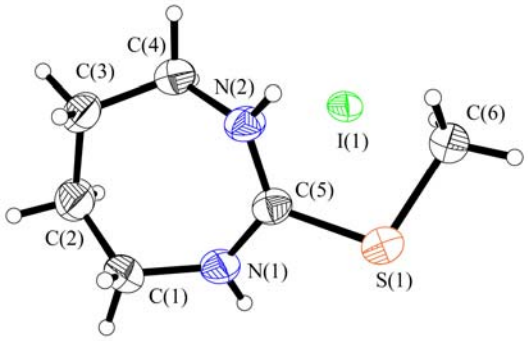

Figure 29. Thermal ellipsoid plot of **27**·HI. Ellipsoids are drawn at the 50% probability level. N(1)–C(5) = 1.326(3) Å, N(2)–C(5) = 1.325(3) Å, S(1)–C(5) =1.750(3) Å. N(1)–C(5)–N(2) = 123.3(2)°, N(1)–C(5)–S(1) =114.2(2)°, N(2)–C(5)–S(1) = 122.6(2)°.

The structure of **28**·HI, prepared by reacting **27**·HI with 3-amino-1-propanol is shown as a thermal ellipsoid plot in Figure 30. This structure shows the formation of the guanidine core by the replacement of the methylmercapto group with the aminoalcohol. The C–C distances and angles are typical for the carbon atoms in their respective environments. The C–O distance is typical of a single bond indicating the presence of an OH group. The N–C(5)–N angles total 360° and the C(5)–N distances lie between the values of a C–N double bond and a C–N single bond indicating sp^2-hybridization.

The presence of the iodide ion is evidence of the ionic nature of this compound and means the guanidine core must be protonated so that it carries a positive charge.

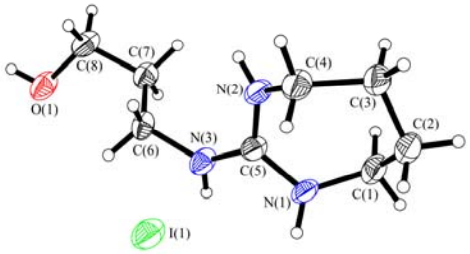

Figure 30. Thermal ellipsoid of **28**·HI. Ellipsoids are drawn at the 50% probability level. N(1)–C(5) = 1.330(5) Å, N(2)–C(5) =1.354(5) Å, N(3)–C(5) = 1.333(4) Å, N(3)–C(6) = 1.427(4) Å. N(1)–C(5)–N(2) = 119.6(3)°, N(2)–C(5)–N(3) = 118.8(3)°, N(1)–C(5)–N(3) = 121.6(3)°.

The thermal ellipsoid plots of **29** and **31** are shown in Figure 31. Compound **31** has been described previously but not characterized crystallographically.[56] Compound **29** is reported for the first time in this work. The carbon atoms on the outer periphery of the bicyclic system have distances and angles typical for their environment. The N–C(4)–N angles add up to 360° and the C(4)–N distances in **29** lie between the values of a single bond and double bond, confirming the sp^2-hybridization of the carbon atom and the delocalization of the guanidine core. The N–C(3)–N angles and C(3)–N distances in **31** are similar to those in **29**.

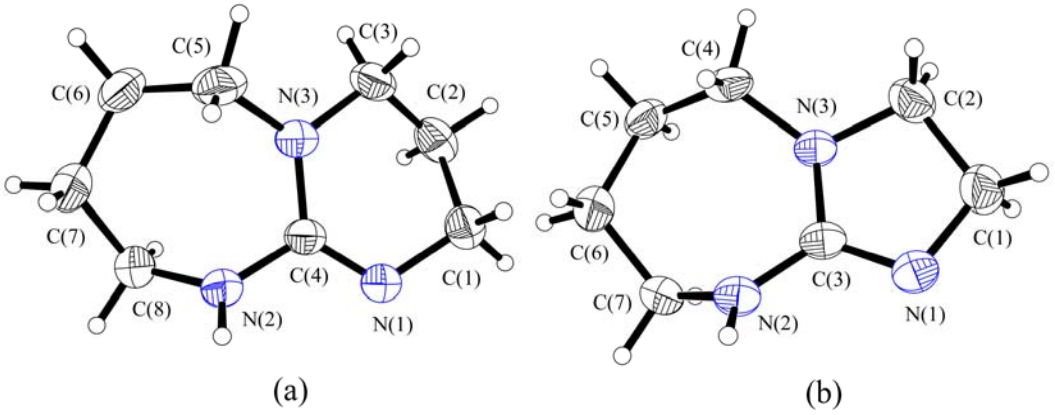

Figure 31. Thermal ellipsoid plots of (a) **29** and (b) **31**. Ellipsoids are drawn at the 50% probability level. Selected interatomic distances and angles for **29** are N(1)–C(4) = 1.291(2) Å, N(2)–C(4) = 1.380(2) Å, N(3)–C(4) = 1.368(2) Å, N(1)–C(4)–N(2) = 118.8(1)°, N(2)–C(4)–N(3) = 115.5(1)°, N(1)–C(4)–N(3) = 125.7(1)°. Selected interatomic distances and angles for **31** are N(1)–C(3) = 1.293(2) Å, N(2)–C(3) = 1.356(2) Å, N(3)–C(3) = 1.394(2) Å, N(1)–C(3)–N(2) = 123.5(2)°, N(2)–C(3)–N(3) = 120.0(2)°, N(1)–C(3)–N(3) = 116.5(2)°.

The structure of $Mo_2(tbd)_4Cl$, **33**, is shown as a thermal ellipsoid plot in Figure 32 with selected interatomic distances and angles included in the caption. There are two crystallographically independent paddlewheels in the structure, each residing on a center of inversion. The ligands are well ordered, allowing for reliable determination of distances and angles. The Mo–Mo distances (2.1711(7) Å and 2.1690 Å) are not very different and are longer than the Mo–Mo distance in $Mo_2(hpp)_4Cl{\cdot}2CH_2Cl_2$ (2.1280 Å).[58] The Mo–Cl distance averages to 3.009[1] Å which is too long to imply any significant bonding between the atoms.

The structure of $Mo_2(tbd)_4Cl_2$, **34**, is shown as a thermal ellipsoid plot in Figure 33 with interatomic distances and angles listed in the caption. The compound

crystallized in a body-centered tetragonal space group, and the difficulties associated with structure determination in such space groups have been previously reported.[59]

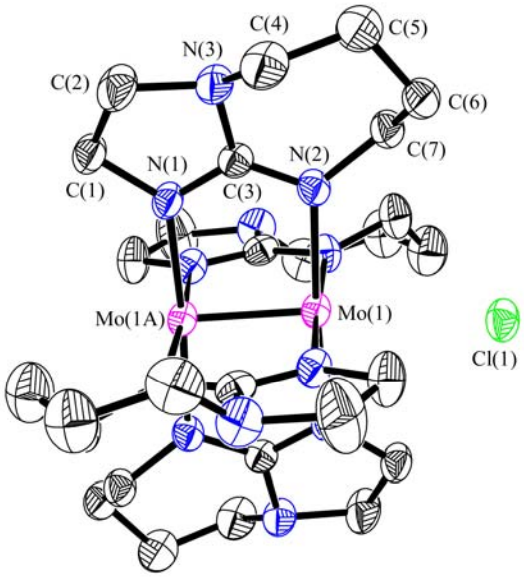

Figure 32. Thermal ellipsoid plot of **33** in **33**·$2CH_2Cl_2$. Ellipsoids are drawn at the 50% probability level. Hydrogen atoms and solvent molecules omitted for clarity. Mo(1)–Mo(1A) = 2.1711(7) Å, Mo(2)–Mo(2A) = 2.1690(7) Å, Mo–N(1)av = 2.116[6] Å, Mo–N(2)av = 2.150[6] Å, Mo(1)–Cl(1) = 2.999(1) Å, Mo(2)–Cl(1) = 3.018(1) Å. Mo(1A)–Mo(1)–Cl(1) = 173.39(3)°, Cl(1)–Mo(2)–Mo(2A) = 172.67(3)°, Mo–Mo–N(1)av = 90.2[2]°, Mo–Mo–N(2)av = 93.4[2]°.

The structure was solved in *I4/m* with the molecule residing on the intersection of a four-fold axis and mirror plane. The asymmetric unit contains a Mo atom, a Cl atom and one half of a ligand. The molecule's residency on a special position produces disorder of the ligands over two positions. The Mo–Mo distance of 2.206(1) Å is longer

than that in **33** by 0.036 Å. By comparison, the difference in Mo–Mo distance between $Mo_2(hpp)_4Cl_2$ and $Mo_2(hpp)_4Cl$ is 0.046 Å.[58]

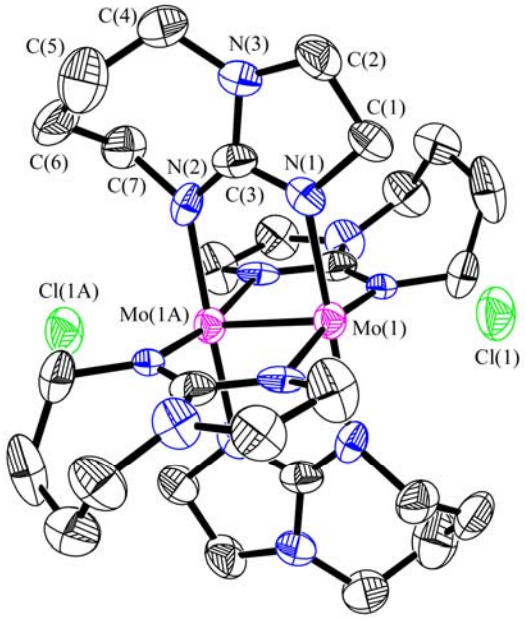

Figure 33. Thermal ellipsoid plot of **34**. Ellipsoids are drawn at the 50% probability level. Hydrogen atoms are removed for clarity. Mo(1)–Mo(1A) = 2.206(1) Å, Mo(1)–Cl(1) = 2.849(2) Å, Mo(1)–N(1) = 2.14(2) Å, Mo(1)–N(2) = 2.06(2) Å, Mo(1A)–Mo(1)–Cl(1) = 180.0°, Mo–Mo–N(1) = 92.2(3)°, Mo–Mo–N(2) = 91.0(3)°.

The thermal ellipsoid plot of $Mo_2(tbu)_4$, **35**, is presented in Figure 34. The molecule resides on a special position at the intersection of two two-fold axes; one axis is along the Mo-Mo axis, the other is perpendicular to it. The special position generates disorder of the ligands over two positions. The Mo–Mo distance is 2.0677(9) Å, very similar to the value found for $Mo_2(hpp)_4$ (2.067(1) Å).[12a]

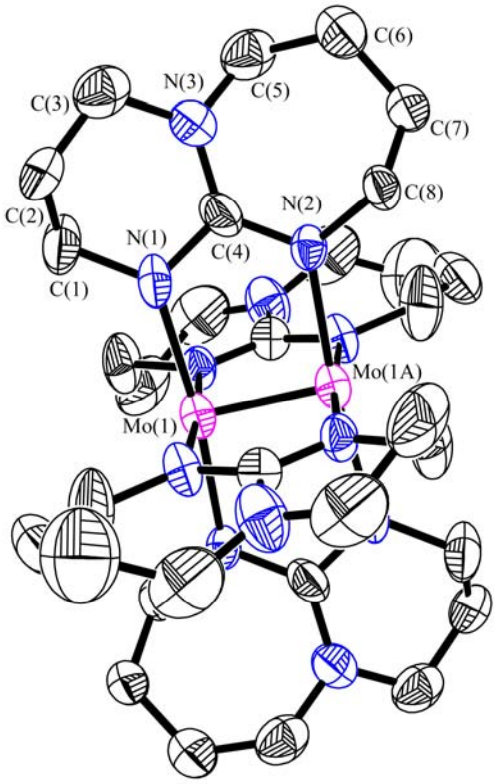

Figure 34. Thermal ellipsoid plot of **35**. Ellipsoids are drawn at the 30% probability level. Hydrogen atoms are removed for clarity. Mo(1)–Mo(1A) = 2.0677(9) Å, Mo–N(1)av = 2.15[3] Å, Mo–N(2)av = 2.14[3] Å. Mo–Mo–N(1)av = 92.9[9]°, Mo–Mo–N(2)av = 92[1]°.

The thermal ellipsoid plot of $Mo_2(tbu)_4Cl$ in **36** is shown in Figure 35. The molecule resides on a 4-fold axis with the ligand disordered over two positions. The Mo–Mo distance of 2.133(2) Å is an increase of 0.065 Å from that found in **35**. This is a similar increase as that found between $Mo_2(hpp)_4Cl$ and $Mo_2(hpp)_4$ (0.061 A).[58] The Mo–Cl distance is 3.705(1) Å, too long to consider any significant bonding interaction.

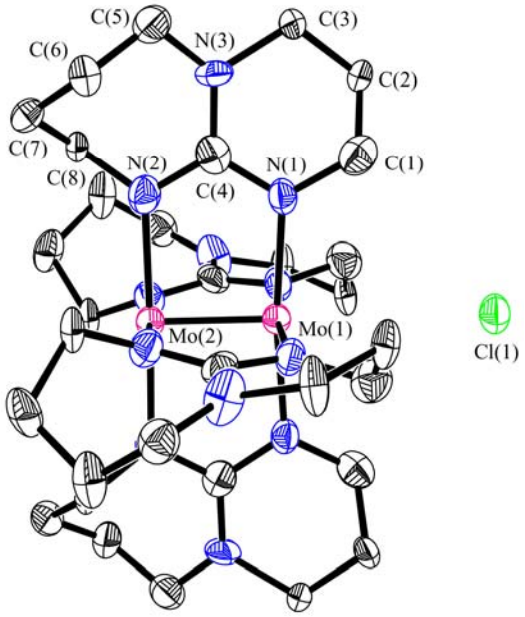

Figure 35. Thermal ellipsoid plot of **36**. Ellipsoids are drawn at the 50% probability level. Disorder is not shown. Hydrogen atoms are removed for clarity. Mo(1)–Mo(2) = 2.133(2) Å, Mo(1)–N(1) = 2.117(6) Å, Mo(2)–N(2) = 2.154(7) Å, Mo(1)–Cl(1) = 3.705(1) Å, Mo(1)–Mo(2)–N(2) = 93.4(2)°, Mo(2)–Mo(1)–N(1) = 91.0(2)°, Mo(2)–Mo(1)–Cl(1) = 180.0°.

Electrochemistry. The CV and DPV of $Mo_2(tbd)_4$ and $Mo_2(tbu)_4$ were observed using THF solutions of approximately 1 mM concentration. The DPVs of these two compounds are depicted in Figure 36. The two peaks observed at –1.059 V and –0.242 V for $Mo_2(tbd)_4$ and at -1.009 V and -0.312 V for $Mo_2(tbu)_4$ are related to successive one-electron oxidations corresponding to:

$$Mo_2^{4+} \xrightleftharpoons{-e^-} Mo_2^{5+}$$

$$Mo_2^{5+} \xrightleftharpoons{-e^-} Mo_2^{6+}$$

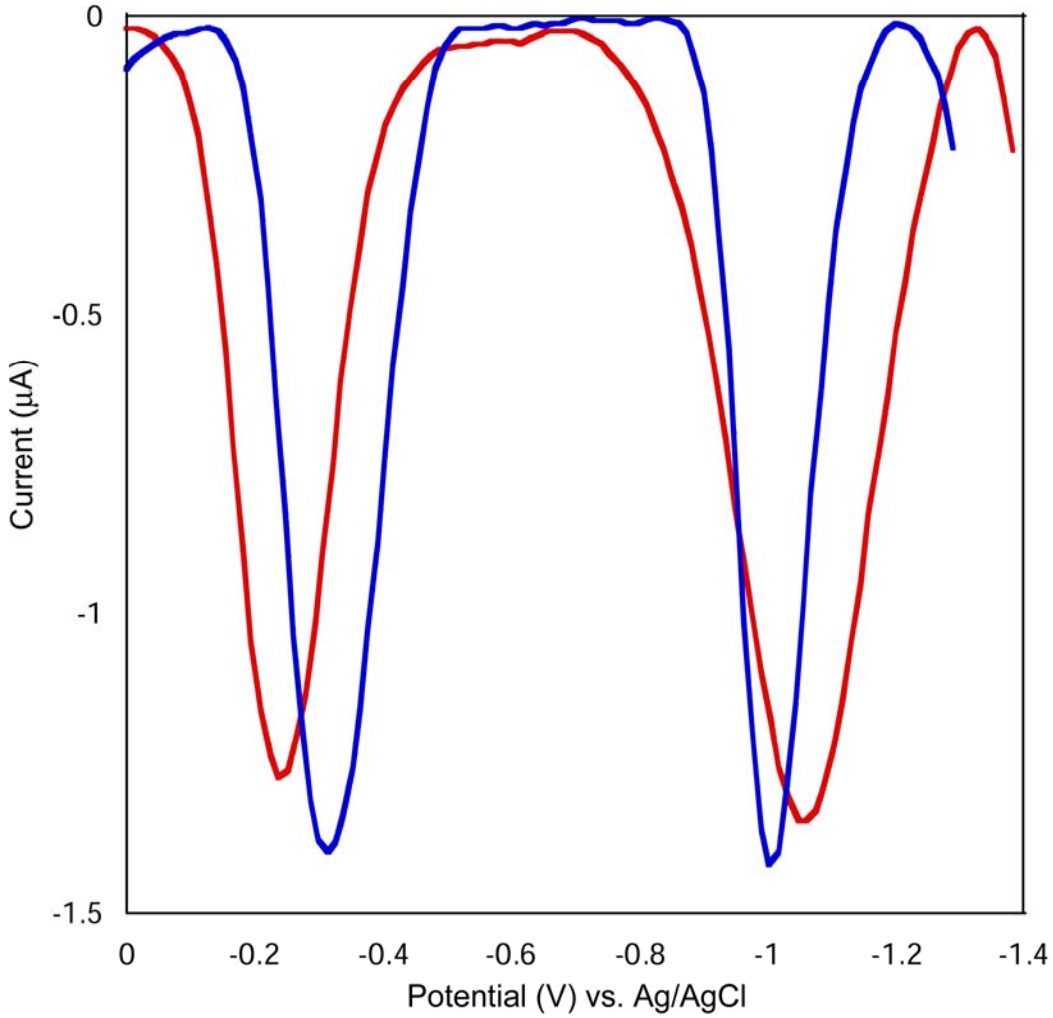

Figure 36. Differential pulse voltammograms of $Mo_2(tbd)_4$ (blue) and $Mo_2(tbu)_4$ (red).

For each of these voltammograms, the Fc/Fc^+ couple was measured at 0.663 V under similar conditions. This places the potentials versus ferrocene at the values seen in Table 19, which also lists the potential versus ferrocene for $Mo_2(hpp)_4$. All three compounds have extremely negative $E_{1/2}^{(1)}$ potentials. These negative potentials mean

that simple dissolution in CH_2Cl_2 leads to the formation of Mo_2^{5+} species (the reduction potential of CH_2Cl_2 has previously been measured at -1.638 V versus ferrocene).[66] The $E_{1/2}^{(2)}$ for both compounds also show that oxidation to the Mo_2^{6+} state is quite easy and may be accomplished by O_2 or other common oxidizing agents.

Table 19. Redox Potential Values for $Mo_2(hpp)_4$, $Mo_2(tbd)_4$ and $Mo_2(tbu)_4$.

	$E_{1/2}^{(1)}$ (Mo_2^{4+}/Mo_2^{5+})		$E_{1/2}^{(2)}$ (Mo_2^{5+}/Mo_2^{6+})		
	Ag/AgCl	Fc/Fc^+	Ag/AgCl	Fc/Fc^+	Ref
$Mo_2(hpp)_4$	-1.271	-1.795	-0.444	-0.968	66
$Mo_2(tbd)_4$	-1.059	-1.722	-0.242	-0.905	this work
$Mo_2(tbu)_4$	-1.009	-1.672	-0.312	-0.975	this work

[a] Bu_4NBF_4·3toluene
[b] THF/Bu_4NBF_4 (0.1 M)

The $\Delta E_{1/2}$ values defined as $E_{1/2}^{(2)} - E_{1/2}^{(1)}$ of both compounds allow for the calculation of the conproportionation constant[50] $K_C = \exp(\Delta E_{1/2}/25.69)$ for the process

$$Mo_2^{6+} + Mo_2^{4+} \rightleftharpoons Mo_2^{5+}$$

The $\Delta E_{1/2}$ for the $Mo_2(tbd)_4$ system is 711 mV and the K_C is 1.05×10^{12}. For the $Mo_2(tbu)_4$ system, the $\Delta E_{1/2}$ is 690 mV and the K_C is 4.62×10^{11}. As with the $Mo_2(hpp)_4$ system ($K_C = 9.56\times10^{13}$) the large values are not due to the instability of the Mo_2^{6+} species, but the greater reactivity of the Mo_2^{4+} species toward even very mild oxidizing agents such as CH_2Cl_2.[66]

Magnetic Behavior. Both $Mo_2(tbd)_4$, **32**, and $Mo_2(tbu)_4$, **35**, are reasonably soluble in common NMR solvents, and their ^1H spectra have been observed in C_6D_6 solutions. The ^1H NMR spectra of the Mo_2^{6+} species **34** and **37** have also been observed

in CD_2Cl_2 solutions. All of the compounds give clean spectra and because all of the signals are in the normal regions and of normal sharpness, it may be concluded that these four compounds are diamagnetic.

The singly oxidized species **33** and **36** show the expected single unpaired electron as evidenced by magnetic susceptibility. The *g* values calculated from these measurements are 1.94 for **33** and 1.92 for **36**, similar to that found for $Mo_2(hpp)_4Cl$ (g = 1.94),[66] and are less than 2.00 due to spin-orbit coupling associated with the molybdenum atoms.

Supplemental Information. A table of information for the LMSB crystallographic database and selected NMR and UV-vis spectra are found in Appendix C.

CHAPTER VI

CONCLUSIONS

Structural Trends in the Dimolybdenum Compounds

Selected values for the Mo_2^{4+} compounds described in Chapters II through V are presented in Table 20. As expected, the Mo–Mo distance is dependant on the bite angle of the bridging ligand. However, the ligand also distorts to accommodate the dimolybdenum unit. In the case of $Mo_2(tbo)_4$ the bite angle calculated from the crystal structure and that found through DFT calculations differ by more than 5°. For the complexes containing asymmetric ligands (tbn, tbd and tbu) the factors affecting the Mo–Mo distance become more complex. Many of the crystal structures for these compounds have disordered ligands. The disorder makes measurements of the angles needed to calculate the bite angle inaccurate. The ligand also lies across the dimolybdenum unit on a tilt as evidenced by the inequivalent Mo–N distances. This tilt serves to further maximize the overlap of the molybdenum and nitrogen orbitals and mitigates the effect of the bite angle.

Figure 37 shows a plot of the Mo–Mo distance versus the bite angle determined from the crystal structure data. For the reasons discussed above, a linear relationship does not exist between the two values. Despite this, the values fit well to a curve defined by the quadratic equation:

$$d = [(a_m + 2.6)^2/10000] + M$$

where d is the calculated M–M distance, a_m is the bite angle of the ligand, and M is the M–M distance in a representative hpp complex (i.e. $Mo_2(hpp)_4$).

Table 20. Selected Values for Mo_2^{4+} Compounds.

Compound	Mo–Mo (Å)[a]	Mo–N (Å)	bite angle (°) (crystal)	bite angle (°) (DFT)
$Mo_2(tbu)_4$	2.068(1)	2.14 2.15	-2.5	1.4
$Mo_2(hpp)_4$	2.067(1)	2.16	-0.3	5.3
$Mo_2(tbd)_4$	2.072	–	–	10
$Mo_2(tbn)_4$	2.082(1)	2.14 2.18	8.9	15
$Mo_2(tbo)_4$	2.132(1)	2.16	23	29
$Mo_2(TMhpp)_4$	2.063(1)	2.14	-2.1	–
$Mo_2(TEhpp)_4$	2.060(1)	2.15	-2.6	–

[a] Values rounded to the third decimal place. Predicted value in red.

The equation can be adjusted to operate using the bite angles determined from DFT calculations on the ligands. This results in a shift of the quatdratic term by -5.1° such that:

$$d = [(a_c - 2.5)^2/10000] + M$$

where a_c is the calculated angle.

With this equation, the M–M distance for a complex with a bicyclic guanidinate ligand may be predicted by calculating the bite angle of the ligand. For example, by using the value of the Ru–Ru distance in $Ru_2(hpp)_4Cl_2$ (2.324(1) Å) the values found in Table 21 may be predicted.

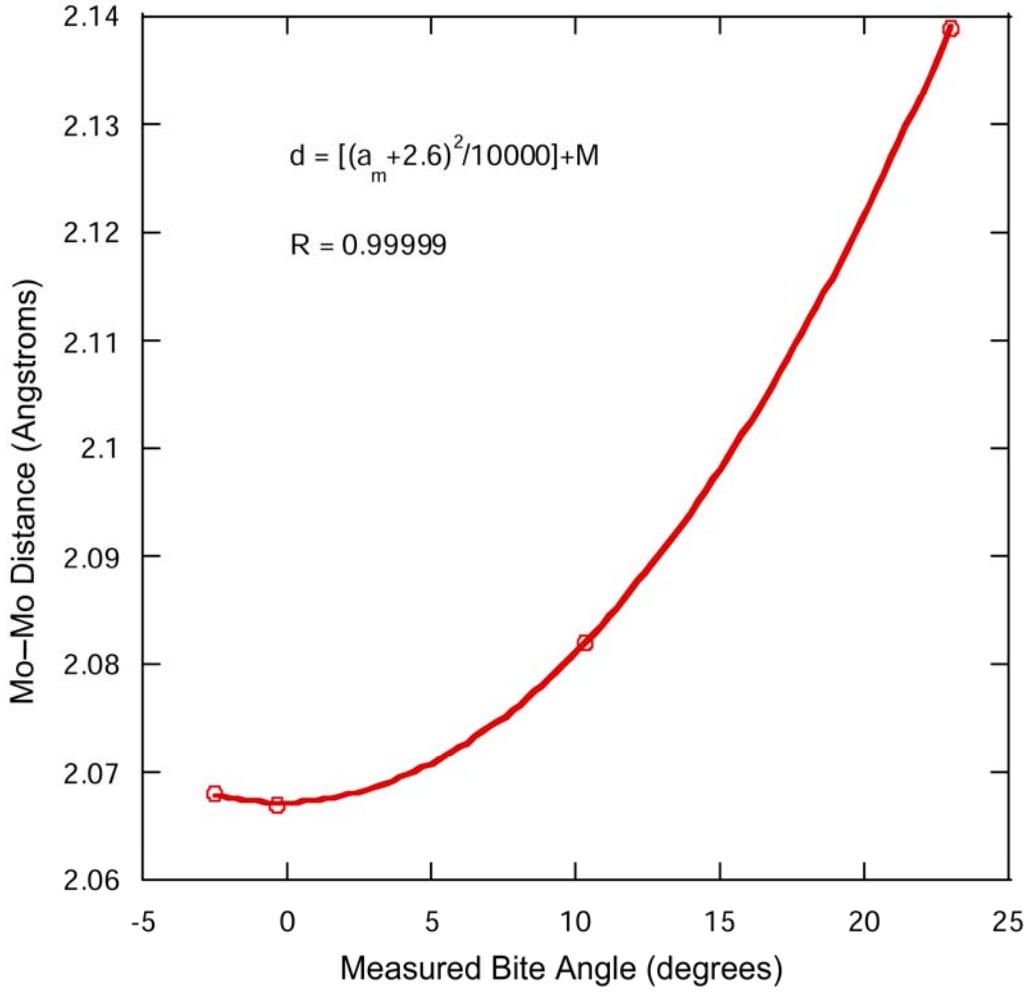

Figure 37. A plot of the Mo–Mo distance versus the measured bite angle.

Table 21. Predicted Values for $Ru_2(L)_4^{2+}$ Compounds.			
Compound	Bite angle (°) (DFT)	Ru–Ru (Å)[a,b]	Bite angle (°)[b] (measured)
$Ru_2(hpp)_4Cl_2$	5.3	2.324(1)	2.1 (2.6)
$Ru_2(tbo)_4Cl_2$	28.5	2.392	23.5
$Ru_2(tbn)_4Cl_2$	14.7	2.339	9.6
$Ru_2(tbd)_4Cl_2$	10.1	2.330	5.2
$Ru_2(tbu)_4Cl_2$	1.4	2.324	2.6
[a] Values rounded to the third decimal place. [b] Predicted values in red.			

Alternatively, by calculating the bite angle of a possible new bicyclic guanidinate ligand (tbh, **XXVII**) of 20°, the Mo–Mo distance in $Mo_2(tbh)_4$ (2.098 Å) may be predicted.

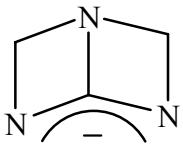

XXVII

These equations appear quite general and should allow for the prediction of the M–M distance for a series of $M_2(L)_4^{n+}$ compounds provided the distance for one of the compounds in the series is already known. These comparisons will hold true provided the only change to the compound is the ligand bridging the dimetal unit. More dimetal complexes with guanidinate ligands will be needed to confirm the validity of the

proposed equations. Most likely, another term or variable will be needed to adjust for the dimetal unit (i.e. differences between Mo_2 units and Ru_2 units).

As seen with the $Mo_2(hpp)_4^{n+}$ (n = 0, 1, 2) system, the Mo–Mo distance increases for the dimolybdenum unit as electrons are removed from the δ-orbital as the compounds are oxidized from the Mo_2^{4+} state to the Mo_2^{5+} and Mo_2^{6+} states. The change in Mo–Mo distance varies between 0.03 Å and 0.11 Å for each electron removed from the δ-orbital. The amount of change is dependent on the bite angle of the ligand, the counterion present and the presence or absence of solvent. The largest measured change in Mo–Mo distance between $Mo_2(tbn)_4Cl_2$ and $Mo_2(tbn)_4$ (0.160 Å) reveals that a wide range in Mo–Mo distance may be achieved. Through modification of the ligand, manipulation of the dimolybdenum oxidation state and careful selection of counterions it may be possible to fine tune the Mo–Mo distance. This capability could provide control of the physical and chemical properties that would be required for applications such as electrochemical sensors.

Electrochemistry

The addition of new dimolybdenum compounds to the guanidinate class of ligands allows for the modification of Figure 7 to include a range for guanidinates, similar to that seen for carboxylates and formamidinates. This modification is made in Figure 38, showing a range for the bicyclic guanidinates from -1.27 V to -0.990 V for the first redox process. As with the carboxylates and formamidinates the voltammetry data were collected under different conditions which might shift the measurements by a few

millivolts. Still, there is an overwhelming trend to shift the redox potential by *ca* -1.5 V compared to the two other common classes of ligands.

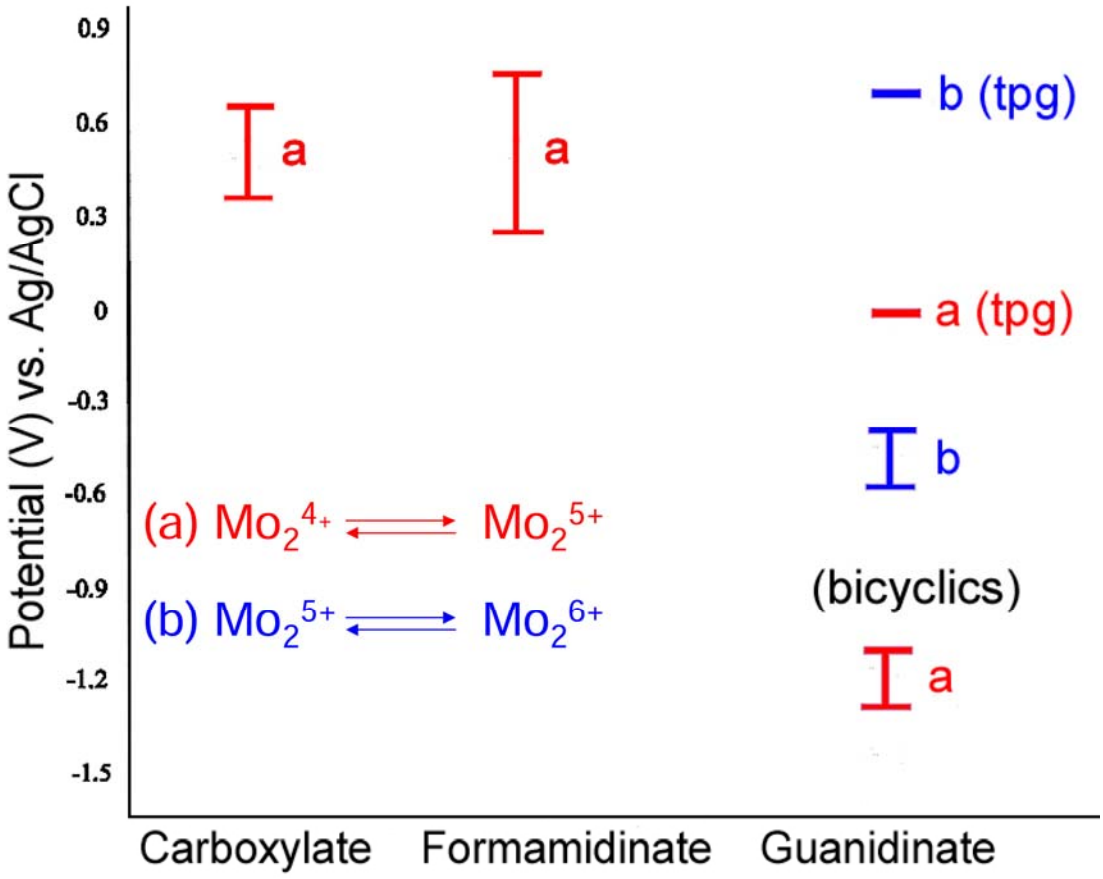

Figure 38. Variation in potentials as a function of ligand for paddlewheel complexes for the type $M_2(L)_4$. The anion of 1,2,3-triphenylguanidine is represented as tpg.

A plot of the $E_{1/2}^{(1)}$ redox potential versus the Mo–Mo distance is shown in Figure 39. Two values were omitted from the curve fit in the plot. One data point belongs to $Mo_2(hpp)_4$ whose voltammetry data was collected under different conditions. The other

belongs to $Mo_2(tbu)_4$. The convergent angle of the ligand in this compound enhances the repulsion between the Mo atoms as the charge increases, making this compound harder to oxidize. A linear relationship is not present, and the redox potential appears to asymptotically approach a value of -0.98 V *vs* Ag/AgCl. This suggests an upper limit to the value $E_{1/2}^{(1)}$ may achieve in $Mo_2(L)_4$ (L = bicyclic guanidinate) complexes, but proper modification of the ligands may allow for lower values to be attained.

Solubility

One of the goals of this project is to provide control over the solubility of the dimolybdenum guanidinate complexes through modification of the ligand. As seen in Table 22, the solubility of $Mo_2(hpp)_4$ is quite low. By modifying the ligand the solubility can be changed. The ligands with smaller rings tend to lower the solubility while the larger rings tend to increase the solubility. The addition of methyl groups causes only a small change in the solubility of the dimolybdenum complexes but the addition of ethyl groups increases the solubility dramatically.

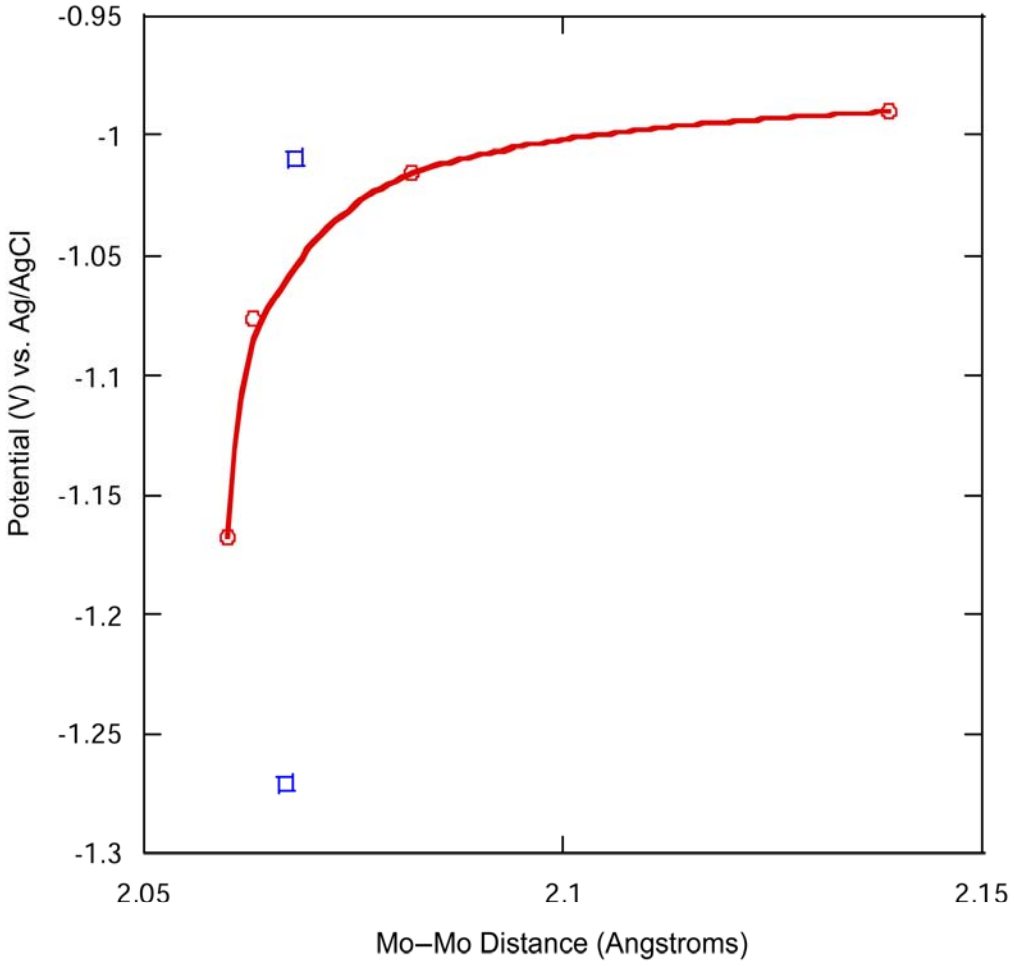

Figure 39. Plot of redox potential *vs* Mo–Mo distance. Values omitted from the curve fit are in blue.

Table 22. Solubility (mg/mL) of Dimolybdenum Compounds.			
Compound	THF	Benzene	Toluene
$Mo_2(hpp)_4$	1.0	1.0	1.0
$Mo_2(tbo)_4$	0.5	0.5	0.5
$Mo_2(tbn)_4$	5.0	2.0	2.5
$Mo_2(tbd)_4$	5.0	2.0	3.0
$Mo_2(tbu)_4$	7.5	2.5	3.0
$Mo_2(TMhpp)_4$	15	1.5	7.5
$Mo_2(TEhpp)_4$	50	10	10

In all cases the solvent of choice appears to be THF. The solubility of the compounds in benzene and toluene tends to be less compared to THF. For the case of THF the trend in solubility may be described as:

$$tbo < hpp < tbn \approx tbd < tbu < TMhpp << TEhpp$$

For all of the compounds, addition of CH_2Cl_2 results in immediate oxidation to the Mo_2^{5+} state. The solubility of the compounds then changes with CH_2Cl_2 becoming the best solvent to use for the oxidized complexes (except for $Mo_2(TEhpp)_4^{n+}$ (n =1, 2) which retains high solubility in many solvents).

Future Work

This work provides a strong basis for understanding the properties of dimolybdenum guanidinates and how the metal-ligand interaction affects the redox potential and Mo–Mo distance. This area of research still has many opportunities for growth in terms of both ligand synthesis and preparation of dimetal complexes.

The preparation of new dimetal complexes offers many avenues for exploration. Considering 16 transition metals known to form paddlewheel complexes, many with multiple oxidation states, combined with the 7 ligands presented the number of potentially available dimetal compounds containing bicyclic guanidinates is in the hundreds. After molybdenum, the most studied $M_2(hpp)_4^{n+}$ compound is the one with M = Ru.[10,59,72] Preparation of a series of $Ru_2(guanidinate)_4^{n+}$ series of complexes would provide interesting opportunities for studying the near-degeneracy of the π* and δ* orbitals in the Ru_2^{n+} core as well as possible access to the Ru_2^{7+} core. New complexes

with Cr and W would allow for further probing of the ligand effects on compounds containing group 6 metals and access to the $MoCr^{4+}$ and MoW^{4+} cores would allow for further control of the redox potential, this time by modification of the dimetal unit as opposed to modification of the ligand.

Further modification of the bicyclic guanidinate ligand system is also possible. Procedures to prepare derivatives with unsaturated C–C bonds (**XXVIII**–**XXXII**) appear in the literature, using much of the methodology described in Chapter V for the preparation of Htbd and Htbu.[73] By preparing such derivatives, the π system of the guanidinate may be extended which would modify the redox potential of the resulting dimetal complex. Such unsaturated systems would also provide a basis for further derivatives by adding halogens or other substituents across the double bond. Dichloroacetaldehyde is commercially available and by using the synthetic strategies from Chapter IV it may be possible to prepare 3,3,6,6-tetrachloro-1,3,5-triazabicyclodec-4-ene (HTClhpp, **XXXIII**). It would be interesting to see if dimolybdenum paddlewheels using such a ligand would be stable, considering the strong reducing power of such systems and their observed tendency to abstract halogen atoms from their surroundings.

The work in this dissertation has established guanidinates as a class of ligands, separate and distinct from halides, carboxylates and formamidinates. Control of the physical properties of the dimolybdenum complexes, particularly solubility and redox potential, has been realized. Many opportunities exist for further expansion and development of the field, both in the preparation of metal complexes and new ligand derivatives.

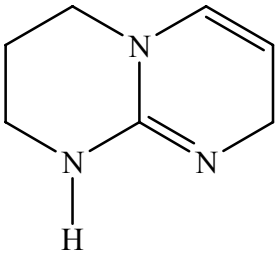

XXVIII

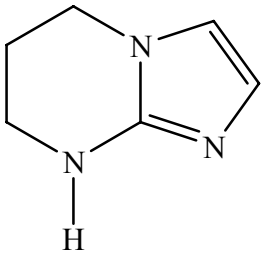

XXIX

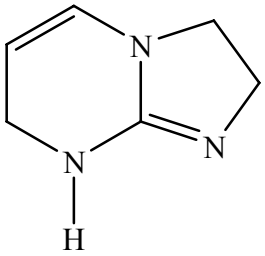

XXX

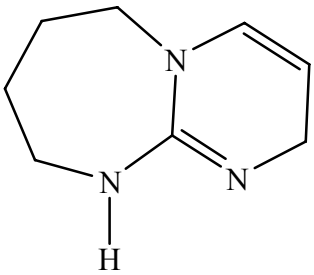

XXXI

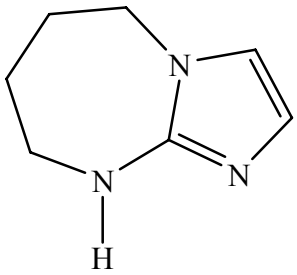

XXXII

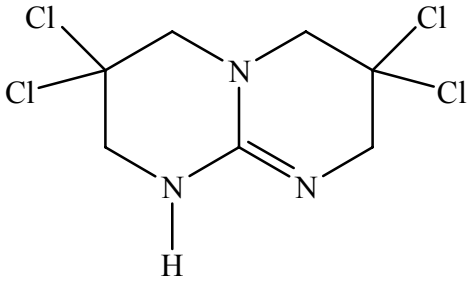

XXXIII

REFERENCES

[1] Cotton, F. A.; Walton, R. A. *Multiple Bonds Between Metal Atoms*, 2nd Ed.; Oxford University Press: Oxford, 1993.

[2] Cotton, F. A.; Harris, C. B. *Inorg. Chem*. **1965**, *4*, 330.

[3] (a) Cotton, F. A.; Matusz, M.; Poli, R. *Inorg. Chem*. **1987**, *26*, 1472. (b) Cotton, F. A.; Matusz, M.; Poli, R.; Feng, X. *J. Am. Chem. Soc*. **1988**, *110*, 1144.

[4] Cotton, F. A.; Daniels, L. M.; Murillo, C. A. *Inorg. Chem*. **1993**, *32*, 2881.

[5] (a) Cotton, F.A.; Daniels, L. M.; Maloney, D. J.; Matonic, J. H.; Murillo, C. A. *Inorg. Chim. Acta* **1997**, *256*, 283. (b) Cotton, F. A.; Daniels, L. M.; Matonic, J. H.; Murillo, C. A. *Inorg. Chim. Acta* **1997**, *256*, 277. (c) Cotton, F. A.; Daniels, L. M.; Falvello, L. R.; Matonic, J. H.; Murillo, C. A. *Inorg. Chim. Acta* **1997**, *256*, 269.

[6] (a) Cotton, F. A.; Daniels, L. M.; Maloney, D. J.; Matonic, J. H.; Murillo, C. A. *Inorg. Chim. Acta* **1997**, *256*, 283. (b) Cotton, F. A.; Daniels, L. M.; Feng, X.; Maloney, D. J.; Matonic, J. H.; Murillo, C. A. *Inorg. Chim. Acta* **1997**, *256*, 291.

[7] Cotton, F. A.; Poli, R. *Polyhedron* **1987**, *6*, 1625.

[8] Cotton, F. A.; Matonic, J. H.; Murillo, C. A. *Inorg. Chim. Acta* **1997**, *264*, 61.

[9] (a) Cotton, F. A.; Daniels, L. M.; Matonic, J. H.; Murillo, C. A.; Wang, X. *Polyhedron* **1997**, *16*, 1177. (b) Cotton, F. A.; Daniels, L. M.; Murillo, C. A.; Wang, X. *Inorg. Chem*. **1997**, *36*, 896.

[10] Bear, J. L.; Li, Y.; Han, B.; Kadish, K. M. *Inorg. Chem*. **1996**, *35*, 1395.

[11] Cotton, F. A.; Matonic, J. H.; Murillo, C. A. *J. Am. Chem. Soc*. **1997**, *119*, 7889.

[12] See for example: (a) Cotton, F. A.; Timmons, D. J. *Polyhedron* **1998**, *17*, 179. (b) Clérac, R.; Cotton, F. A.; Daniels, L. M.; Donahue, J. P.; Murillo, C. A.; Timmons, D. J. *Inorg. Chem*. **2000**, *39*, 2581.

[13] Novak, I.; Wei, X.; Chin, W. S. *J. Phys. Chem. A* **2001**, *105,* 1783.

[14] Schwesinger, R. *Chimia*, **1985**, *39*, 269.

[15] Simoni, D.; Rondanin, R.; Morini, M.; Baruchello, R.; Invidiata, F. P. *Tetrahedron Lett*. **2000**, *41*, 1607.

[16] Gelbard, G.; Vielfaure-Joly, F. *Tetrahedron Lett*. **1998**, *39*, 2743.

[17] (a) Maksić, Z. B.; Kovačevic, B. *J. Org. Chem*. **2000**, *65*, 3303. (b) Kovačevic, B.; Maksić, Z. B. *Org. Lett*. **2001**, *3*, 1523.

[18] Bailey, P. J.; Pace, S. *Coord. Chem. Rev*. **2001**, *214*, 91.

[19] Cotton, F. A.; Daniels, L. M.; Murillo, C. A.; Timmons, D. J. *Chem. Commun*. **1997**, 1449.

[20] Cotton, F. A.; Gu, J.; Murillo, C. A.; Timmons, D. J. *J. Am. Chem. Soc*. **1998**, *120*, 13280.

[21] Cotton, F. A.; Murillo, C. A.; Timmons, D. J. *Chem. Commun*. **1999**, 1427.

[22] Timmons, D. J. Ph.D. *Dissertation*, Texas A&M University, College Station, TEXAS 1999.

[23] See for example: Katz, E.; Bückmann, A. F.; Willner, I. *J. Am. Chem. Soc*. **2001**, *123*, 10752 and references therein.

[24] Mori, A.; Cohen, B. D.; Lowenthal, A. Eds. *Guanidines: Historical, Biological, Biochemical and Clinical Aspects of the Naturally Occurring Guanidino Compounds*; Plenum Press: New York, 1985.

[25] Pickett, C. J. *Chem. Commun*. **1985**, 323.

[26] Fry, A. J.; Touster, J. *J. Org. Chem*. **1986**, *51*, 3905.

[27] SMART Version 5.618, Bruker AXS, Madison, WI, 2001.

[28] SAINT Version 6.02, Bruker AXS, Madison, WI, 2000.

[29] Sheldrick, G. M., SHELXTL V .5; Siemens Industrial Automation Inc.: Madison, WI, 1994.

[30] Canich, J. A. M.; Cotton, F. A.; Dunbar, K. R.; Falvello, L. R. *Inorg. Chem*. **1988**, *27*, 804.

[31] See for example: (a) Savéant, J.-M. *Acc. Chem. Res*. **1993**, *26*, 455. (b) Pause, L.; Robert, M.; Savéant, J.-M. *J. Am. Chem. Soc*. **2000**, 122, 9829. (c) Savéant, J.-M. *J. Am. Chem. Soc*. **1987**, *109*, 6788.

[32] If the stoichiometry was not carefully controlled during the preparation of **3** and less than 1 equiv of $TlBF_4$ was added to **2**, crystals of $Mo_2(hpp)_4Cl_{0.5}(BF_4)_{0.5}$ were obtained. These crystallized in the tetragonal space group $P42_12$ with the following

crystallographic parameters: a = 14.2091(8), c = 16.415(1) Å, V = 3314.3(4) Å^3. The structure was highly disordered. The Mo–Mo distance was 2.1193(6) Å.

[33] Crystals of **3**·2CH_2Cl_2 have been obtained and crystallographic characterization has revealed the presence of a highly disordered $Mo_2(hpp)_4^+$ cation and BF_4 anion. Crystallographic data are: monoclinic space group $P2_1/c$, a = 9.820(3), b = 20.859(5), c = 19.797(3) Å, β = 96.44(1)°, V = 4029(2) Å^3. The Mo–Mo distance was 2.110(1) Å.

[34] Cotton, F. A.; Huang, P.; Murillo, C. A.; Timmons, D. J. *Inorg. Chem*. *Commun*. **2002**, *5*, 501.

[35] Cotton, F. A.; Feng, X.; Matusz, M. *Inorg. Chem*. **1989**, *28*, 594.

[36] (a) Bailey, P. J.; Bone, S. F.; Mitchell, L. A.; Parsons, S.; Taylor, K. J.; Yellowless, L. J. *Inorg. Chem*. **1997**, *36*, 867. (b) Bailey, P. J.; Bone, S. F.; Mitchell, L. A.; Parsons, S.; Taylor, K. J.; Yellowless, L. J. *Inorg. Chem*. **1997**, *36*, 5420.

[37] Angell, C. L.; Cotton, F. A.; Frenz, B. A.; Webb, T. R. *J. Chem. Soc., Chem. Commun* **1973**, 399.

[38] Cotton, F. A.; Frenz, B. A.; Webb, T. R. *J. Am. Chem. Soc*. **1973**, *95*, 4431.

[39] Cotton, F. A.; Daniels, L. M.; Hillard, L.; Murillo, C. A. *Inorg. Chem*. **2002**, *41*, 1639.

[40] Chisholm, M. H.; Clark, D. L.; Huffman, J. C.; Van Der Sluys, W. G.; Kober, E. M.; Lichtenberger, D. L.; Bursten, B. E. *J. Am. Chem. Soc*. **1987**, *109*, 6796.

[41] Cotton, F. A.; Daniels, L. M.; Huang, P.; Murillo, C. A. *Inorg. Chem*. **2002**, *41*, 317.

[42] (a) Cotton, F. A.; Lin, C.; Murillo, C. A. *Acc. Chem. Res*. **2001**, *34*, 759. (b) Cotton, F. A.; Lin, C.; Murillo, C. A. *Proc. Natl. Acad. Sci*. USA **2002**, *99*, 4810.

[43] See for example: Cotton, F. A.; Donahue, J. P.; Lin, C.; Murillo, C. A. *Inorg. Chem*. **2001**, *40*, 1234.

[44] Cotton, F. A.; Lin, C.; Murillo, C. A. *J. Am. Chem. Soc*. **2001**, *123*, 2670.

[45] Lin, C.; Protasiewicz, J. D.; Smith, E. T.; Ren, T. *Inorg. Chem*. **1996**, *35*, 6422.

[46] See for example: (a) Cotton, F. A. Pederson, E. *Inorg. Chem*. **1975**, *14*, 399. (b) Santure, D. J.; Huffman, J. C.; Sattelberger, A. P. *Inorg. Chem*. **1985**, *24*, 371. (c) Cotton, F. A.; Ren, T. *J. Am. Chem. Soc*. **1992**, *114*, 2237.

[47] Cotton, F. A.; Gu, J.; Murillo, C. A.; Timmons, D. J. *J. Chem. Soc., Dalton Trans*. **1999**, 3741.

[48] Cotton, F. A.; Huang, P.; Murillo, C. A. *Inorg. Chem*. **2003**, *42*, 670.

[49] Berry, J. F.; Cotton, F. A.; Huang, P.; Murillo, C. A. *Dalton Trans*. **2003**, *7*, 1218.

[50] Richardson, D. E.; Taube, H. *Inorg. Chem*. **1981**, *20*, 1278.

[51] See for example: (a) Cotton, F. A.; Donahue, J. P.; Lin, C.; Murillo, C. A. *Inorg. Chem*. **2001**, *40*, 1234. (b) Flanagan, J. B.; Margel, S.; Bard, A. J.; Anson, F. C. *J. Am. Chem. Soc*. **1978**, *100*, 4248. (c) Ito, T.; Hamaguchi, T.; Nagino, H.; Yamaguchi, T.; Kido, H.; Zavarine, I. S.; Richmond, T.; Washington, J.; Kubiak, C. P. *J. Am. Chem. Soc*. **1999**, *121*, 4625.

[52] Cotton, F. A.; Norman, Jr., J. G. *J. Coord. Chem*. **1971**, *1*, 161.

[53] A'Court, R. *Eur. Pat*. 0198680, **1986**.

[54] McKay, A. F.; Hatton, W. G.; Braun, R. O. *J. Am. Chem. Soc*. **1956**, *78*, 6144.

[55] McKay, A. F.; Kreling, M.-E.; Paris, G. Y.; Braun, R. O.; Whittingham, D. J. *Can. J. Chem*. **1957**, *35*, 843.

[56] McKay, A. F.; Kreling, M.-E. *Can. J. Chem*. **1957**, *35*, 1438.

[57] Li, C.; Mella, S. L.; Sartorelli, A. C. *J. Med. Chem*. **1981**, *24*, 1089.

[58] Cotton, F. A.; Daniels, L. M.; Murillo, C. A.; Timmons, D. J.; Wilkinson, C. C. *J. Am. Chem. Soc.* **2002**, *124*, 9249.

[59] Cotton F. A.; Murillo, C. A.; Wang, X.; Wilkinson, C. C. *Inorg. Chim. Acta* **2003**, *351*, 191.

[60] Cotton, F. A.; Wilkinson, G.; Gaus, P. L. *Basic Inorganic Chemistry*, 3rd Ed.; John Wiley & Sons, Inc.: New York, 1995, p. 278.

[61] Cotton, F. A.; Daniels, L. M.; Hillard, E. A.; Murillo, C. A. *Inorg. Chem*. **2002**, *41*, 2466.

[62] Cotton, F. A.; Daniels, L. M.; Murillo, C. A.; Zhou, H. C. *Inorg. Chim. Acta* **2000**, *300-302*, 319.

[63] Buschmann, W. E.; Miller, J. S.; Bowman-James, K.; Miller, C. N. *Inorg. Synth.* **2002**, *33*, 83.

[64] Hopfinger, A.; Söderlund, M.; Reni, S. *Finn. Pat*. 82445, **1988**.

[65] Arend, M.; Westermann, B.; Risch, N. *Angew Chem. Int. Ed*. **1998**, *37*, 1044.

[66] Thompson, B.B. *J. Phar. Sci*. **1968**, *57*, 715.

[67] Huebner, C. F.; Donoghue, E. M.; Novak, C. J.; Dorfmann, L.; Wenkert, E. *J. Org. Chem.* **1970**, *35*, 1149.

[68] Reeve, W.; Christian, J. *J. Am. Chem. Soc*. **1956**, *78*, 860.

[69] Bartoszak-Adanska, E.; Bregier-Jarzebowska, R.; Lmozik, L. *Polyhedron* **2002**, *21*, 739.

[70] Cotton, F. A.; Gruhn, N. E.; Gu, J.; Huang, P.; Lichtenberger, D. L.; Murillo, C. A.; Van Dorn, L. O.; Wilkinson, C. C. *Science*, **2002**, *298*, 1971.

[71] Cotton, F. A.; Villagrán, D. unpublished results.

[72] Cotton, F. A.; Murillo, C. A.; Reibenspies, J. H.; Villagran, D.; Wang, X.; Wilkinson, C. C. *Inorg. Chem*. **2004**, *43*, 8373.

[73] Arya, V. P.; Nagarajan, K.; David, J.; Shenoy, S. J.; Gokhale, N. G. *Indian J. Chem*. **1978**, *16B*, 226.

APPENDIX A

SUPPLEMENTAL MATERIAL FOR CHAPTER III

Table 23. LMSB Database Information for the Compounds in Chapter III.			
Compound	Formula	Number	STR Number
1-(2-Aminoethyl)-2-imidazolidinethione	$C_5H_{11}N_3S$	**6**	3912
Htbo	$C_5H_9N_3$	**7**	3926
Htbn	$C_6H_{11}N_3$	**8**	4023
$[H_2tbn][HCO_3]$	$C_7H_{13}N_3O_3$	**-**	4013
$Mo_2(tbo)_4$	$C_{20}H_{32}Mo_2N_{12}$	**9**	4049
$Mo_2(tbo)_4$·THF	$C_{24}H_{40}Mo_2N_{12}O$	**9**	3998
$Mo_2(tbo)_4Cl$	$C_{20}H_{32}ClMo_2N_{12}$	**10**	3959
$Mo_2(tbn)_4$	$C_{24}H_{40}Mo_2N_{12}$	**11**	4028
$Mo_2(tbn)_4Cl_2$	$C_{24}H_{40}Cl_2Mo_2N_{12}$	**13**	4273
$Mo_2(tbn)_4Cl_2$·$2CH_2Cl_2$	$C_{26}H_{44}Cl_6Mo_2N_{12}$	**13**·$2CH_2Cl_2$	4080
$Mo_2(tbn)_4Cl_2$·$3CHCl_3$	$C_{27}H_{43}Cl_{11}Mo_2N_{12}$	**13**·$3CHCl_3$	4271

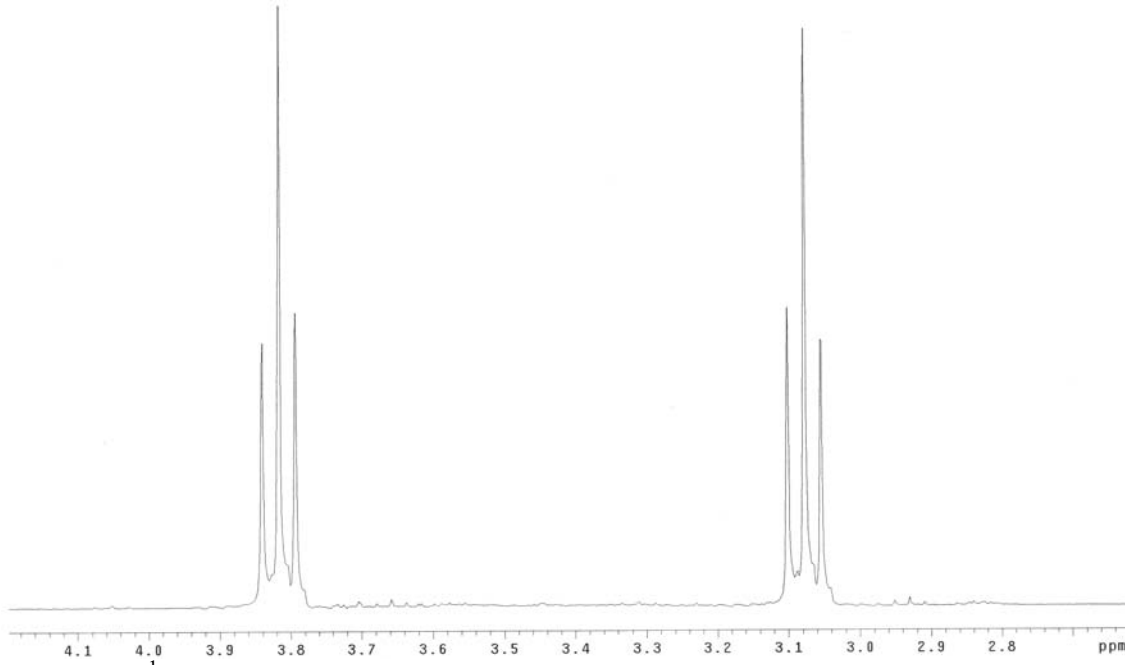

Figure 40. ^{1}H NMR spectrum of Htbo.

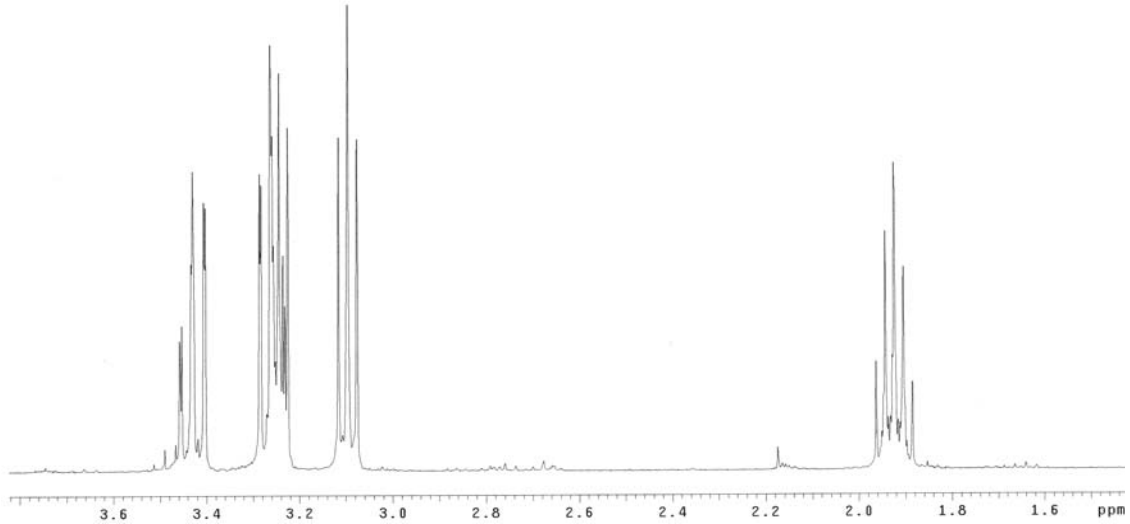

Figure 41. ^{1}H NMR spectrum of Htbn.

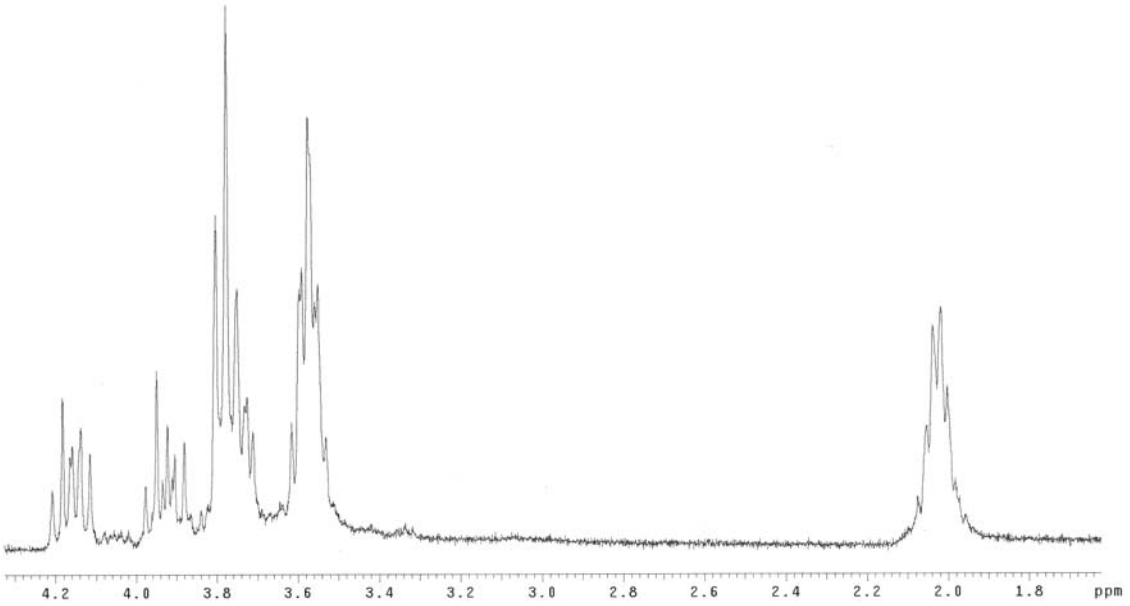

Figure 42. ^{1}H NMR spectrum of $Mo_2(tbn)_4Cl_2$.

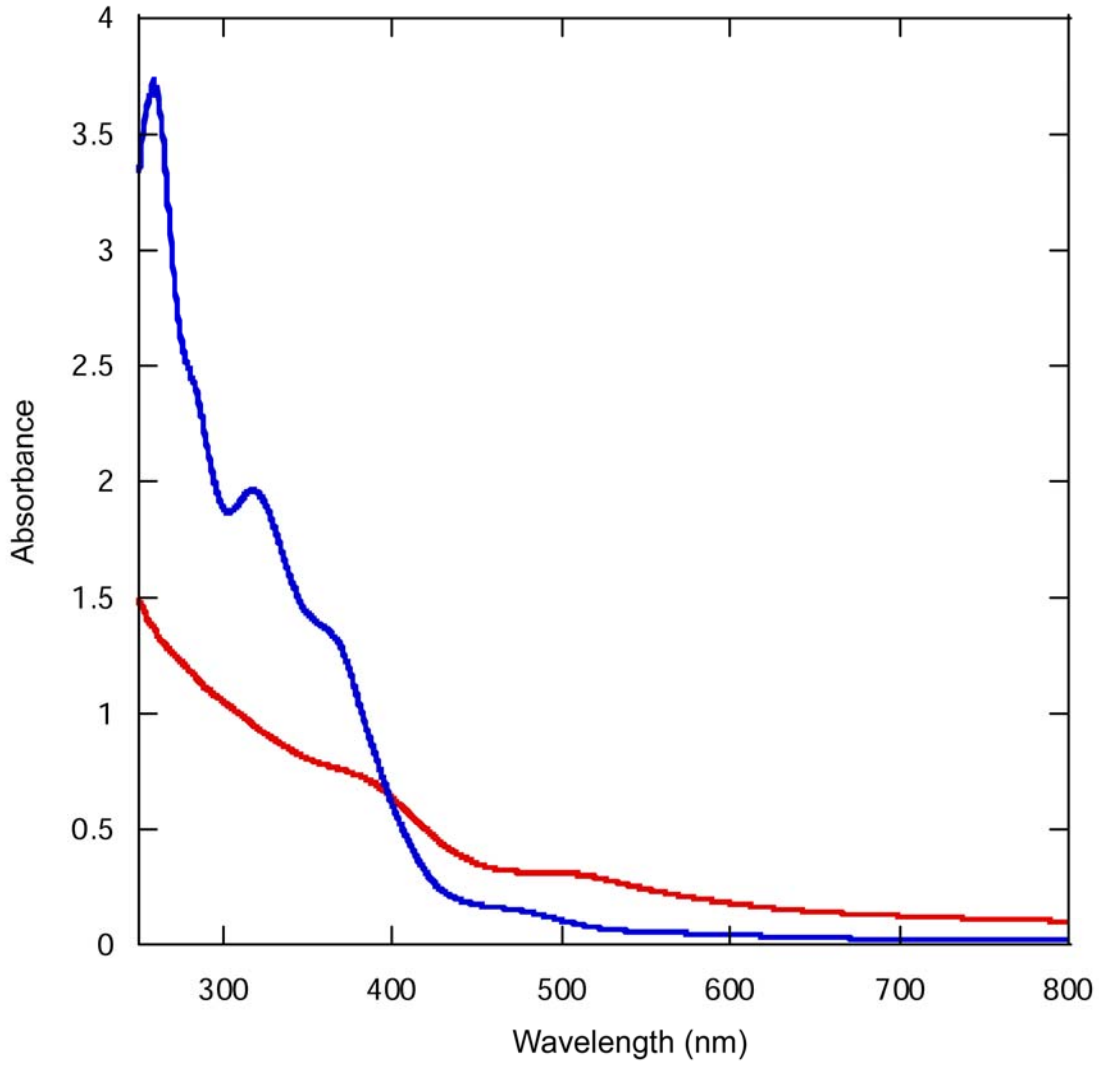

Figure 43. UV-Visible Spectra of $Mo_2(tbo)_4$ (red) and $Mo_2(tbn)_4$ (blue).

APPENDIX B

SUPPLEMENTAL MATERIAL FOR CHAPTER IV

Table 24. LMSB Database Information for the Compounds in Chapter IV.			
Compound	Formula	Number	STR Number
N,N-bis(2,2-dimethyl-3-iminohydroxypropyl)amine	$C_{10}H_{22}ClN_3O_2$	**14**·HCl	3879
N,N-bis(2,2-dimethyl-3-iminohydroxypropyl)amine	$C_{10}H_{21}N_3O_2$	**14**	3901
N,N-bis(3-amino-2,2-dimethyl-propyl)amine	$C_{20}H_{52}CdN_8O_7$	$Cd(\mathbf{15})_2(NO_3)_2\cdot H_2O$	3907
$[H_2TMhpp][HCO_3]$	$C_{12}H_{23}N_3O_3$	-	4002
N,N-bis(2,2-diethyl-3-iminohydroxypropyl)amine	$C_{14}H_{32}ClN_3O_3$	**17**·HCl·H_2O	3923
N,N-bis(3-amino-2,2-diethyl-propyl)amine	$C_{30}H_{72}CdN_8O_7$	$Cd(\mathbf{18})_2(NO_3)_2\cdot$ EtOH	3981
HTEhpp	$C_{15}H_{29}N_3$	**19**	4016
$Mo_2(TMhpp)_4$	$C_{44}H_{80}Mo_2N_{12}$	**20**	4042
$Mo_2(TMhpp)_4(TFPB)$	$C_{76}H_{92}BF_{24}Mo_2N_{12}$	**21**	4228
$Mo_2(TMhpp)_4(TFPB)$	$C_{77}H_{94}BCl_2F_{24}Mo_2N_{12}$	**21**·CH_2Cl_2	4206
$Mo_2(TMhpp)_4(TFPB)_2$	$C_{108}H_{104}B_2F_{48}Mo_2N_{12}$	**22**	4105
$Mo_2(TEhpp)_4$	$C_{60}H_{112}Mo_2N_{12}$	**23**	4118
$Mo_2(TEhpp)_4(TFPB)$	$C_{96}H_{136}BF_{24}Mo_2N_{12}O_2S_2$	**24**·2DMSO	4290

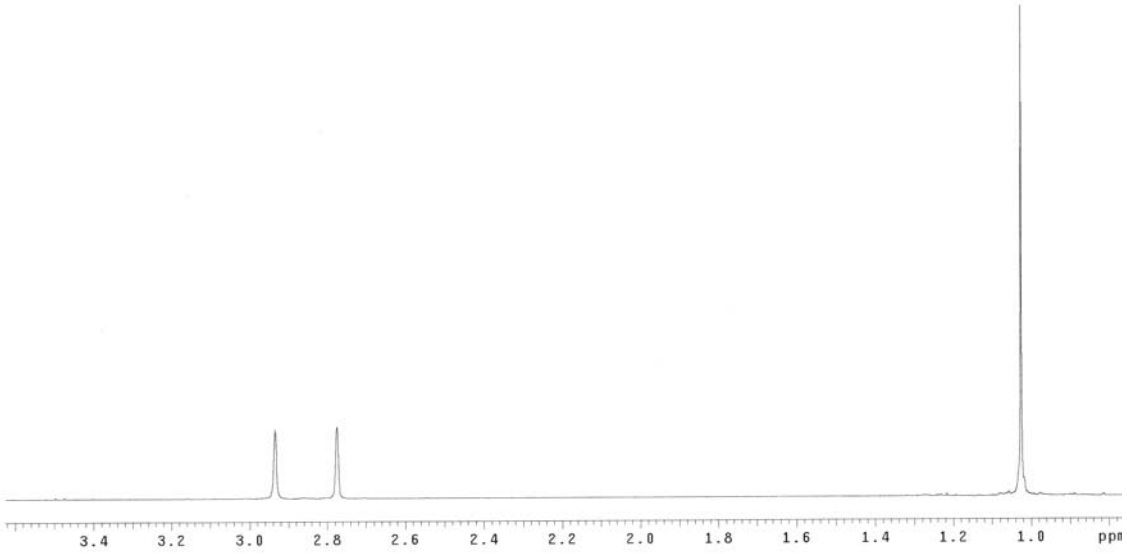

Figure 44. ^{1}H NMR of HTMhpp.

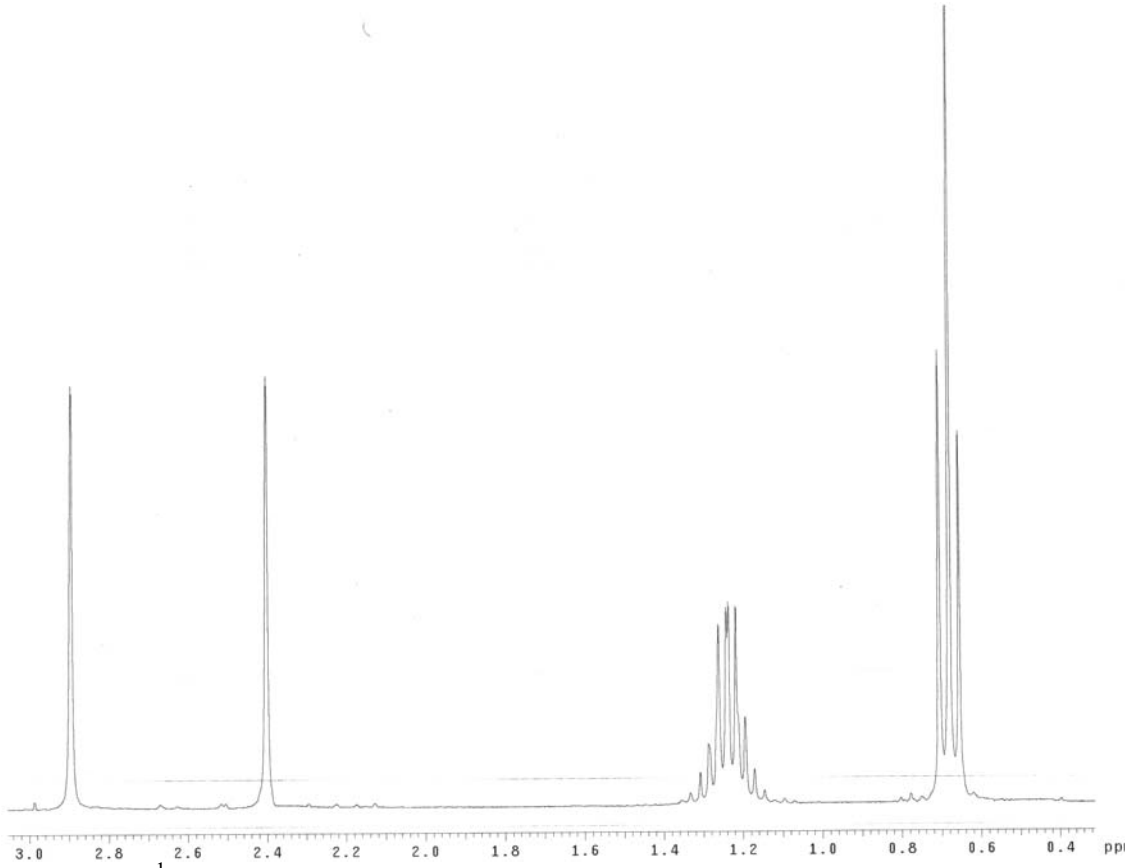

Figure 45. ^{1}H NMR of HTEhpp.

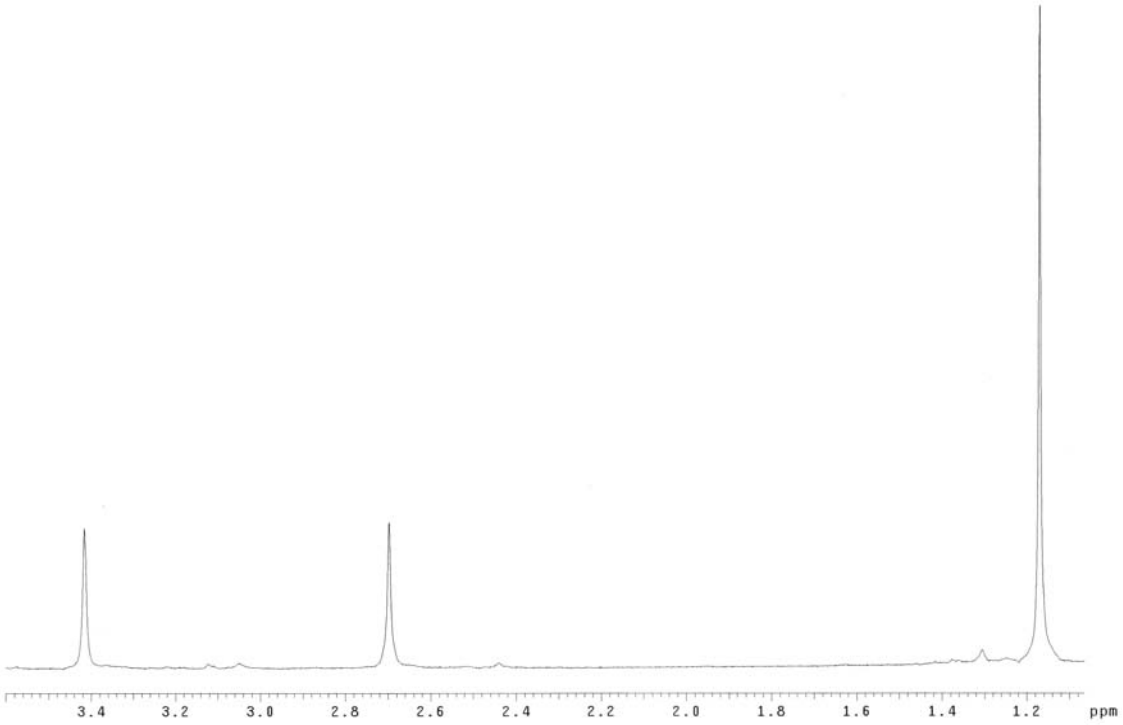

Figure 46. ^{1}H NMR spectrum of $Mo_2(TMhpp)_4$.

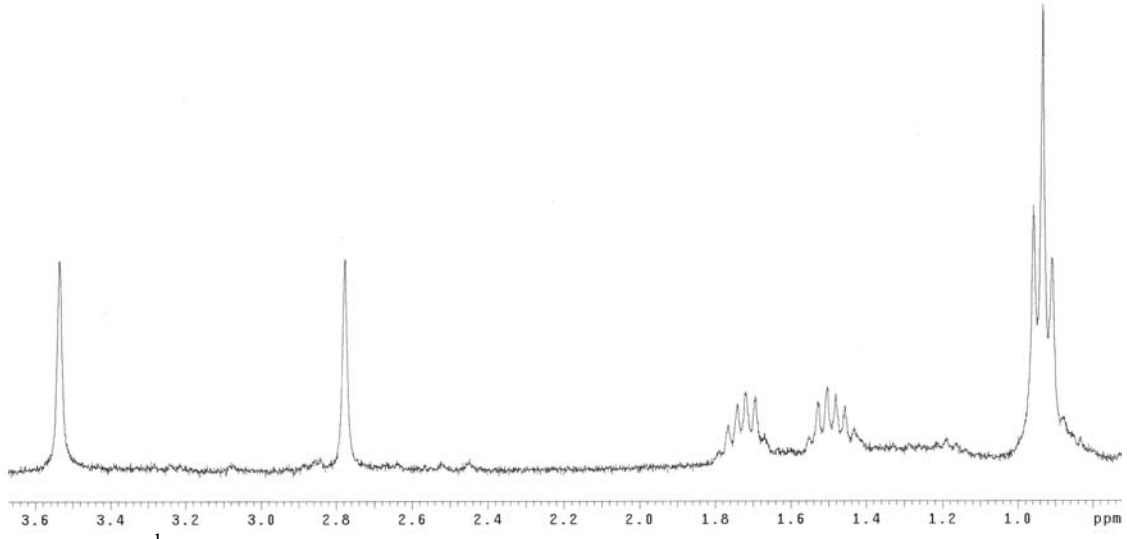

Figure 47. ^{1}H NMR spectrum of $Mo_2(TEhpp)_4$.

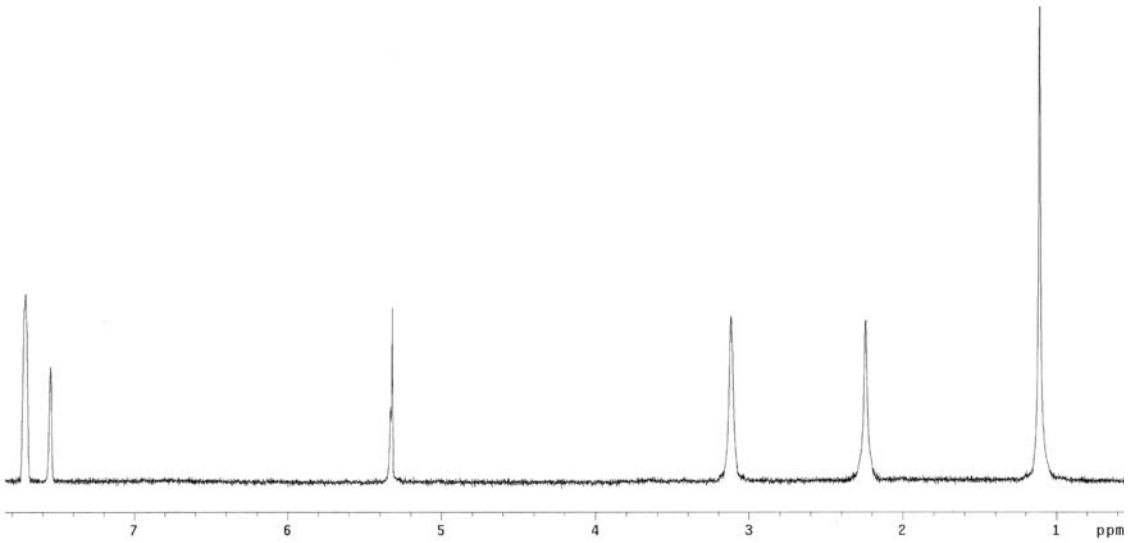

Figure 48. ^{1}H NMR of $Mo_2(TMhpp)_4(TFPB)_2$.

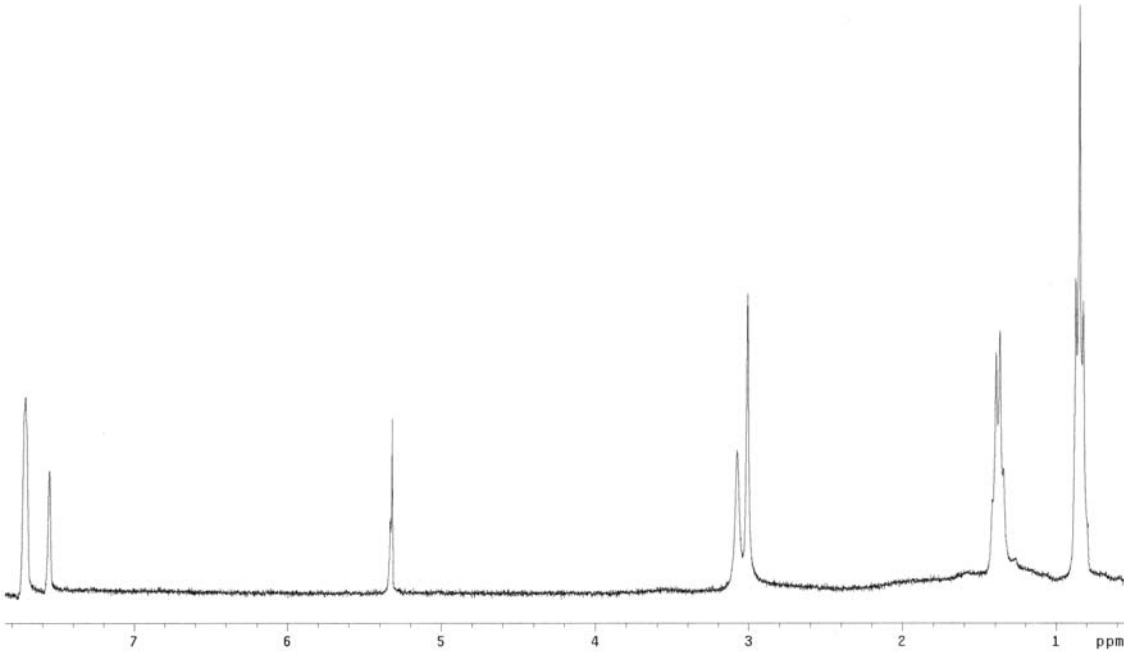

Figure 49. ^{1}H NMR spectrum of $Mo_2(TEhpp)_4(TFPB)_2$.

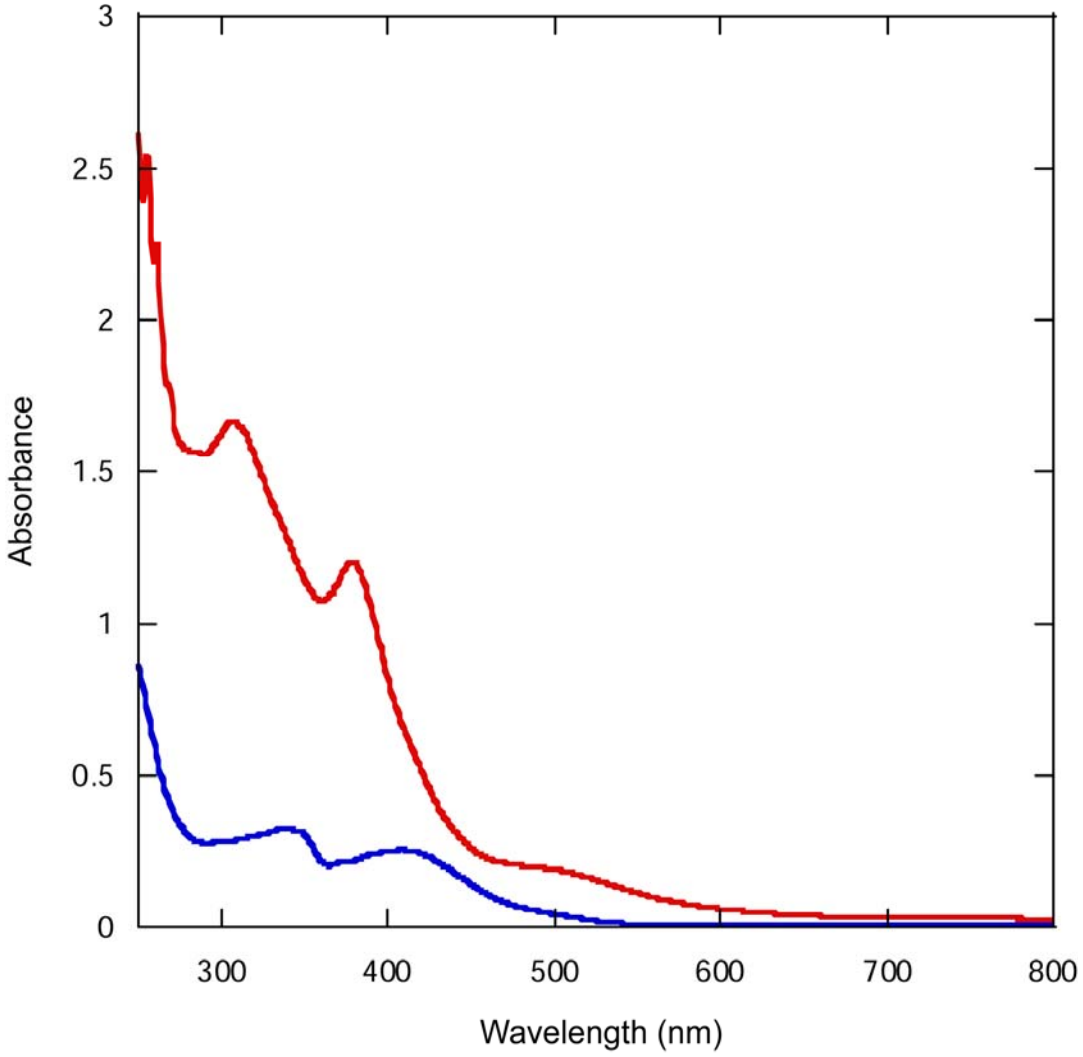

Figure 50. UV-Visible spectra of $Mo_2(TMhpp)_4$ (red) and $Mo_2(TEhpp)_4$ (blue).

APPENDIX C

SUPPLEMENTAL MATERIAL FOR CHAPTER V

Table 25. LMSB Database Information for the Compounds in Chapter V.			
Compound	Formula	Number	STR Number
1,3-Diazacycloheptane-2-thione	$C_5H_{10}N_2S$	**26**	4121
2-Methylmercapto-Δ^2-1,3-diazacycloheptane	$C_6H_{13}N_2SI$	**27**·HI	4120
2-(γ-Hydroxypropylamino)-Δ^2-1,3-diazacycloheptene	$C_8H_{17}N_3O$	**28**·HI	4132
Htbu	$C_8H_{15}N_3$	**29**	4232
Htbd	$C_7H_{13}N_3$	**31**	4171
$Mo_2(tbd)_4Cl$	$Mo_2(C_7H_{12}N_3)_4Cl$	**33**	4248
$Mo_2(tbd)_4Cl_2$	$Mo_2(C_7H_{12}N_3)_4Cl_2$	**34**	4225
$Mo_2(tbu)_4$	$Mo_2(C_8H_{15}N_3)_4$	**35**	4236
$Mo_2(tbu)_4Cl$	$Mo_2(C_8H_{15}N_3)_4Cl$	**36**	4278

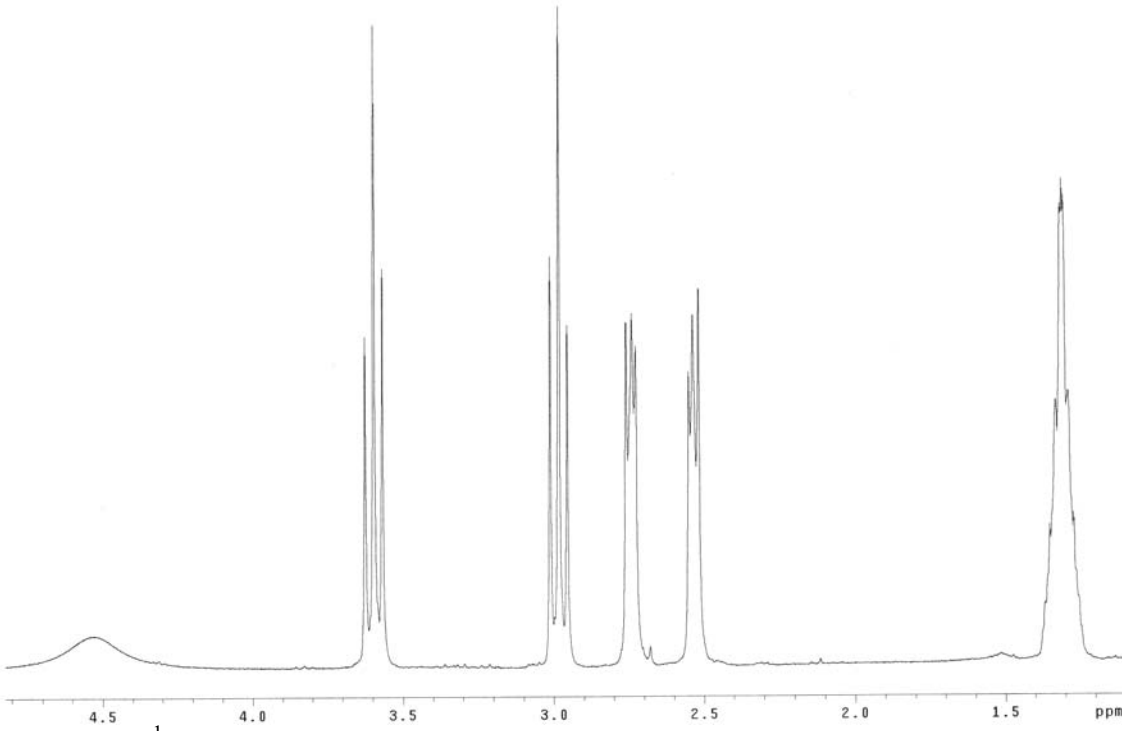

Figure 51. ^{1}H NMR of Htbd.

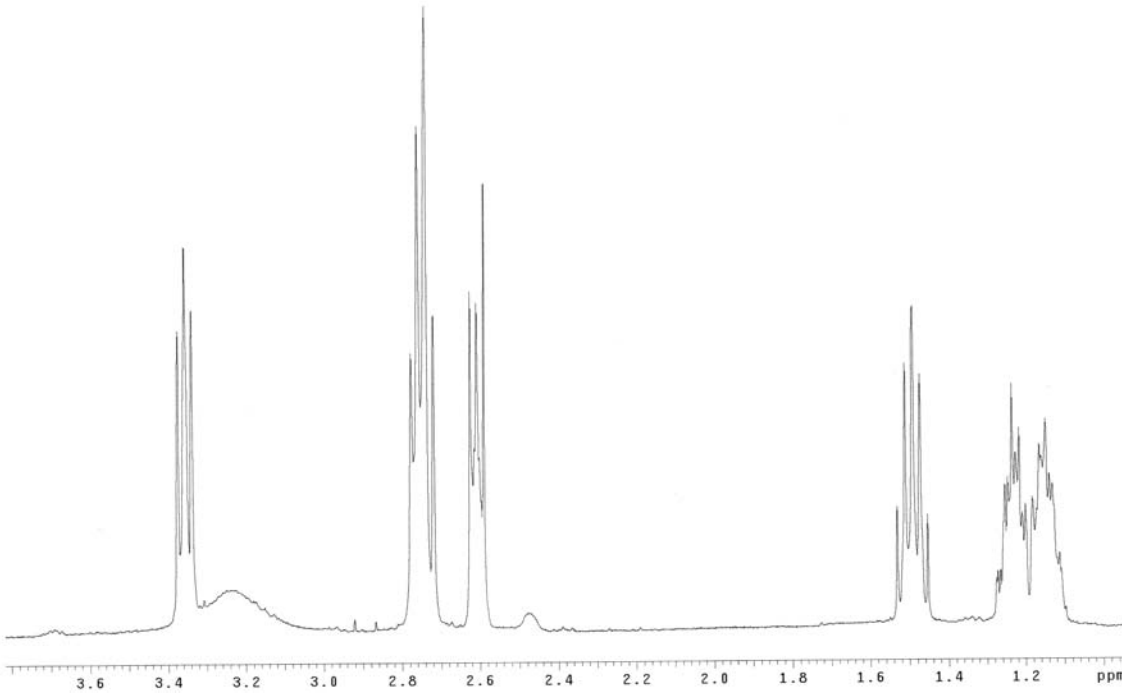

Figure 52. ^{1}H NMR of Htbu.

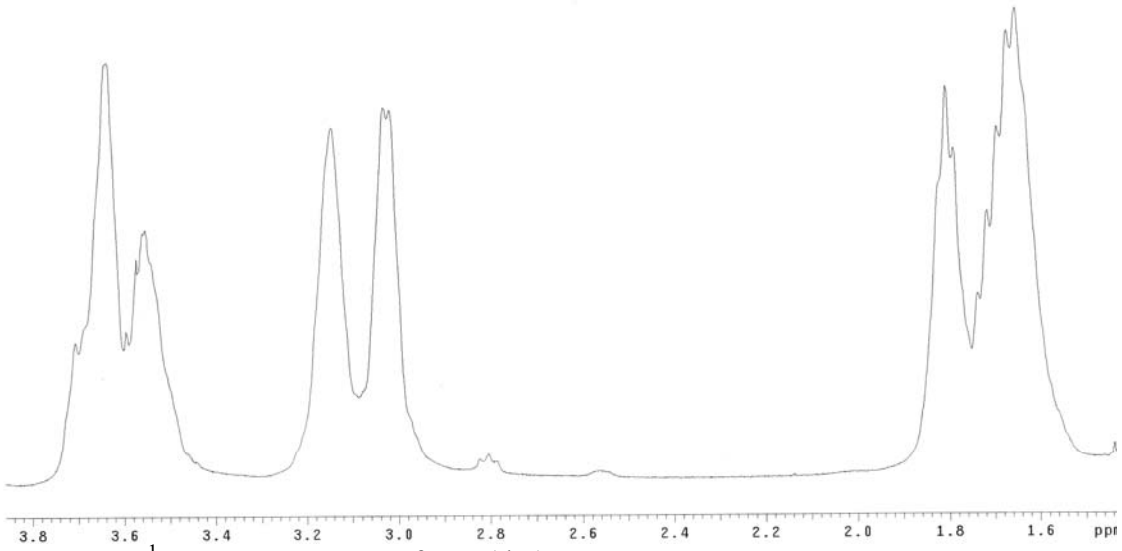

Figure 53. ^{1}H NMR spectrum of $Mo_2(tbu)_4$.

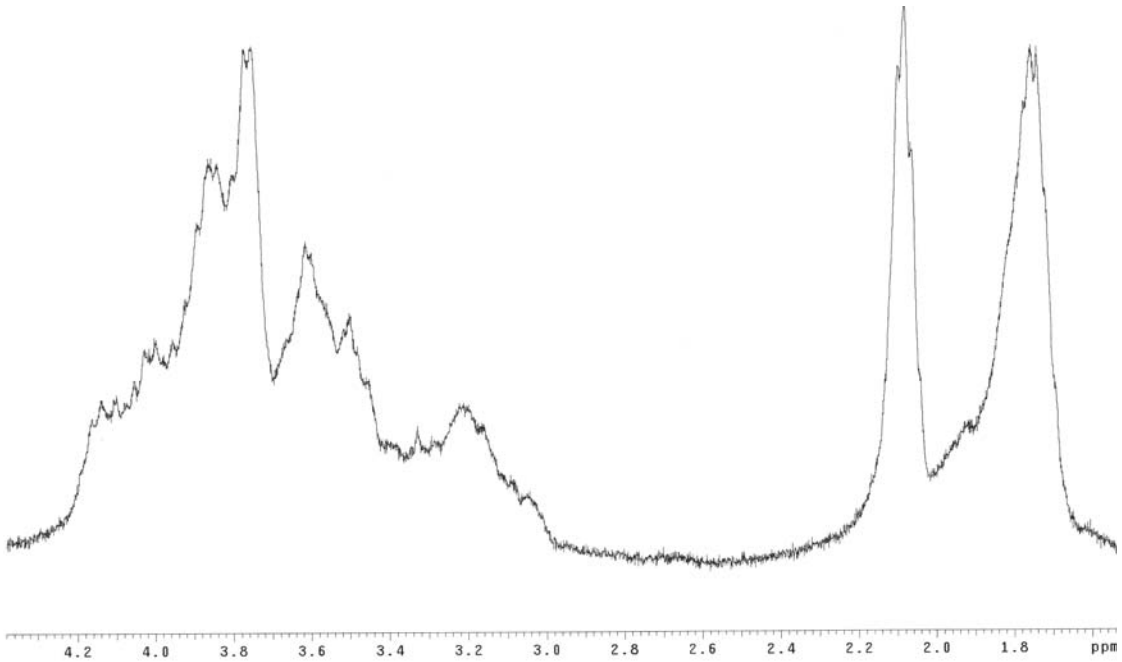

Figure 54. ^{1}H NMR spectrum of $Mo_2(tbd)_4Cl_2$.

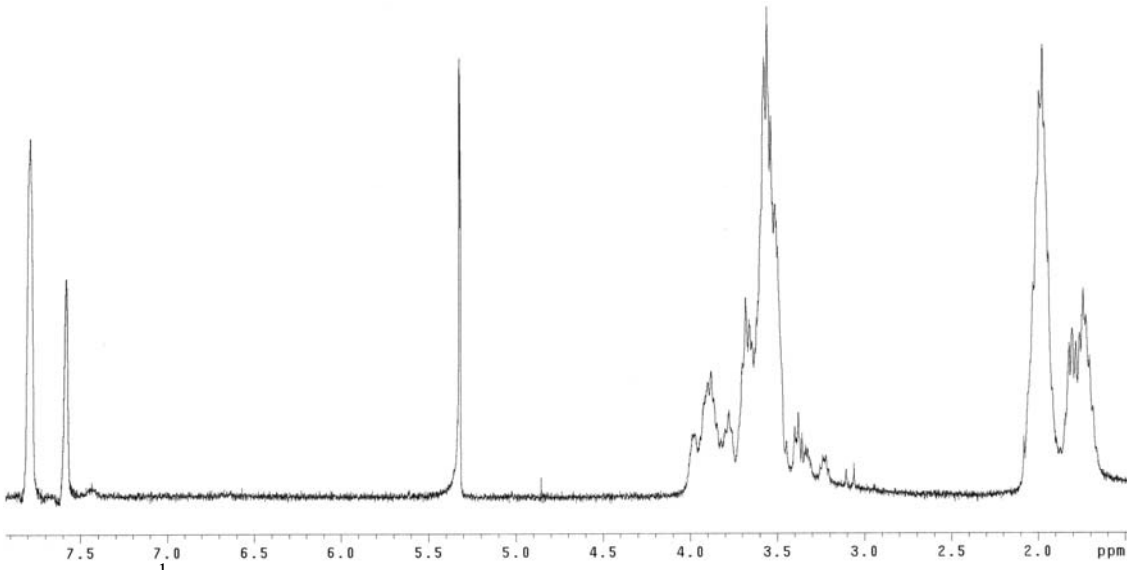

Figure 55. ^{1}H NMR spectrum of $Mo_2(tbu)_4(TFPB)_2$.

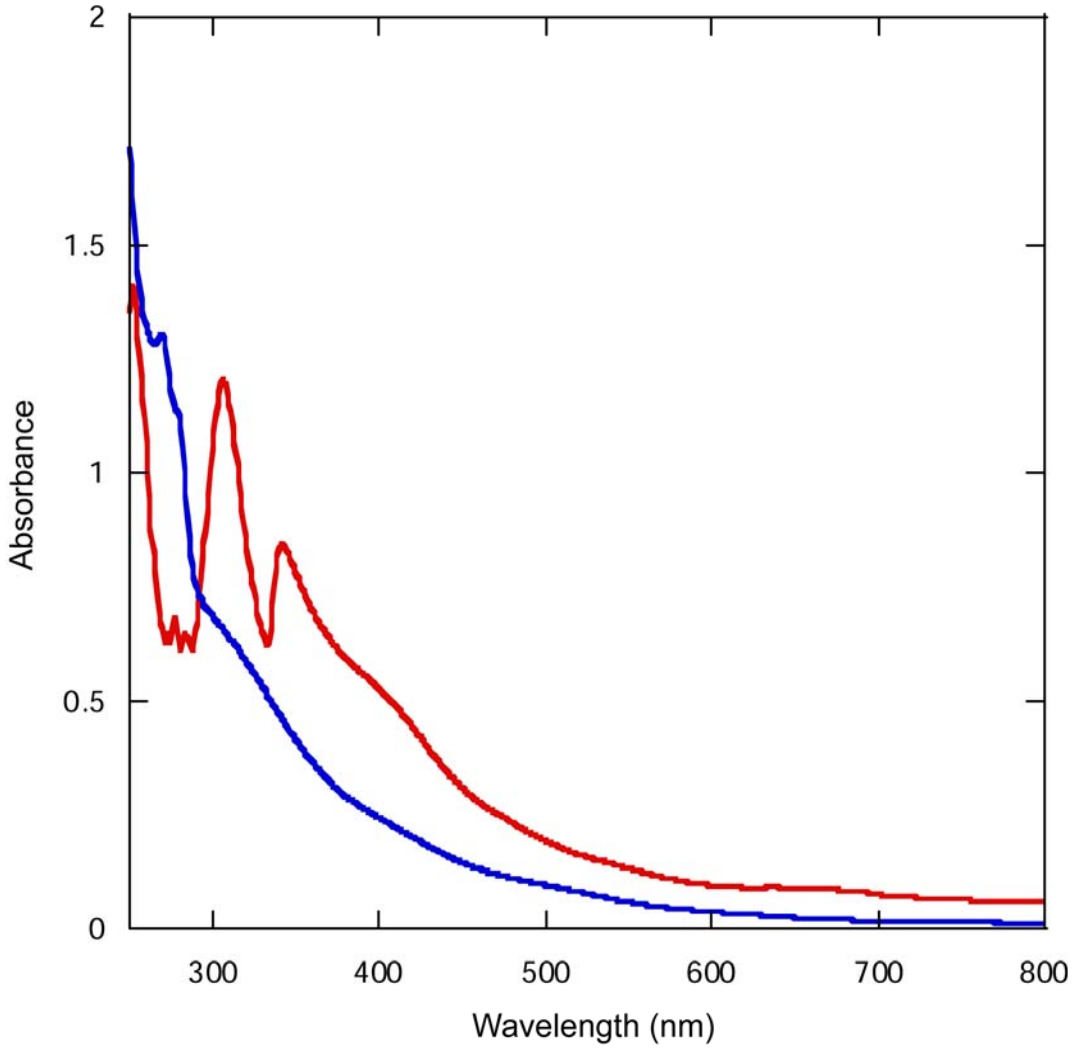

Figure 56. UV-Visible spectra of $Mo_2(tbd)_4$ (red) and $Mo_2(tbu)_4$ (blue).

VITA

Chad C. Wilkinson received his B.S. Chemistry degree from Baylor University in December, 1999. During his time there, he worked in the research laboratory of Dr. Stephen L. Gipson studying the electrochemistry of organometallic complexes. His degree was conferred with distinction from the honors program of Baylor University and is also certified by the American Chemical Society. He then began his graduate career under the guidance of Dr. F. A. Cotton in August, 2000.

His permanent address is: 3702 Auburn Dr., Abilene, Texas 79602, USA.